# IDENTIFICATION OF EPIGENETIC CHANGES IN PROSTATE TISSUES WITH PREMALIGNANT CHARACTERISTICS

by

**Ceren Şeref**

A dissertation submitted to the

Graduate School of Health Sciences

in Partial Fulfillment of the requirements

for the Degree of

Doctor of Philosophy

in

Cellular and Molecular Medicine


December 10, 2020

*To Ivan Vujaklija,*

*who lifts the weight of the world off my shoulders.*

# ABSTRACT


Identification of Epigenetic Changes in Prostate Tissues

with Premalignant Characteristics

Ceren ŞEREF

Doctor of Philosophy in Cellular and Molecular Medicine

December 10, 2020

Prostate cancer (PCa) is one of the most commonly diagnosed, non-cutaneous malignancy and a leading cause of cancer-related death worldwide. Conventional methods of diagnosis include prostate specific antigen testing, digital rectal examination, and transrectal ultrasound guided prostate biopsies. The limitation of these approaches has led to the development of multiparametric MRI (mpMRI) guided biopsies. Significantly more sensitive, mpMRI can accurately identify radiographically suspicious lesions that are likely to be malignant and guide biopsy collection. However, even with this approach, ~10% of suspicious biopsies are found to be histopathologically benign. Given the sensitivity of mpMRI, it is unclear if these lesions harbor premalignant features or are technical artifacts.

Epigenetic alterations, including DNA hypermethylation, are commonly found early in the development of PCa. Therefore, using these as premalignant markers, we characterized the epigenetic signatures of those radiographically suspicious lesions that were deemed to be benign by histology. Focusing on three well-characterized tumor suppressors, APC, GSTP1 and RARβ2 we developed a highly sensitive quantitative methylation specific PCR method to quantify promoter methylation. This method could robustly identify malignant and benign samples with the limited genetic material from FFPE biopsies. With this we quantified the promoter methylation of radiographically suspicious lesions from patients with either histopathology positive ("malignant"; n=28, 82 biopsies) or negative ("MRI"; n=18, 56 biopsies) biopsies. We found that the observed methylation levels of MRI cohort were markedly higher than benign samples yet lower than malignant tumors. This difference was highly gene specific. In our MRI cohort we did not observe any methylation positive cores at the APC promoter while almost all samples were positive for GSTP1 methylation. Even in the malignant cohort, only 37% of biopsies were methylation positive with the APC gene. Further, the relative methylation of the MRI cohort was heterogeneous with several cores biopsied from the same patient being positive for different markers. Intriguingly, when we investigated the clinical outcome of this cohort, almost none of the lesions in the MRI cohort had progressed into a neoplastic lesion. Overall, our results demonstrate that radiographically suspicious non-malignant lesions carry premalignant epigenetic alterations.

# ÖZETÇE

Premalign Özellikli Prostat Dokularında

Epigenetik Değişikliklerin Karakterizasyonu

Ceren ŞEREF

Hücresel ve Moleküler Tıp, Doktora

December 10, 2020

Prostat kanseri (PKa), dünya çapında en yaygın olarak teşhis edilen, kutanöz olmayan malignitelerden ve kansere bağlı ölümlerin önde gelen nedenlerinden biridir. Geleneksel tanı yöntemleri prostat spesifik antijen testi, dijital rektal muayene ve transrektal ultrason klavuzluğunda yapılan prostat biyopsileridir. Bu yaklaşımların karşılaştığı kısıtlamalar multiparametrik MRI (mpMRI) kılavuzluğunda yapılan biyopsilerin geliştirilmesinde rol oynamıştır. Oldukça hassas bir görüntüleme yöntemi olan mpMRI, şüpheli radyografik lezyonları doğru şekilde tanılamada ve biyopsi alınmasında rehberlik etmektedir. Ancak bu yaklaşımla bile şüpheli biyopsilerin ~% 10'unun histopatolojik olarak iyi huylu olduğu gözlemlenmiştir. mpMRI'nin hassasiyeti göz önüne alındığında, bu lezyonların premalign özellikler barındırma olasılığı ya da bu gözlemlerin teknik bir problemden kaynaklanıyor olma ihtimali açık değildir.

DNA hipermetilasyonu da dahil olmak üzere, epigenetik değişiklikler genellikle prostat kanserinin erken dönemlerinde gözlenebilmektedir. Bu değişiklikleri premalign belirteçler olarak kullanarak, histolojik olarak iyi huylu tanımlanmış ancak radyografik olarak şüpheli lezyonların epigenetik imzalarını karakterize ettik. İyi karakterize edilmiş tümör baskılayıcı APC, GSTP1 ve RARβ2 genlerine odaklanarak, promotör metilasyonunu ölçmek için oldukça hassas, kantitatif metilasyona özgü PCR yöntemini optimize ettik. Bu yöntemin, iyi ve kötü huylu örnekleri FFPE biyopsilerinden elde edilen sınırlı genetik materyalle tanımlayabildiğini saptadık. Bu yaklaşımla, histopatolojisi pozitif ("malign"; n = 28, 82 biyopsi) veya negatif ("MRI"; n = 18, 56 biyopsi) hastalardan alınan radyografik olarak şüpheli lezyonların promotör metilasyonunu ölçtük. MRI kohortunuda metilasyon seviyelerinin, iyi huylu örneklerden belirgin şekilde yüksek, ancak kötü huylu tümörlerden daha düşük olduğunu gözlemledik. Ayrıca, bu değişkenliğin oldukça gen spesifik olduğunu saptadık. MRI kohortunda, APC'de herhangi bir metilasyon pozitif kor gözlemlenemezken, korların tamamına yakını GSTP1 metilasyonu için pozitifti. Malign örneklerin bulunduğu kohortta bile, biyopsilerin sadece %37'si APC geni için metilasyon pozitifti. Ayrıca, MRI kohortunda aynı hastadan analiz edilmiş farklı kor biyopsilerinde heterojen bir pozitiflik gözlemlendi. Bu kohortun klinik bulgularını araştırdığımızda ise, şaşırtıcı bir şekilde, MRI kohortundaki örneklerin neredeyse hiçbirinin neoplastik bir lezyona dönüşmediğini gördük. Sonuç olarak, DNA metilasyon profilimiz, radyografik olarak şüpheli lezyonların premalin epigenetik değişiklikler taşıdığını gösterdi.

# ACKNOWLEDGEMENTS

First and foremost, I would like to thank my advisor Dr. Nathan Lack for giving me the opportunity to work in this amazing environment. Although it is always told, a journey as complicated and tough as this, is a completely different experience on its own. I'm grateful for his continuous support in this journey, and the guidance for the life that "no one would understand".

I would also like to thank my thesis progress committee members Dr. Müjdat Zeybel for his guidance and understanding and Dr. Yeşim Sağlıcan for her support, being available all the time, day and night. I also would like to thank Dr. Ömer Faruk Bayrak for kindly accepting to be a member of my thesis defense jury.

I would like to thank Prof. Dr. Tarık Esen for enabling me to work with such an important and unique cohort. Also, coming up with interesting ideas and bringing the nice team together, letting us come this far.

I am so grateful to Dr. Ömer Acar, not only his scientific contribution but also his never ending support, enthusiasm and optimism. He made everything look so easy and manageable, even though we are not even in the same time zones! I cannot thank him enough for the trust he placed in me, no matter what happens. I also want to thank Dr. Mert Kılıç for his continuous support, valuable insights and discussions throughout the project, being there all the time for help.

My sincere thanks goes to the Lack Lab members. Especially our "TR team", Doğancan Özturan and Betül Ersoy, you were there at bench with me all the time. You are the lab mates everyone would wish for. My other long-distance lab mates, my mentors, my PhD sisters, Hilal Saraç, Fatma Özgün and Fidan Şeker, you are the best! From hours and hours of Zoom meetings to every single text, being there all the time for me, solving anything and everything instantly. I'm so sorry, no way you will be free from me even after my graduation! Mohammad Haroon Qureshi and Özen Leylek, I will miss our coffee times when we hopelessly try to solve our PhD and life problems. Thanks for sharing the journey with me!

I want to express how lucky I am to be able to work with and share this PhD life with Betül Ersoy once again. The person who is always on my side, picks me up when I fall, enjoys the good, gets angry for the bad. I can only wish my fellow PhD candidates out

there to have someone indestructible as she is. If you can sit with someone without uttering a word yet share the world, that's him or her, then you will know what I'm talking about.

Gizem Yılmaz Durmuşoğlu, you always kept my head above the surface, and helped me in everything coming into my way. I am grateful for your friendship, support and understanding. You always put everything aside going on in your life to share even the smallest unimportant things and be there for me. Thank you!

I want to thank Koç University Graduate School of Health Sciences (GSHS) and Koç University Research Center for Translational Medicine (KUTTAM) for the funding and great research environment they provided, bringing all these beautiful people together.

There is someone I cannot thank enough even if I wrote hundreds of pages. What he did for me cannot be simply described as supporting or sharing the process. I want to thank Ivan Vujaklija, being the impossible person, going through another PhD with me, step by step. Being a mentor, being a wailing wall, being a sanctuary of my mind that is never at ease. But above all, embracing everything and being the "That is fine, how can I help?" person. I don't know how to thank you for all.

Last but not the least, if anyone suffered all the ups and downs of these years as much as me, they are surely my mum Selma Şeref and dad Sabahattin Şeref. Listening to all the complains, keeping my head in the game but reminding me all the time that I am the most important thing in the world and no matter what happens, they are the ones comforting me that we will figure it out. I wouldn't be able to do it without you. I am an incredibly lucky daughter.

Also my special thanks goes to the biggest support team ever, the Vujaklija family, cheering me up all the time, reminding me that I am surrounded by the most beautiful people. Thank you so much!

# TABLE OF CONTENTS

# LIST OF TABLES

# LIST OF FIGURES

# ABBREVIATIONS

| | |
|---|---|
| ACTB | Actin Beta |
| ADC | Apparent Diffusion Coefficient |
| APC | Adenomatous polyposis coli |
| Ct | Cycle Threshold |
| CZ | Central Zone |
| DCE | Dynamic Contrast-Enhanced |
| DRE | Digital Rectal Examination |
| DWI | Diffusion-Weighted Imaging |
| gDNA | Genomic DNA |
| GSTP1 | Gluthathion S-trasferase Pi 1 |
| HGPIN | High-Grade Prostatic Intraepithelial Neoplasia |
| ISUP | International Society of Urologic Pathologists |
| mpMRI | Multiparametric MRI |
| MRI | Magnetic Resonance Imaging |
| MGMT | $O^6$-methylguanine DNA methyltransferase |
| PIA | Proliferative Inflammatory Atropy |
| PB | Prostate Biopsy |
| PCa | Prostate Cancer |
| PI-RADS v2 | Prostate Imaging - Reporting and Data System version 2 |
| PZ | Peripheral Zone |
| RA | Retinoic Acid |
| RARE | Retinoic Acid Response Element |
| RARβ2 | Retinoic Acid Receptor Beta 2 |
| TRUS | Transrectal Ultrasound |
| TW1 | T1 Weighted Imaging |
| TW2 | T2 Weighted Imaging |
| TZ | Transition Zone |
| QMSP | Quantitative Methylation Specific Polymerase Chain Reaction |
| QPCR | Quantitative Polymerase Chain Reaction |

# 1. INTRODUCTION

## 1.1 The prostate gland

The prostate is a walnut shaped gland positioned at the subperitoneal portion between the pelvic diaphragm and the peritoneal cavity. It is located posterior to the symphysis pubis, anterior to rectum and inferior to the urinary bladder. The prostate surrounds the proximal urethra that exits from the bladder **(Figure 1.1)** (1). It consists of a central zone (CZ), transition zone (TZ) and peripheral zone (PZ) **(Figure 1.2)**. These three zones arise from different embryonic origins (2) and have unique histological, anatomical, functional properties and susceptibility to pathological disorders including prostate cancer (PCa). The PZ is primarily derived from the urogenital sinuses and is the most common site of PCa with 70% of all tumours arising from this zone. The TZ is also derived from the urogenital sinuses but only 25% of PCa is found in this zone. The difference in PCa incidence between PZ and TZ has been proposed to be due to the differing stromal components of these zones (1). The TZ is composed of more fibromuscular stroma which is involved in benign prostatic hyperplasia (BPH) (3). Finally, the CZ is derived from the Wolffian duct and has a very low incidence of cancer and similar to seminal vesicles (1).

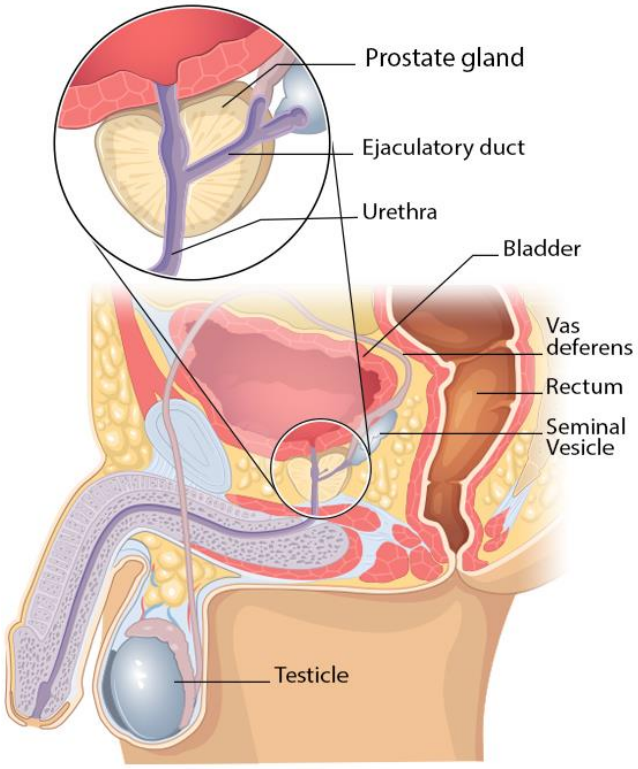


**Figure 1.1 Location of the prostate.** *Adopted from (4).*

The prostate is comprised of two major cell types: epithelial and stromal cells. Epithelial cells are further categorized in four classifications including basal, secretory or luminal, intermediate and neuroendocrine cells (5). Basal cells are undifferentiated cells that are non-secretory with a low proliferative capacity. Luminal cells are terminally differentiated and non-dividing. Intermediate cells connect the luminal and basal cells. Finally, neuroendocrine cells are intraepithelial regulatory cells that are scattered among basal and luminal cells (6,7).

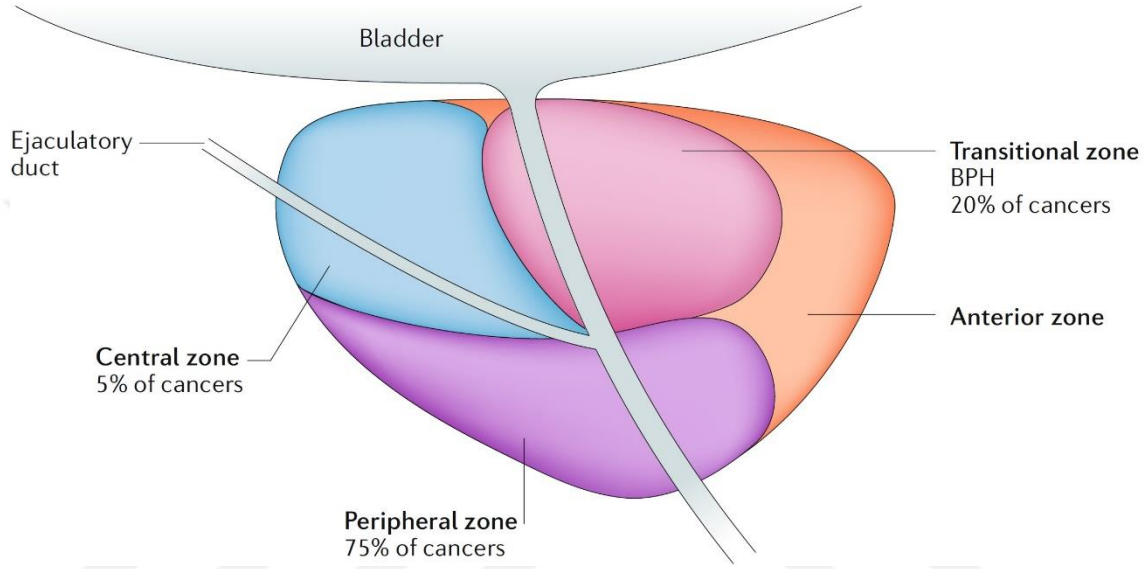


**Figure 1.2 Zones of the prostate gland.** *Adopted from (8).*

## 1.2 Prostate Cancer

### 1.2.1 Epidemiology

PCa is the most commonly diagnosed, non-cutaneous malignancy and the second cause of cancer-related deaths among men in USA and Europe. An estimated 1.6 million men worldwide are diagnosed with PCa and 366,000 die of this disease each year (9). Incidence rates of prostate cancer are highly variable between countries. This has been partially attributed to the extent of screening as well as the putative risk factors including age, race and family history (9). While still unclear, other risk factors such as physical activity, diet, obesity, sexual factors and inflammation have all been associated with increased PCa (10). While the prevalence may have increased, the disease is typically indolent and most patients die “with” rather than “of” PCa (11).

### 1.2.2 Development of PCa

PCa is proposed to be initiated at the ages between 20-30 years (12). However, these tumors are only detected decades later when the PCa associated symptoms emerge in more advanced disease (13). The development of PCa is a multistep process **(Figure 1.7)** that is initiated from benign epithelial which proceeds into a premalignant lesion and eventually invasive prostate carcinoma. Hyperplastic lesions increase with age, but not all, particularly BPH, are a precursor for PCa (14). High-grade prostatic intraepithelial neoplasia (HGPIN) is defined as preinvasive state of ongoing cellular proliferations (15). HGPIN appears as a collection of atypical and irregular epithelial cells, forming a pseudo-multilayer appearance within the lining of prostatic ducts and acin. In this the basal cell layers are disrupted but still present (14). HGPINs are frequently observed in PZ. Since HGPIN is an established precursor, it is considered as an *in situ* carcinoma of prostate, which is a localized cancer. However, in contrast to a localized cancer, HGPINs can stay unchanged. Spontaneous regression can also be observed in some cases (16,17). Proliferative inflammatory atrophy (PIA) is proposed to be an even earlier precursor of PCa (18). However, the role of PIA in malignant transformation remains controversial. Some studies associate PIA with a lower risk PCa (19), while others suggest it is a precursor to HGPIN (20). Overall, while both HGPIN and PIA are potential precursors of PCa development, HGPIN is the most likely precursor due to its high resemblance in morphological structure and genetic properties (21,22).

### 1.2.3 PCa Diagnosis

Various symptoms such as pain in the lower back, hips and/or thighs, erectile dysfunction, blood in the semen, urinary problems or prostate enlargement are associated with PCa. However, all of these symptoms are also associated with BPH and other urinary system disorders. Therefore, accurate and effective diagnostic tests are essential to correctly diagnose PCa. Standard PCa tests include prostate-specific antigen (PSA) blood testing, digital rectal examination (DRE), transrectal ultrasound (TRUS), magnetic resonance imaging (MRI) and biopsy (23). Histopathology of the sampled biopsy remains the gold standard of PCa diagnosis. With each biopsy the cores are scored based on the Gleason system. As shown in **Figure 1.3**, evaluation criterion of the Gleason system is the loss of the normal tissue architecture (24). They are graded on a scale of 1 to 5 and a cumulative score is produced that incorporates a principal and major secondary score (e.g. 4+3). A clear understanding of the classification system is critical for accurate diagnosis.

Given the confusion around this scoring method, growth patterns of prostate adenocarcinomas, modifications in surgical approaches and biopsy protocols and increased serum PSA screening a new Gleason Grade grouping was incorporated into the 2016 edition of World Health Organization classification of prostate tumors (25). The new Gleason groups corresponding to the Gleason scores are depicted in **Figure 1.3**.

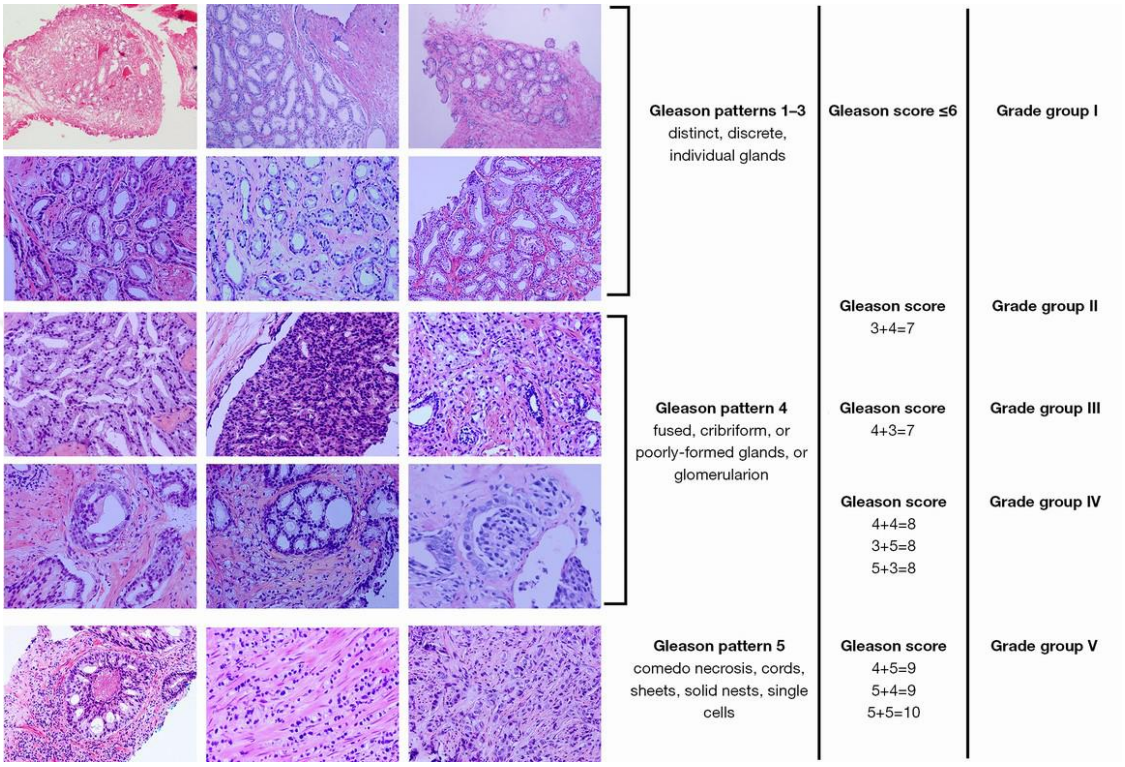


**Figure 1.3 Associated Gleason patterns, scores and Gleason Group system.** *Adopted from (24).*

TRUS guided prostate biopsies remain the gold-standard for PCa diagnosis (PB) (26). However, these biopsies, which samples a region in the prostate, are prone to systematic sampling errors (27,28). Anterior prostate, midline and extreme apex are particularly under sampled and it is believed that up to half of PCa cases the cancer is missed and the aggressiveness in one third is underestimated (29,30). The detection rate of 12-core systematic biopsy sampling for men with an elevated PSA going under an initial biopsy is 30-55% (31) with a false-negative rate of 20-24% (32). The sextant biopsy protocol improved detection rate by a factor of 1.3 compared to the laterally directed 12-core biopsies (33). Some experts suggest using a template for transperinal mapping biopsies to systematically sample all quadrants of the prostate (34). However, this approach has higher morbidity as each additional biopsy increase the infection rate (35).

To overcome the limitations of systematic biopsies, multiparametric MRI (mpMRI) has been developed over the last decade (35). In comparison to conventional imaging techniques, MRI provides the best imaging modality of the gland contours and the zone anatomy (36). An MRI sequence a set of radiofrequency pulses and gradients that produce images with a distinct appearance (37). Traditional MRI of the prostate composed of only T1 and T2 weighted imaging (T1W and T2W) and these two sequences could only be used for local staging of the known cancer (38). The addition of functional parameters to MRI provides increased predictive value (39). Usually, preferred functional assessment sequences that supplement T1W and T2W include dynamic contrast-enhanced (DCE) MRI and diffusion-weighted imaging (DWI) with apparent diffusion coefficient (ADC) maps (36). These different parameters allow significantly better resolution of the prostate. Images based on T1W are used to detect the hemorrhages within prostate and seminal vesicles. T2W can evaluate gland anatomy, detection of abnormalities in morphology together with extraprostatic extensions and seminal vesical invasion (40). DWI is used for differentiation of benign lesions from clinically significant prostate cancer and aggressiveness prediction. The differences in the appearance of lesions due to their free water content observed with DWI is depicted on ADC maps (36). Finally, DCE is used to assess lesion vascularity, therefore aiding in differentiation of high grade tumors and low grade lesions **(Figure 1.4)** (41). Indeed, with these three one can achieve a 98% positive predictive value for cancer detection, which is significantly better than T2W imaging alone (68%) (42). mpMRI can therefore increase the detection of clinically significant PCa while reducing over-identification of low-risk ones (43). However, regardless of the imaging modality, a biopsy is still required to confirm the PCa diagnosis.

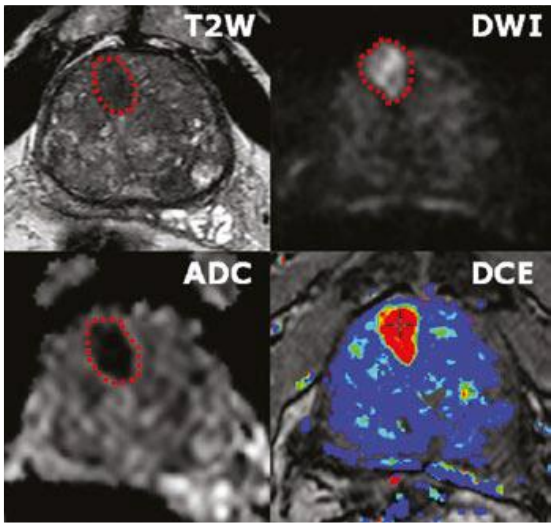


**Figure 1.4 mpMRI images includes several functional parameters.** *Adopted from* (44). *Suspicious areas in prostate (red dashed line) are identified by anatomical and functional characteristics, T2W, fusion weighted and DCE imaging. Combined these approaches are called mpMRI.*

### 1.2.4 MRI-guided biopsies

The introduction of mpMRI guided biopsies has significantly improved the PCa detection rate while reducing morbidity. An MRI-guided biopsy will determine the location of a suspicious area in the prostate with mpMRI before or during biopsy (45). Cognitive/visual methods or software dependent techniques are employed to join the two approaches and collects fewer cores compared to standard biopsies (46). Overall this approach combines the superior imaging characteristics of mpMRI with the accuracy of TRUS biopsy (35).

The standards for acquiring images and reporting, as well as the precise parameters for significant disease prediction are described by Prostate Imaging-Reporting and DATA System (PI-RADS) with a 1-5 scale based on the features of T2WI, DWI and DCE (47). Scores assigned to each sequence reflects the degree of abnormality and probability of clinically significant prostate cancer (44) **(Table 1.1).** There are multiple approaches for MRI-guided biopsies including a visual estimation TRUS- guided biopsy or cognitive fusion biopsy, MRI-TRUS fusion biopsy and direct in-bore biopsy (44,48).

**Table 1.1 PI-RADS Scoring Criteria** *Adopted from (49)*.

| Score | Criteria |
|---|---|
| | ***T2W for the peripheral zone (PZ)*** |
| 1 | Uniform signal intensity (SI) |
| 2 | Linear, wedge shaped, or geographic areas of lower SI, usually not well demarcated |
| 3 | Intermediate appearances not in categories 1/2 or 4/5 |
| 4 | Discrete, homogeneous low signal focus/mass confined to the prostate |
| 5 | Discrete, homogeneous low signal intensity focus with extra-capsular extension/invasive behaviour or mass effect on the capsule (bulging), or broad (>1.5 cm) contact with the surface |
| | ***T2WI for the transition zone (TZ)*** |
| 1 | Heterogeneous TZ adenoma with well-defined margins: "organised chaos" |
| 2 | Areas of more homogeneous low SI, however well marginated, originating from the TZ/BPH |
| 3 | Intermediate appearances not in categories 1/2 or 4/5 |
| 4 | Areas of more homogeneous low SI, ill defined: "erased charcoal sign" |
| 5 | Same as 4, but involving the anterior fibromuscular stroma or the anterior horn of the PZ, usually lenticular or water-drop shaped. |
| | ***Diffusion weighted imaging (DWI)*** |
| 1 | No reduction in ADC compared with normal glandular tissue. No increase in SI on any high b-value image (≥b800) |
| 2 | Diffuse, hyper SI on ≥b800 image with low ADC; no focal features, however, linear, triangular or geographical features are allowed |
| 3 | Intermediate appearances not in categories 1/2 or 4/5 |
| 4 | Focal area(s) of reduced ADC but iso-intense SI on high b-value images (≥b800) |
| 5 | Focal area/mass of hyper SI on the high b-value images (≥b800) with reduced ADC |
| | ***Dynamic contrast enhanced (DCE)-MRI*** |
| 1 | Type 1 enhancement curve |
| 2 | Type 2 enhancement curve |
| 3 | Type 3 enhancement curve |
| +1 | For focal enhancing lesion with curve type 2–3 |
| +1 | For asymmetric lesion or lesion at an unusual place with curve type 2–3 |

*Cognitive-fusion biopsy:*

Also referred as cognitive registration this approach identifies the suspicious lesion with mpMRI before biopsy sampling. Having identified the lesion, it is then targeted with TRUS by the biopsy operator. The location of the suspicious area can be saved within the mpMRI file either as snapshots or hand drawings. After acquisition, the images are reviewed immediately before biopsy. The operator therefore must transfer visual information between different formats. Yet despite these technical challenges, the accuracy and detection rate of MRI-targeted biopsies with visual registration are still higher than systematic biopsies (50,51).

*MRI-TRUS fusion biopsy:*

In MRI-TRUS, suspicious areas are identified with mpMRI prior to biopsy and then contoured together with the whole prostate. The fusion software platform then uploads these images in a 2D or 3D model. During the procedure, real time ultrasound images are matched or fused (registered) with these models and suspicious areas are identified and targeted (52). Two types of registration are used, rigid and elastic. In rigid registration, mpMRI images are directly superimposed over ultrasound images. The elastic registration accounts for the shape difference of the prostate between MRI and TRUS scan as the ultrasound probe can deform the gland. Swelling and motion can also be considered by some software during the procedure. As with visual registration, MRI/TRUS biopsies are superior compared to systematic biopsies, specifically for higher-grade disease (53,54).

*In-bore MRI biopsy*:

This approach takes serial scans during the procedure with a mpMRI scanner to guide biopsy collection. Suspicious areas are identified with the aid of diagnostic quality images and are registered together with interventional images (55). In-bore biopsy technique have three different approaches including transperineal, transgluteal and the most commonly, transrectal. The registration of two different sets of mpMRI images, obtained in similar positions, is one of the main advantages of this technique. Multiple registrations allow the correct alignment of the images for further analysis, such as aiding in possible motion corrections. To reduce over-diagnosis and morbidity, only 1-2 suspicious areas are generally targeted with 2 cores sampled per target. However, depending on the number of targets, an 8 additional cores can be sampled (56). In the cases where prebiopsy mpMRI

identifies more than 2 suspicious areas, it is recommended to perform biopsies on the 2 most suspicious areas (56). The tumour detection rates of in-bore biopsies to range from 8% to 59% (median of 42%) and of those radiographically suspicious lesions almost all are clinically significant (81-93%) (57). Furthermore, Kilic et al. showed that the detection rate of clinically significant cancer in suspicious regions can differ depending on the PIRADS score of the lesions. They reported a detection rate of 63% for PI-RADS 4 and 89% for PI-RADS 5 lesions (58). However, while markedly better than TRUS biopsies, this approach requires intense training both for the radiologist and the biopsy operator.

While there is no consensus which of these three biopsy approaches is superior to the others, all MRI guided biopsy methods listed here address the flaws of TRUS biopsies such as under or over sampling, poor risk stratification and false negative rates (59). Yet while increased use of mpMRI has improved the accuracy of routine biopsies (60) there is still a 7-17% false positive rate (57). It is unclear if these false positive MRI-guided biopsies contain anatomical, genetic or epigenetic premalignant alterations.

## 1.3 Epigenetics

The epigenome is a cell-specific profile comprised of DNA methylation, histone modifications, nucleosome remodeling and RNA-associated silencing. Collectively, these result in heritable changes to gene expression that, unlike genetic alterations, do not alter the DNA sequence. Importantly, both genetic and epigenetic alterations can act as drivers in cancer. Altering the chromatin accessibility or activity of gene promoters can silence tumor suppressor genes or reactivate oncogenes.

### 1.3.1 DNA methylation

One of the common modifications of eukaryotic DNA is methylation of cytosine residues at cytosine-guanine (CpG) dinucleotides (61). In humans, 70 to 90% of CpGs are methylated (62). Importantly, the distribution of CpG dinucleotides is not random. Retrotransposons, protein coding regions and transposons contain the majority of the CpG dinucleotides present in the human genome (61). Further, around 1% of the human genome have short, dense areas of CpG dinucleotides that are approximately 200-2000 bp named CpG islands (61,63–65). These CpG islands primarily occur in the 5´ regions of genes including promoters and untranslated regions. They are also found in the first exon of approximately half of all the human genes (66). Excluding imprinted genes and

the inactive X chromosome, promoter-CpG islands are generally not methylated (67). However, when methylated these promoter-CpG islands cause gene silencing by blocking the binding of transcription factors and transcriptional machinery. This occurs through the recruitment of methyl-CpG-binding domain proteins (MBDs), histone deacetylases (HDACs) and chromatin remodeling factors that when bound to hypermethylated promoters, induce chromatin condensation and make the promoters inaccessible to the transcriptional machinery **(Figure 1.5)** (68–70). DNA methylation correlates with specific histone modifications, genomic locations and nucleosome positioning (67). The transcriptionally inactive heterochromatin is comprised of methylated DNA that is tightly bound around the histone octamers methylated at lysine 9 or 27 of histone 3 (H3K9, H3K27), and lysine 20 of histone 4 (H4K20) (67). Studies by Chodavarapu *et al.* demonstrated that nucleosomal DNA is more highly methylated than unbound flanking DNA and that this nucleosome-bound DNA is itself preferentially targeted by methyltransferases (71). Consistent with DNA methylation targeting to nucleosomes, intron-exon and exon-exon boundaries are both enriched for nucleosomes and DNA methylation. Collectively, the methylation status of DNA is affected by the positioning of the nucleosome (71).

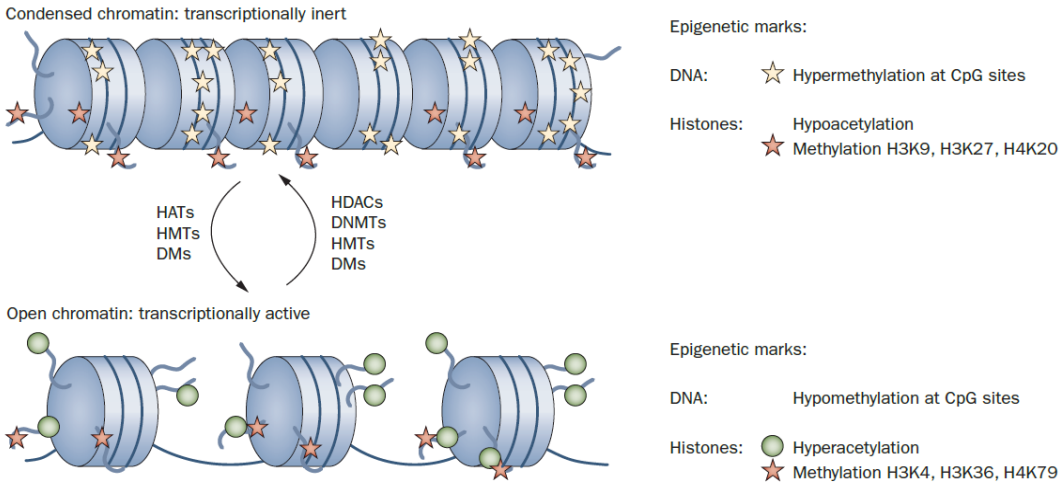


**Figure 1.5. Epigenetic marks that correlate with different methylation status.** *Adopted from* (67).

The balance between DNA hypermethylation and hypomethylation is altered in cancer and can act as a driver of neoplastic carcinogenesis. This can occur through several mechanisms including promoter hypermethylation of tumour suppressors or hypomethylation of proto-oncogenes **(Figure 1.6)** (72). Genome-wide hypomethylation

can also activate proviral sequences and retrotransposons that can disrupt nearby genes and causes loss of imprinting (65). This is not a binary event and the type of DNA methylation including density or the spread the methylation, level (ratio of methylated and unmethylated DNA copy number) and frequency (percentage of a methylated tumors at a given locus) all affect gene silencing (67).

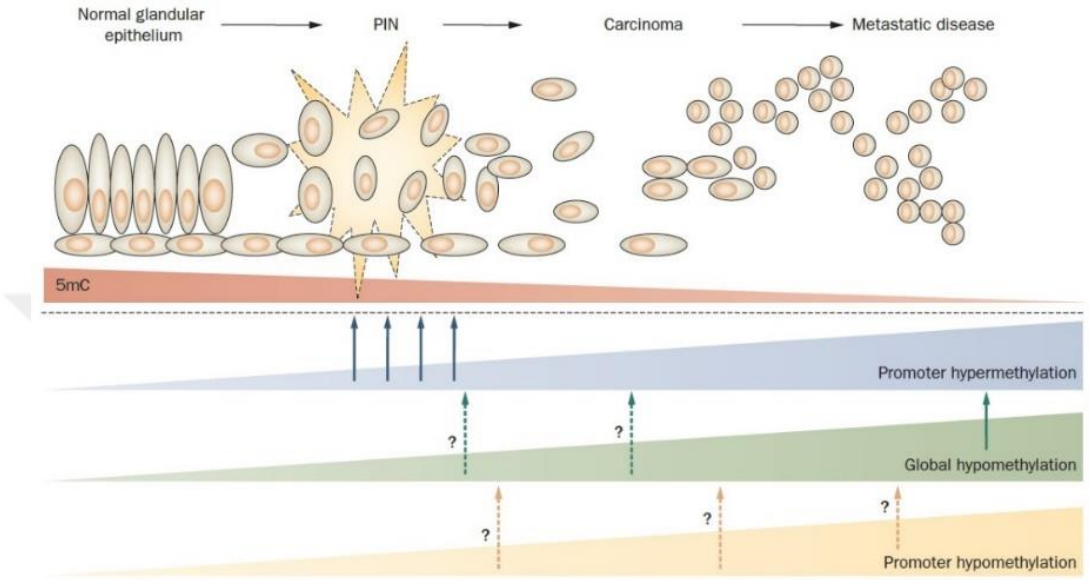


**Figure 1.6. Different methylation events throughout the transformation from normal cells to metastatic state.** *Adopted from* (67).

### 1.3.2 Epigenetic modifications in prostate cancer

#### 1.3.2.1 DNA methylation in prostate cancer

CpG islands are commonly methylated in PCa and cause gene silencing by promoter inactivation (73). Common hypermethylation events occur at different stages of tumor progression including premalignant lesions and strongly correlates with clinical stage or pathological grade of PCa **(Figure 1.7)**. The hypermethylation of the genes that are commonly associated with PCa development and growth is shown in (74). These genes are involved in DNA damage repair, hormonal response, cell cycle control and tumor invasion and metastasis pathways (75).

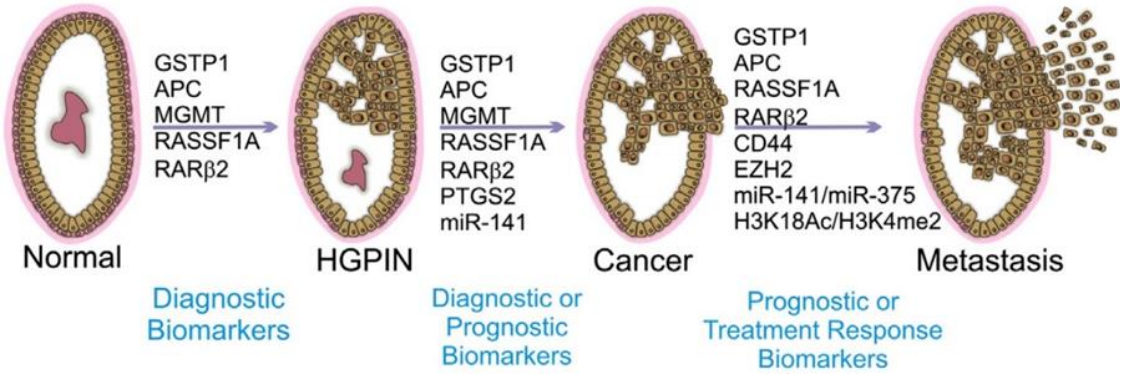


**Figure 1.7. Epigenetic alterations accompanying PCa initiation, progression and metastasis.** *Adopted from* (76).

**Table 1.2. Genes frequently hypermethylated in PCa.** *Adapted from* (74).

| Gene | Hypermethylation |
|---|---|
| APC, COX2, GSTP1, HIC1, MDR1, RARβ2, RASSF1A | 70-95% |
| 14-3-3 σ, CD44, CDH1, CSH13, CDKN1C, ESR2, ETNRB, MGMT, RUNX3, SFRP1, THBS1, TMS1 | 20-70% |
| AR,CDKN2A, CDKN1B, DAPK, ESR1, NKX3.1 | >20% |

### 1.3.2.2 DNA damage repair

In PCa, DNA repair enzymes that maintain genomic stability during replication and repair of damage are commonly inactivated by loss-of-function mutations (77). The expression of these DNA repair genes can also be downregulated by hypermethylation. Specifically, DNA alkyl-repair gene $O^6$-methylguanine DNA methyltransferase (MGMT) and glutation S-transferase (GSTP1) has been reported to be frequently hypermethylated in PCa (75).

*Glutathione S-transferase P1 (GSTP1)*: The GST family (α, μ, π, σ, Θ) of enzymes protect DNA from damage by detoxifying and eliminating potential genotoxic agents (78). GSTP1, a product of π gene, prevents oxidant and electrophilic DNA damage (75). Suppressing the activity of GSTP1 renders the cells more prone to DNA damage and subsequently increases the probability of somatic driver mutations in cancer (79,80). In 1994, the first report of GSTP1 hypermethylation in PCa was demonstrated (77). This epigenetic modification is found in 90% of cancerous samples and 70% in PIN (81,82).

In contrast, methylation is rarely detected in normal prostate tissues and BPH (82). These findings suggest that the cancer gain a selective growth advantage due to accumulation of genetic defects induced by methylated GSTP1. However, the exact mechanisms of how GSTP1 is methylated and inactivated during the neoplastic transformation from PIA to PIN remains unknown. GSTP1 methylation could also be detected at a high frequency in various samples such as urine, blood and ejaculate from PCa patients while low levels or no methylation is observed in healthy controls (83–85) . This difference in frequencies between tumor and normal samples make GSTP1 an ideal candidate biomarker for PCa (86).

#### 1.3.2.3 Hormonal response

The prostate is an endocrine gland that responds to signaling molecules including growth factors and hormones. Given this critical role, cancer initiation and advancement is associated with dysregulation of signaling pathways involved in growth control and homeostasis (75). Several different genes including androgen receptor, estrogen receptor and retinoic acid receptor are critical in mediating this control.

*Retinoic acid receptor β (RARβ):* Retinoic acid receptor (RAR) is a nuclear receptor that is activated by retinoic acid (RA) and 9-cis retinoic acid (87). There are three differentially expressed RAR receptors (α, β, γ) shown to play key roles in epithelial cell growth and tumorigenesis (88). Two different promoters exist for RARβ gene that in combination with alternative splicing leads to several different isoforms. Of these, RARβ2 is the biologically active isoform and is regulated by P2 promoter (89). The P2 promoter has a high affinity retinoic acid response element (RARE), associated with RA-induced transcriptional activation of RARβ2 (90). Downregulation of *RARβ2* expression via DNA methylation has been observed in numerous malignant cell lines. Promoter hypermethylation of *RARβ* leads to cell cycle dysregulation and carcinogenesis (91). Loss of RARβ is observed in many epithelial cancers including PCa (92,93). This can occur by aberrant promoter methylation in bladder, breast, cervical and PCa (94–96). Hypermethylation of RARβ2 is observed in 79% of primary prostate and 90% of hormone refractory PCa, while no hypermethylation is observed in BPH or normal prostate samples. Furthermore, 20% of PIN samples show RARβ2 promoter methylation suggesting that this occurs early in PCa etiology and is associated with cancer initiation. (96–98).

#### 1.3.2.4 Tumor cell invasion and metastasis

Cell adhesion molecules (CAMs) are responsible for regulation of cell-cell/cell-substrate adhesions and play a critical role in maintaining normal tissue structure. Cadherins and cathenins are the major elements of this cell adhesion system. Tumor infiltration and metastasis is believed to be caused by the dysregulation of this system (99). In PCa, CD44 and APC are the most common CAMs that are impaired due to promoter hypermethylation and are associated with cancer stage and prognosis (98).

*Adenomatous polyposis coli (APC):* APC inactivation caused by promoter methylation and mutation plays roles in cell-cell adhesion and Wnt signaling pathway (100,101). Canonical Wnt signaling pathway is associated with normal cell growth and differentiation. Wnt antagonists, including APC, regulate cell proliferation and differentiation. Wnt proteins bind to transmembrane receptors, transducing a signal to the cytoplasmic protein Dishevelled (Dvl) (102). Dvl is a cytoplasmic protein recruited to the membrane where it dephosphorylates the protein Axin that maintains the integrity of a complex including APC and β-catenin (103). It also induces the phosphorylation of APC and β-catenin by glycogen synthase kinase 3β (GSK3β). Phosphorylation, ubiquitination and the following proteolytic degredation of β-catenin occurs in APC/axin/GSK3β complex (104). The role of APC in Wnt signaling is to negatively regulate this complex and prevent the binding of β-catenin to the transcription factors that activate genes including c-MYC (105) and Cyclin D1 (106,107), which drives progression through G1 phase of the cell cycle (108). Loss of APC constitutively activates the pathway by stabilizing β-catenin thereby even without the presence of Wnt proteins (104). In pancreatic, liver, colon, esophageal, stomach and PCa promoter methylation of APC is commonly observed (109). Hypermethylated APC renders the cell vulnerable to both epigenetic and genetic changes (110). The APC promoter is hypermethylated in 27-90% of PCa samples while it is observed only 5-6% in non-cancerous tissues (111–113). PIN samples show 36% promoter methylation, suggesting the it can be detected at early onset PCa (98,113).

### 1.3.3 Potential of DNA methylation in clinical diagnosis

Aberrant DNA methylation can serve as a diagnostic marker for PCa (74,114). However, in clinical samples, the amount of tumor tissue is typically very limited or highly diluted

with normal DNA. Therefore, a clinical methylation assays must be sensitive, specific, easy to analyze and compatible with limited clinical material (115).

### 1.3.4 Detection of DNA methylation from clinical samples

There are numerous DNA methylation assays. **Table 1.2** and **Table 1.3** show commonly used assays, however, it should be noted that current available methods are not limited to those listed here (116). While all methods quantify DNA methylation, they can vary from a few specific loci (typing technique) to a whole-genome methylation pattern (profiling technique) (117). Given this diversity, choosing the right method for DNA methylation analysis is challenging. This is influenced by both the available samples and the specific goal of the study.

**Table 1.3. Overview of methods for DNA methylation analysis.** *Adopted from* (118).

| | Analytical readout | | | | |
|---|---|---|---|---|---|
| | Column-based | PCR-based | Gel-based | Array-based | HTS-based |
| Enzymatic digestion | RL-HPLC | HpaII-PCR | RLGS-M | HELP | HELP-seq |
| Affinity enrichment | NA | MeDIP-PCR | NA | MeDIP-chip | MeDIP-seq |
| Bisulfite converstion | NA | qMSP/MethyLight | Bisulfite sequencing | Golden Gate methylation assay | RRBS |
| | | | MSP | Infinium methylation assay | WGSBS |

*RP-HPLC: Reversed-phase high-performance liquid chromatography; HELP: HpaII tiny fragment enrichment by ligation-mediated PCR; MeDIP: methylated DNA immunoprecipitation; MSP: methylation-specific PCR; HTS: high-throughput sequencing; RLGS-M: restriction landmark genome scanning for methylation; RRBS: reduced representation bisulfite sequencing; WGSBS: whole-genome shotgun bisulfite sequencing.*

DNA methylation can be analyzed in either a quantitative or qualitative assay (75). The choice of the method used for methylation analysis depends on the type of information needed. Initial techniques were more focused on gaining information about overall methylation levels while more recent scientific work will characterize methylation status of specific DNA sequences or even genomes (119–121). Qualitative methylation assays provide binary results about the presence or absence of methylation rather than the specific location of a methylcytosine or different levels of methylation (122). These types of detections are advantageous in terms of their simplicity and short time of analysis. Furthermore, the ability of differentiating the methylation status of normal and tumor

tissue samples has made these approaches of great interest for cancer research (123). On the other hand, quantitative methylation measurements use explicit sequence context and provide results from individual or multiple CpG sites with single base resolution. Since each methylation analysis technique has its own strengths and limitations, nowadays it is also preferred using a combination of strategies for methylation status (123).

The earliest DNA methylation assays such as HPLC, radiolabeling S-adenosylmethionine or using antibodies against methylcytosine could detect, but not locate, the site of methylation (124). Methods were then developed that could identify specific methylation sites, but were limited to those genomic regions with methylation-specific restriction enzyme sites with *HpaII and MspI* (125). The discovery of bisulfite conversion reaction combined with Sanger sequencing finally allowed single-base resolution detection of methylation status to be achieved. Bisulfite conversion can effectively differentiate between methylated and unmethylated cytosines. The bisulfite reaction causes deamination of unmethylated cytosines to uracil and upon subsequent PCR reactions are amplified as thymine. In contrast methylated cytosines (5-methylcytosines) are shielded from deamination and remain intact as cytosines (**Figure 1.8**) (126).

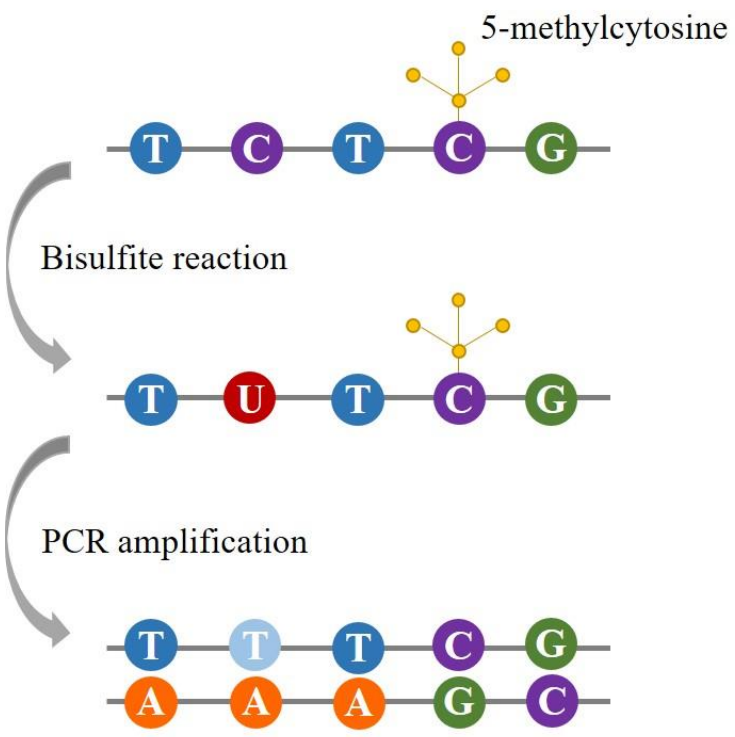


**Figure 1.8 Principle behind bisulfite conversion reaction.** *Adapted from* (127).

The introduction of DNA microarrays and then next-generation sequencing (NGS) made it possible to analyze the entire methylomes of bisulfite converted samples (128). While suitable for large-scale discovery these NGS-based assays are not amenable to large clinical samples due to the low-throughput. The most common method for clinical studies is quantitative real-time methylation specific PCR (QMSP), also known as MethyLight (129). This sensitive, high-throughput method can quantify of DNA methylation with good accuracy and very low DNA input **(Figure 1.10).** Further, methylation can be quantified with QMSP from paraffin-embedded tissues, bodily fluids such as blood and urine and others clinical material (**Figure 1.9).** QMSP quantifies the proportion of methylated targets following bisulphite conversion of genomic DNA using PCR primers specific to the converted unmethylated cytosine. With this, the proportion of methylated regions are then normalization to a standard reference region that is not methylated. One of the strengths of QMSP is the ability to detect methylation with a 10,000-fold excess of unmethylated DNA (129). Overall, QMSP is a sensitive and reliable approach to quantify methylation at known genomic regions from a large number of clinical samples.

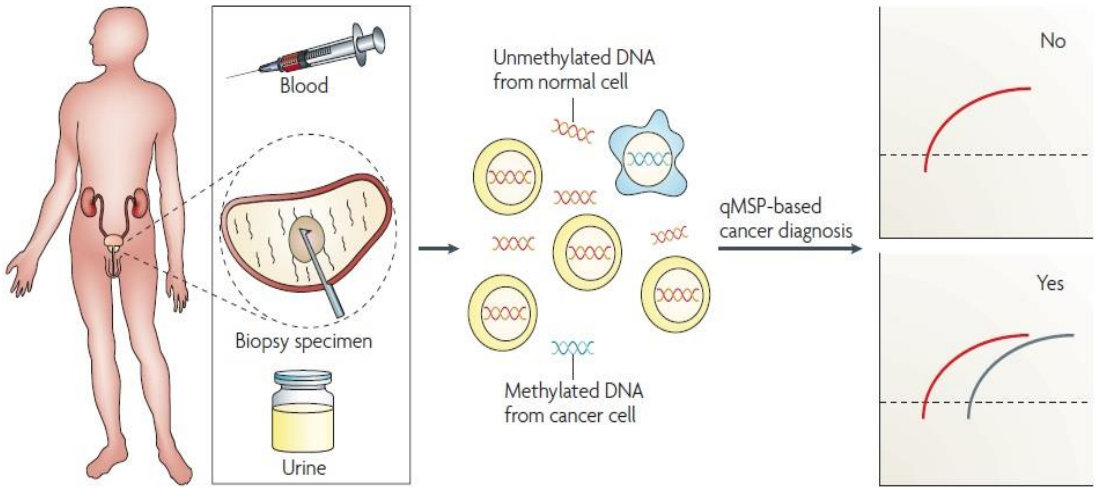


**Figure 1.9. QMSP method can use various clinical samples as templates.** *Adopted from* (130) .

QMSP reactions can be carried out with several different probe and primer approaches. The most commonly used are either Molecular Beacons (3-5) and Taqman probes (6,7). However, scorpion primers that combine both the primer and probe have also been successfully used in QMSP reactions **(Figure 1.10)**. These contain a probe sequence that is held together in a hairpin-loop structure that brings the fluorophore on the 5' end in close proximity to the quencher at the 3' end thereby preventing fluorescence (131).

However, following PCR amplification, the probe sequence can bind to its complementary sequence causing the hairpin loop to open and separate the fluorophore and quencher. The introduction of a PCR stopper stops the detection of non-specific products such as primer dimers or mispriming events by preventing read-through (131,132).

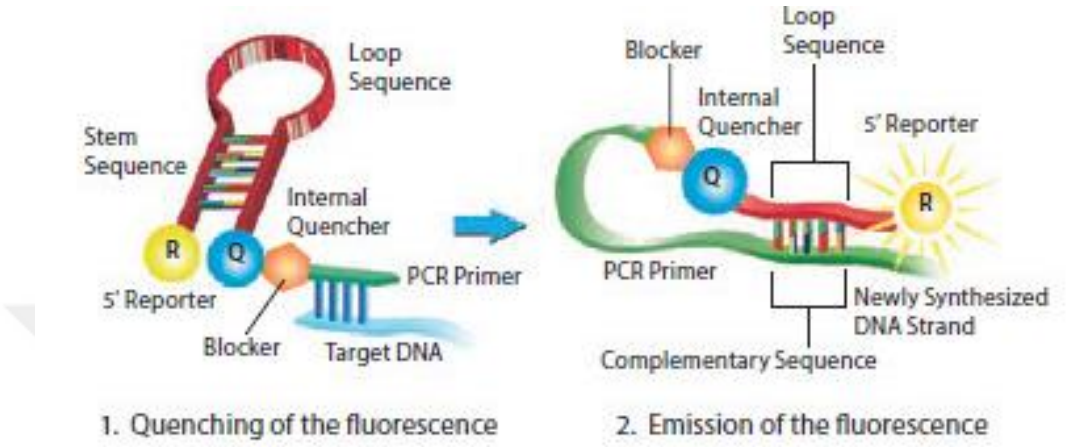


**Figure 1.10. Mode of action of Scorpion primers in QMSP reactions.** *Adopted from* (132).

### 1.3.4.1 Tissue based biomarker assays

Tissue based biomarkers assays are very useful for the representation of tumor environment. While considerable improvements were made with liquid biomarker assays, tissue based assays became standard care for PCa patients undergoing biopsy or radical prostatectomy. Molecular Diagnostic Services Program recommends tissue based assays, including Confirm MDx, Oncotype Dx GPS, Prolaris and and Decipher. These assays were also included in NCCN guidelines (Clinical Practice Guidelines in Oncology) (133).

Specifically, Confirm MDx is recommended as a patient management strategy with a history of negative biopsy and potentially would undergo repeat diagnostic biopsy (134–136).The assumption is that normal tissues in the vicinity of a tumor might have an altered epigenetic, genetic or protein expression profile. Therefore, following these epigenetic changes can be used to decrease false negative biopsy outcome (137). For that purpose, the methylation status of the three tumor suppressor genes, APC, GSTP1 and RASSF1, are observed with multiplex QMSP reactions to determine DNA methylation status (133).

## 1.4 Aim of the study

We propose that false positive MRI-guided biopsies contain epigenetic pre-malignant alterations. Therefore, the aim of this study is to characterize the epigenetic alterations of radiographically suspicious yet histopathologically benign prostate needle biopsies collected with mpMRI guidance. With this aim, we will quantify the promoter DNA methylation of several genes including APC, GSTP1 and RARβ2 that specifically mark premalignant stages of PCa. Specifically, we will optimize a QMSP assay that is compatible with FFPE fixed mpMRI in bore biopsy samples. Overall, this thesis will explore the potential use of DNA methylation markers for early detection, disease prediction and the correlation to clinical outcomes.

# 2. MATERIALS AND METHODS

## 2.1 Materials

### 2.1.1 Chemicals and reagents

All chemicals used in this thesis work is purchased from Sigma-Aldrich or Merck unless otherwise stated. Antibiotics were purchased from Goldbio Biotechnology. Bacterial growth media is purchased from Becton Dickinson (BD). Molecular biology reagents were purchased from Thermo Fisher Scientific, Sigma-Aldrich, New England Biolabs, Macherey-Nagel and Zymo Research. Cell culture reagents were purchased from Gibco, Lonza and Invitrogen.

### 2.1.2 Plasmids

#### 2.1.2.1 Plasmids generated for standard curves

Plasmids containing pCR4 vector **(Figure 2.1)** and the promoter region of either *ACTB* **(Figure 2.2),** *APC* **(Figure 2.3),** *GSTP1* **(Figure 2.3)** and *RARβ2* **(Figure 2.4)** was generated with TOPO® TA cloning kit of Invitrogen (Carlsbad, California, United States), according to the manufacturer's protocol with a modification in the incubation time.

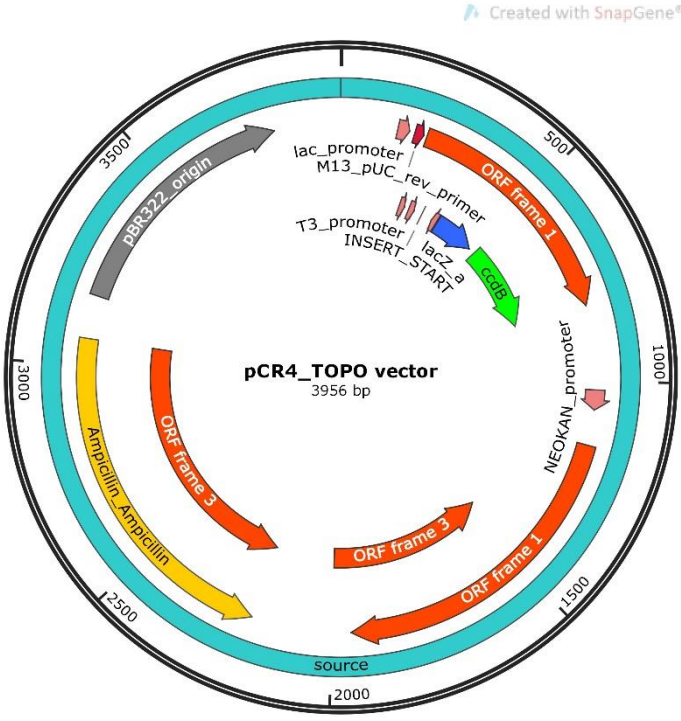


**Figure 2.1. pCRTM4-TOPO® vector for cloning.**

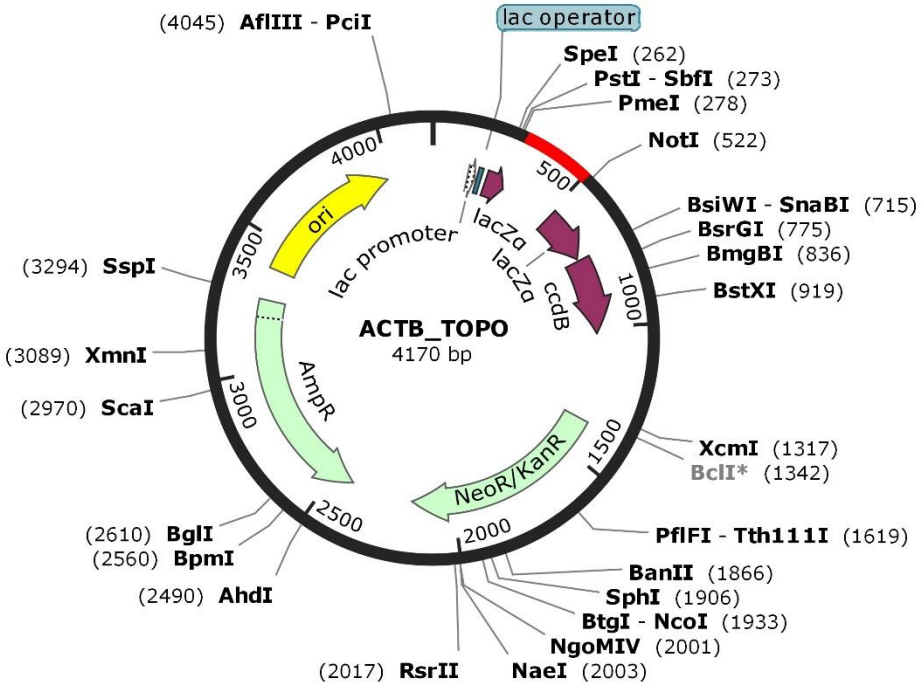


**Figure 2.2 ACTB TOPO plasmid.**

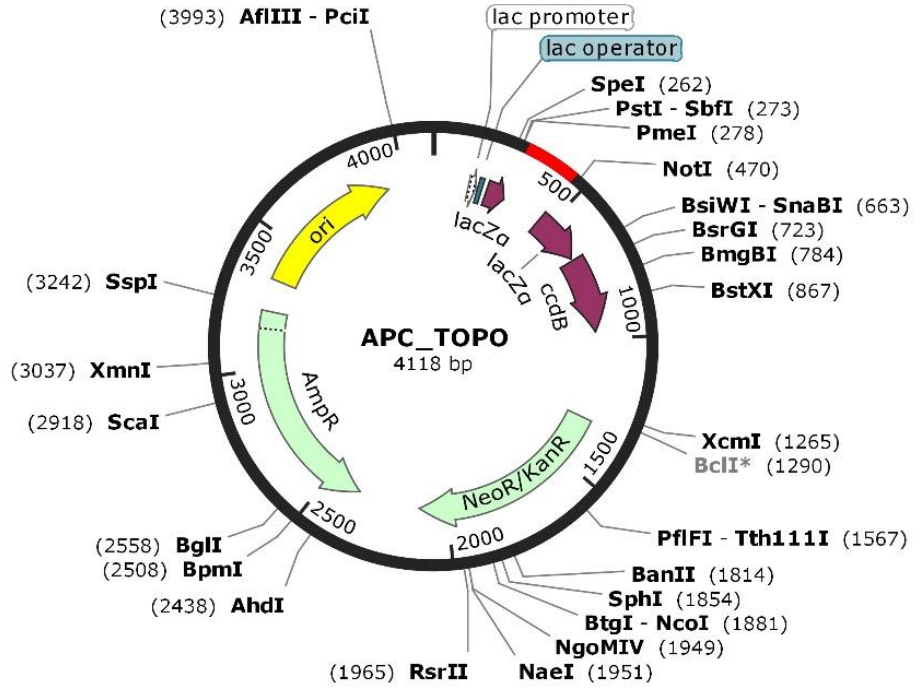


**Figure 2.3 APC TOPO plasmid.**

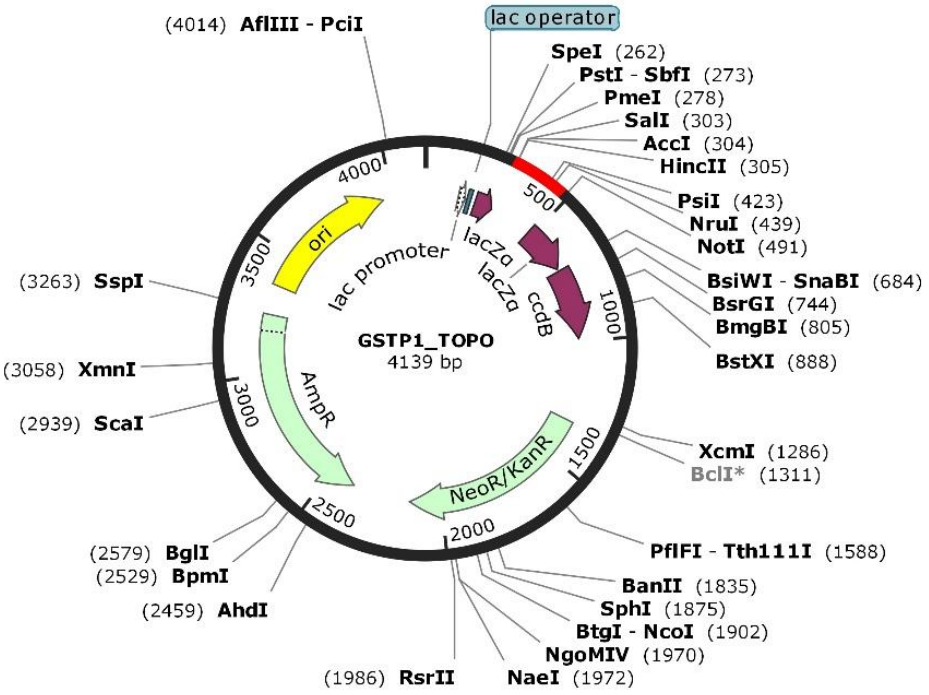


**Figure 2.4 Cloned GSTP1 TOPO plasmid.**

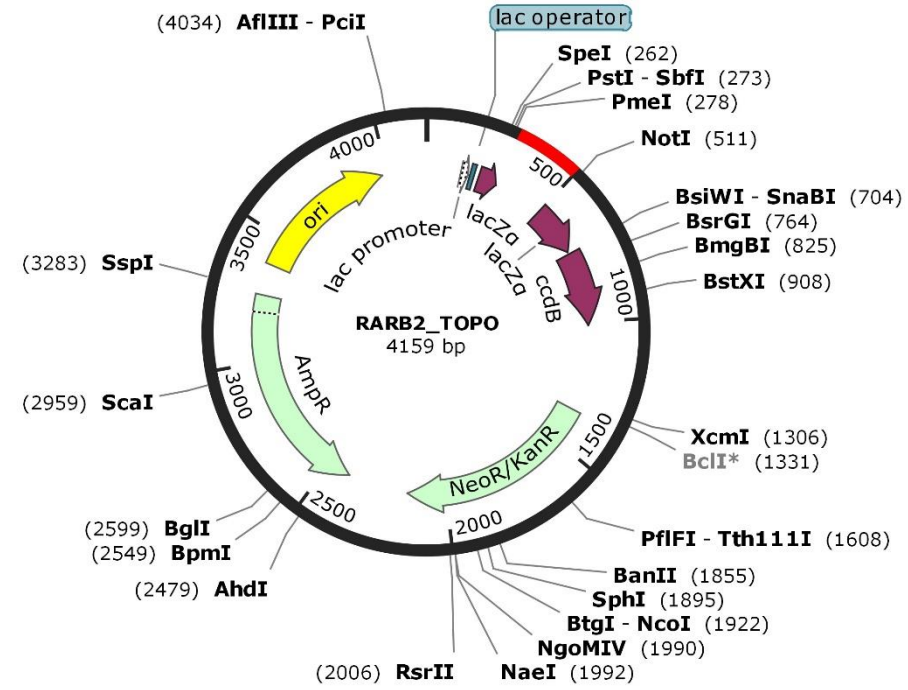


**Figure 2.5 Cloned RARB2 TOPO plasmid.**

### 2.1.3 Bacterial strains

*E.coli* strain STBL3, with genotype $F^{-}$mcrB mrr hsdS20 ($rB^{-}$, $mB^{-}$) recA13 supE44 ara14 galK2 lacY1 proA2 rpsL20 ($Str^{R}$) xyl5 $\lambda^{-}$leu mtl1 is used for the propagation and cloning of bacterial plasmids.

### 2.1.4 Bacterial growth media

Liquid and solid bacterial growth media was prepared from LB broth and LB agar powder. Indicated amount by the manufacturer was dissolved in distilled water, autoclave sterilized in 121ºC for 30mins. **Table 2.1** shows the content of LB Broth and LB Agar. SOC outgrowth medium was used to dilute outgrowth prior to plating.

**Table 2.1 Media used for bacterial growth.**

| Media | Components |
|---|---|
| **244620-BD Difco™ LB Broth, Miller (Luria-Bertani)** | 10.0 g Tryptone, 5.0 g Yeast Extract, 10.0g Sodium Chloride in 25g/L medium |
| **244520-BD Difco™ LB Agar, Miller (Luria-Bertani)** | 10.0 g Tryptone, 5.0 g Yeast Extract, 10.0g Sodium Chloride, 15.0 g Agar in 40g/L medium |
| **#NEB B9035 SOC Outgrowth Medium** | 2% Vegetable Peptone, 0.5% Yeast Extract, 10mM NaCl, 2.5mM KCl 10mM $MgCl_2$, 10mM $MgSO_4$, 20mM Glucose |

### 2.1.5 Antibiotics

Carbenicillin (100µg/ml) was used for cloning and propagation of the bacterial plasmids.

### 2.1.6 Primers

**Table 2.2 - Table 2.5** show the primers used for amplification of promoter regions of the genes, sequencing, qMSP and qPCR.

**Table 2.2 Primers used for amplification of promoters from bisulfite converted genomic DNA.**

| Gene | Name | Sequence (5'-3') | Abbreviation |
|---|---|---|---|
| ACTB | ACTB_outer_F | GATATAAGGTTAGGGATAGGATAG | βO_F |
| | ACTB_outer_R | AACCAATAAAACCTACTCCTCC | βO_R |
| APC | APC_outer_F | CCTATACCCCACTACGAAATACGA | AO_F |
| | APC_outer_R | GGCGGGTTGTATTAATATAGTTATA | AO_R |
| GSTP1 | GSTP1_outer_F | TTTTTGCGGTCGACGTTCG | GO_F |
| | GSTP1_outer_R | ACGAAAACTACGACGACGAAA | GO_R |
| RARβ2 | RARB2_outer_F | GGGGATTAGAATTTTTTTATGCG | RO_F |
| | RARB2_outer_R | TCCAAACTTACTCGACCAATCCAAC | RO_R |

**Table 2.3. Primers used for sequencing confirmation of cloned plasmids.**

| Name | Sequence (5'-3') |
|---|---|
| M13_rev | CAGGAAACAGCTATGAC |

**Table 2.4. Primers and probes used for qMSP experiments.**

| Gene | Oligo Type | Sequence (5'-3') | Abbrv. |
|---|---|---|---|
| ACTB | Scorpion probe_1 | [6FAM]CCGGGGCCTCCATCACCACCCCGG[BHQ1dt][HEG]TATAGGTTGGGGAAGTTTGTTTTTG | β_Sc1 |
| | Scorpion probe_2 | [6FAM]CCGCGCATCACCACCCCACACGCGCGG[BHQ1dt][HEG]GGAGTATATAGGTTGGGGAAGTTTG | β_Sc2 |
| | Forward primer of β_Sc1 | TATAGGTTGGGGAAGTTTGTTTTTG | β_F1 |
| | Forward primer of β_Sc2 | GGAGTATATAGGTTGGGGAAGTTTG | β_F2 |
| | Reverse primer | AACACACAATAACAAACACAAATTCAC | β_R1 |

| | | | |
|---|---|---|---|
| APC | Scorpion probe | [6FAM]GCCGGCGGGTTTTCGACGGGCCGGC[BHQ1dt][HEG]CGAACCAAAACGCTCCCCA | A_Sc1 |
| | Reverse primer | GTCGGTTACGTGCGTTTATATTTAG | A_R1 |
| GSTP1 | Scorpion probe_1 | [6FAM]CCGGGCGAACTCCCGCCGAGCCCGG[BHQ1dt][HEG]TCGGGGTGTAGCGGTCGTCG | G_Sc1 |
| | Scorpion probe_2 | [6FAM]CGCACGGCGAACTCCCGCCGACGTGCG[BHQ1dt][HEG]TGTAGCGGTCGTCGGGGTTG | G_Sc2 |
| | Forward primer of G_Sc1 | TCGGGGTGTAGCGGTCGTCG | G_F1 |
| | Forward primer of G_Sc2 | TGTAGCGGTCGTCGGGGTTG | G_F2 |
| | Reverse primer | CGCCCCAATACTAAATCACG | G_R1 |
| | Reverse primer | GCCCCAATACTAAATCACGACG | G_R2 |
| | Reverse outer primer | ACGAAAACTACGACGACGAAA | GO_R |
| RARβ2 | Scorpion probe_1 | [6FAM]CGCGGGCTACCCCGACGATACCCGCG[BHQ1dt][HEG]GGGATGTCGAGAACGCGAGCGA | R_Sc1 |
| | Scorpion probe_2 | [6FAM]CGGCGCCCGACGATACCCAAAGCGCCG[BHQ1dt][HEG]AACGCGAGCGATTCGAGTAG | R_Sc2 |
| | Forward primer of RR_Sc1 | GGGATGTCGAGAACGCGAGCGA | R_F1 |

| | | | |
|---|---|---|---|
| | Forward primer of RR_Sc2 | AACGCGAGCGATTCGAGTAG | R_F2 |
| | Reverse primer | CTTACAAAAAACCTTCCGAATACG | R_R2 |

**Table 2.5. Primers used for qPCR experiments.**

| Gene | Name | Sequence (5'-3') | Abbreviation |
|---|---|---|---|
| ACTB | Forward primer of β_Sc1 | TATAGGTTGGGGAAGTTTGTTTTTG | β_F1 |
| | Reverse primer | AACACACAATAACAAACACAAATTCAC | β_R1 |

### 2.1.7 Ethical approval

This study was approved by the local ethical board of Koç University has received approvals 2014.113.IRB1.0004 and 2018.359.IRB2.059. All the related activities have conformed to the Declaration of Helsinki.

## 2.2 Methods

### 2.2.1 Bacterial Growth Conditions

Liquid bacterial cultures were prepared from single colonies and inoculated in 5ml LB Broth for small scale plasmid isolations. A starter culture of 2ml LB Broth was used for scaling up in 100ml culture in 500ml round bottom flasks for overnight shaking incubation. After the confirmation of correct colonies, glycerol stocks from the cultures were prepared. LB Broth medium was supplemented with 50% glycerol for preservation of the cultures in 2ml cryovials. Cryovials were stored in -20ºC for later use.

### 2.2.2 Molecular Biology

#### 2.2.2.1 In-silico Cloning and Sequencing Analysis

In-silico clonings and alignments were completed in Serial Cloner version 2.6.1 and SnapGene 5.0.7.

#### 2.2.2.2 Polymerase Chain Reaction (PCR)

All PCR reactions for annealing temperature optimizations for qMSP and TOPO® TA clonings were completed with DreamTaq Green PCR Master Mix (2X) containing

DreamTaq DNA polymerase, 2X DreamTaq Green buffer, dATP, dCTP, dGTP and dTTP, 0.4 mM each, and 4 mM MgCl2. The reaction mixture and the cycling conditions were shown in **Table 2.6** and **Table 2.9.**

**Table 2.6. Reaction mix for PCR reactions.**

| Component | Volume |
|---|---|
| DreamTaq Green MM (2X) | 25µl |
| Forward primer (10µM) | 1µl |
| Reverse primer (10µM) | 1µl |
| $dH_2O$ | 22µl |
| Template (1ng/µl) | 1µl |
| Total | 50µl |

**Table 2.7. Cycling conditions of PCR for promoter amplification.**

| Step | | Temperature | Duration |
|---|---|---|---|
| Initial denaturation | | 98ºC | 00:30 |
| Amplification (30 cycles) | Denaturation | 98ºC | 00:10 |
| | Annealing | 60ºC (50-55-60-65 gradient for optimizations) | 00:20 |
| | Extension | 72ºC | 00:30 |
| Final extension | | 72ºC | 04:00 |
| Hold | | 4ºC | infinite |

### 2.2.2.3 DNA isolation

***Plasmid DNA isolation***

Plasmid DNA was isolated with Macherey-Nagel Nucleospin® Plasmid or Nucleobond Xtra Midi Kits. Plasmid isolation protocol is based on a SDS/alkaline lysis of pelleted bacteria, followed by a neutralization step of the lysate to create appropriate binding conditions of plasmid DNA to a silica membrane. Protein, genomic DNA, cell debris are precipitated by a centrifuge step, followed by several wash steps with ethanol buffers.

Plasmid DNA is eluted with a slightly alkaline, low ionic buffer, 5mM Tris/HCl at pH 8.5.

***Genomic DNA isolation***

*Genomic DNA isolation from cell pellets*

Confluent cells in 10cm cell culture dishes were detached from the plate with 0.05% Trypsin-EDTA (Gibco™ #25300062), and pelleted. MN NucleSpin® Tissue kit is used for genomic DNA isolation from cell pellets. Cell lysis achieved by the incubation with proteinase K/SDS mixture. Then chaotropic and ethanolic buffers are added on to the lysate to create appropriate binding conditions. After several washing steps to remove contaminants, genomic DNA is eluted with a slightly alkaline, low ionic buffer, 5mM Tris/HCl, pH 8.5.

*Genomic DNA isolation from FFPE samples*

Genomic DNA isolation from formalin fixed, paraffin-embedded (FFPE) samples were completed with NucleoSpin® DNA FFPE XS kit. First, paraffin around the samples are dissolved with an odorless paraffin dissolver. Then tissues are digested by proteinase K. After fixed tissues are solubilized and released into the solution, a decrosslinking solution is applied with heat to prevent crosslinking with the released DNA. Ethanol is added into the lysate before it is applied to the column. DNA binds to the silica membrane and the contaminants such as metabolites, salts, macromolecular cellular compounds are removed with washing steps. Genomic DNA is eluted with slightly alkaline, low ionic buffer, 5mM Tris/HCl, pH 8.5.

#### 2.2.2.4 Determination of DNA concentration

*Quantification of isolated plasmid DNA*

Plasmid DNA yields were measured with Thermo Scientific™ Nanodrop 2000, full-spectrum UV-Vis spectrophotometer.

*Quantification of isolated genomic DNA*

Genomic DNA yields were measured with Qubit®2.0 fluorometer.

#### 2.2.2.5 Agarose gel electrophoresis

Agarose powder (Sigma-Aldrich, #A9539) was dissolved in 1X TAE buffer, diluted with distilled water of 50X TAE (Thermo Scientific™, B49). 1.5%(w/v) agarose powder was used. 0.5µg/ml ethidium bromide (Sigma-Aldrich, #E1510) was added. 50bp, 100bp or

1kb Gene Ruler™ (Thermo Scientific ™, SM0373, SM1153, SM1553) was used as a marker, mixed with 6x Loading Dye (Thermo Scientific ™, R0611) with 1:6 DNA to dye ratio. Samples were run in a gel under constant voltage and visualized with Bio-Rad Gel Doc™ XR+ Gel Documentation System.

#### 2.2.2.6 Restriction enzyme digestion

Standard curve plasmids generated by TOPO® TA cloning protocol, were restriction enzyme digested to be selected for sequencing. 10 units of restriction enzyme (EcoRI #3101, New England Biolabs®) used for 1µg plasmid DNA. Digested for 1h at 37ºC in 20µl reaction.

#### 2.2.2.7 Molecular cloning

*TOPO TA cloning of PCR products*

Promoter sequences of the genes of our interest (ACTB, APC, GSTP1, RARβ2) are inserted into the pCR™4-TOPO® plasmid **(Figure 2.1)** according to manufacturer's protocol. (TOPO® TA Cloning® Kit for Sequencing, Invitrogen™ by Life Technologies™, Thermo Fisher Scientific™) Sequences amplified from a bisulfite converted LNCaP genomic DNA with the PCR protocol indicated in **Table 2.6,** and cycling conditions in

**Table 2.7.** Outer primers shown in **Table 2.2** were used for amplification. Following PCR, products were loaded in 1.5% agarose gel, run for 1h, 100volts. Single band PCR products were then cut out and gel purified as described in **2.2.2.5**. TOPO® TA Cloning® Kit has pCR™4-TOPO® vector in linear form with 3' thymidine (T) overhangs for TA cloning **(Figure 2.6).** *Taq* polymerase amplified PCR products are easily ligated to this vector since nontemplate-dependent terminal transferase activity of *Taq* adds single deoxyadenosine (A) to the 3' ends of the PCR products. Topoisomerase I cleaves the phosphodiester backbone after 5'-CCCTT in one strand. The energy released is conserved with the formation of a covalent bond between 3' phosphate and a tyrosyl residue of Topoisomerase I. 5' hydroxyl group of the cleaved strand reverses the reaction by attacking the phospho-tyrosil bond between DNA and Topoisomerase I (138). TOPO® Cloning benefits the same reaction for the cloning of PCR products.

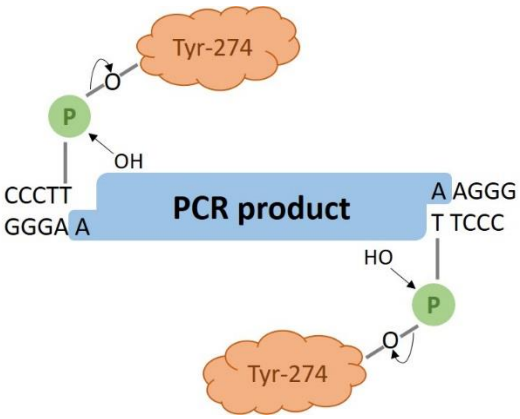


**Figure 2.6. Topoisomerase I activity exploited in TOPO® TA Kit for cloning of PCR products.**

Gel purified PCR product is then combined with TOPO® vector. Incubated at room temperature for 30mins. Transformed into *E.coli* Stbl3 cells. Reaction recipe for TOPO® TA cloning is shown in **Table 2.8.** TOPO® vector has lethal ccdB gene fused to C-terminus of the Lac*Z*α, allowing only positive recombinants to grow as ligation disrupts the *lacZα-ccd*B fusion.

**Table 2.8. TOPO® TA cloning reaction.**

| Reagent | Volume |
|---|---|
| Gel purified PCR product | 2 µL |
| Salt solution | 1 µL |
| Water | 3 µL |
| TOPO® vector | 1 µL |

### 2.2.2.8 Transformation

Generated TOPO® TA clones were amplified in *E.coli* Stbl3 cells. Heat-shock transformation protocol was applied. 2 µL from the TOPO® TA cloning reaction was incubated with 50 µL competent bacteria for 15mins on ice. After that, 45 seconds of 42ºC in water bath and placed on ice for 2mins. After heat-shock, SOC medium **Table 2.1** was added for recovery. Incubated at 37ºC at 225 rpm for 45min. Cultures were spread onto LB agar plates **(Table 2.1)** with carbenicillin or ampicillin. Plates were incubated overnight (12-16h) at 37ºC for single cell colonies.

### 2.2.3 Cell Culture

#### 2.2.3.1 Cell lines

HEK 293T cells are embryonic human kidney epithelial cells. Grown for genomic DNA isolation to use as a methylation negative cell line control. LNCaP WT cells are a lymph node metastasis epithelial cell line of prostate adenocarcinoma. Grown for genomic DNA isolation to use as a methylation positive cell line control.

#### 2.2.3.2 Cell culture conditions

HEK293T cells were cultured in in RPMI 1640 (Gibco™ #11875093) with 10% FBS (Gibco™ #10438034) and 1% penicillin-streptomycin (Gibco™ #15140122). LNCaP cells were cultured in RPMI 1640 (Gibco™ #11875093) with 10% tet-free FBS (Biowest #S181T) and 1% penicillin-streptomycin (Gibco™ #15140122).

### 2.2.4 Methylation analysis

#### 2.2.4.1 Quantitative real time polymerase chain reaction (qRT-PCR)

qRT-PCR reactions were carried out in Thermo Scientific™ PikoReal Real-Time PCR System in 96-well white plates (Thermo Scientific™, SPL0961) in a final volume of 10 µl with LightCycler® 480 SYBR Green I Master (Roche, # 04707516001). 0.5 µl from each primer (10 µM) and 1 µl of template DNA was used. The reaction mixture and cycling conditions were shown in **Table 2.9** and **Table 2.10.**

**Table 2.9. Reaction mix for qPCR reactions.**

| Component | Volume |
|---|---|
| LightCycler® 480 SYBR Green I Master (2X) | 5.0 µl |
| Forward primer (10µM) | 0.25 µl |
| Reverse primer (10µM) | 0.25 µl |
| $dH_2O$ | 3.50 µl |
| Template | 1.0 µl |
| Total | 10.0 µl |

**Table 2.10. Cycling conditions for qPCR reactions.**

| Step | | Temperature (ºC) | Duration (mm:ss) | Ramp Rate(ºC/s) |
|---|---|---|---|---|
| Initial denaturation | | 95ºC | 05:00 | 4.4 |
| Amplification (45 cycles) | Denaturation | 95ºC | 00:10 | 4.4 |
| | Annealing | 52ºC | 00:30 | 2.2 |
| | Extension | 72ºC | 00:30 | 4.4 |
| Melting curve | | 95ºC | 00:05 | 4.4 |
| | | 52ºC | 01:00 | 2.2 |
| | | 72ºC | - | 0.11 |
| Cooling | | 40ºC | 00:30 | 2.2 |
| Hold | | 4ºC | infinite | |

### 2.2.4.2 Bisulfite conversion

Purified genomic DNA is bisulfite converted with EZ DNA Methylation-Direct Kit (Zymo Research, D5021). Bisulfite conversion is achieved by incubating the DNA in a bisulfite solution at elevated temperatures, binding the DNA to silica membrane, desulfonation of sulfonyl uracil adducts at alkaline pH, removing of desulfonation solution, consequent washing steps with an ethanolic buffer and elution with a high pH buffer **(Figure 2.7).**

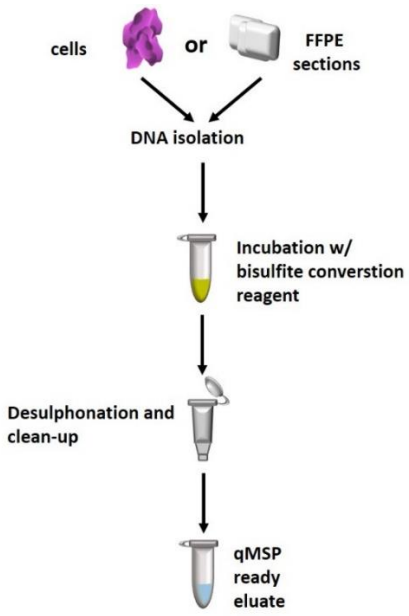


**Figure 2.7. Bisulfite conversion steps.**

### 2.2.4.3 Quantitative Methylation Specific PCR (qMSP)

***Scorpions Uni-Probes***

Scorpions Uni-probes are a bi-labelled fluorescent probe-primer hybrids designed for highly sensitive, sequence specific qPCR experiments. A 5'end reporter and an internal quencher are directly linked at the end of a hairpin-loop structure. A blocker is directly linking the quencher to the 5' end of a PCR primer. With the aid of the blocker, polymerase cannot extend the PCR primer **(Figure 2.8).** Reaction kinetics of Scorpions Uni-Probes are very fast due to the incorporation of the probe and the primer into a single molecule. Fluorescent signal generation is instantaneous and occurs before background reactions. Therefore, Scorpions Uni-Probes provide increased specificity and better discrimination due to signal-noise ratio.

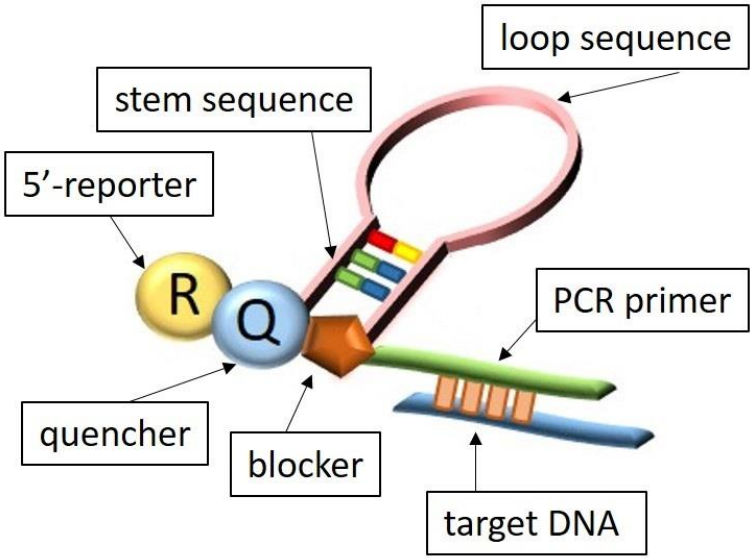


**Figure 2.8. Structure of a Scorpions uni-probe.**

Polymerase extends the PCR primer and complementary strand of the target sequence is synthesized at the beginning of the qPCR reaction. In the next PCR cycle, hairpin-loops unfolds and the loop sequence hybridizes with the quencher. With that, since the reporter and quencher is no longer in close proximity, fluorescence emission takes place **(Figure 2.9)**. Fluorescent signal detected is proportional to the amount of the target DNA.

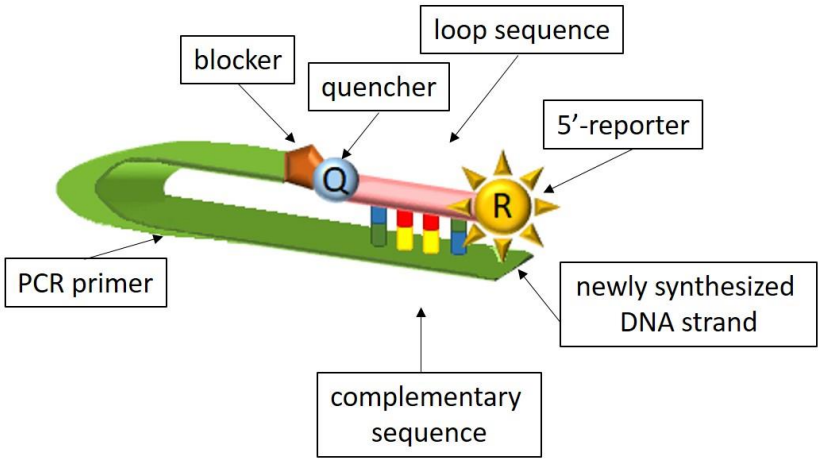


**Figure 2.9. Emission of fluorescence with Scorpions uni-probe.**

***MethyLight assay***

MethyLight is a fluorescence-based, quantitative real-time PCR method. It is sodium-bisulfite dependent and used for sensitive detection and quantification of DNA methylation. MethyLight harbors the use of methylation-specific priming and methylation-specific fluorescent probing. This sensitive methylation-specific approach allows detection of very low frequency DNA hypermethylation as diagnostic and prognostic biomarkers of diseases.

qMSP reactions were prepared according to the mixture in **Table 2.11** and the cycling conditions were summarized in **Table 2.12.** Scorpions probes stocks were dissolved in TE buffer (10mM Tris/HCl, pH7.5, 1mM EDTA) to 100mM prior further dilutions. All the reactions were carried out in Thermo Scientific™ PikoReal Real-Time PCR System in 96-well white plates (Thermo Scientific™, SPL0961).

**Table 2.11. Reaction mixture of qMSP protocol.**

| Component | Volume |
|---|---|
| PCR MM (2X) | 5.0 µl |
| Scorpion probe (10µM) | 0.1 µl |
| Reverse primer (10µM) | 0.1 µl |
| $dH_2O$ | 3.8 µl |
| Template | 1.0 µl |
| Total | 10.0 µl |

**Table 2.12. Cycling conditions of qMSP protocol.**

| Step | | Temperature | Duration | Ramp rate |
|---|---|---|---|---|
| Initial denaturation | | 95ºC | 10:00 | 7ºC/s |
| Amplification (45 cycles) | Denaturation | 95ºC | 00:10 | 4.4ºC/s |
| | Annealing/extension | 60ºC | 02:00 | 2.2ºC/s |
| Hold | | 25ºC | infinite | 7ºC/s |

# 3. RESULTS

Although the introduction of mpMRI has significantly improved PCa detection, false-positives still commonly occur. It is unclear if these false-positive biopsies contain pre-malignant features or are radiographic artifacts. The goal of this thesis therefore is to characterize the epigenetic features of radiologically suspicious but histopathologically benign needle prostate biopsies. Focusing on promoter DNA methylation, which has been shown to cause gene silencing early in carcinogenesis, we chose to quantify the promoter methylation of the tumour suppressors APC, GSTP1 and RARB2. These specific regulatory regions have a well-demonstrated correlation with early stage PCa. This work will therefore design and optimize a DNA methylation that is compatible with mpMRI-guided biopsies **(3.2)** and then test the epigenetic alterations in radiologically suspicious but histopathologically benign biopsies **(3.3)**.

## 3.1 DNA methylation assay

To quantify the promoter methylation of these clinical biopsies we utilized a methylation assay that was compatible with bisulfite converted DNA. Conversion of genomic DNA for differentiating between unmethylated and methylated cytosines is the gold standard for DNA methylation analysis. Upon treatment with a sodium bisulfite, unmodified cytosines are deaminated to uracil while methylated (5-mC) cytosines are unaffected **(Figure 3.1).** This conversion can be detected by several different approaches including targeted PCR amplification where the primer is designed to be complimentary to the modified sequence of the bisulfite converted target area so that primer cannot bind if the cytosines were to be unmethylated, or vice versa.

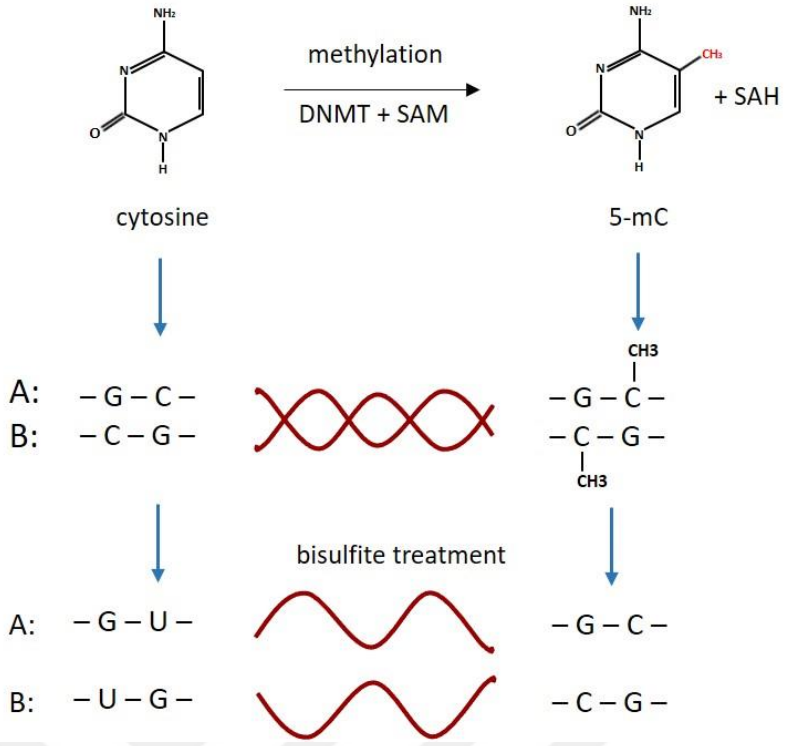


**Figure 3.1 DNA methylation and bisulfite conversion.** *Upon treatment with bisulfite solution, unmethylated cytosines become uracils while methylated ones remain the same. This sequence difference can be observed with amplification based assays.*

### 3.2 QMSP assay design

After comparing several different experimental approaches, we chose to use an QMSP assay to quantify the relative DNA methylation in our bisulfite converted clinical samples. This was selected as mpMRI-guided in bore biopsies are taken with a 16-18 gauge needles and therefore have very limited genetic material. Thus we needed a method that could sensitively detect and quantify DNA methylation in samples that contain little bisulfite converted gDNA. QMSP has been previously demonstrated to effectively quantify DNA methylation from low DNA clinical samples (129). QMSP amplifies the methylated DNA target with sequence specific primers which is detected with a real-time PCR instrument. The real time detection of the QMSP method can be achieved in two different approaches. One of them is by using a fluorescent dye such as SYBR Green. In solution this dye is weakly fluorescent but when bound to double stranded DNA the fluorescence significantly increases. Therefore, by quantifying the relative increase in fluorescence with each round of PCR amplification you can quantify the relative double-stranded PCR product (139). While easy, this approach is not selective for a specific region and will detect any amplified double-stranded DNA including non-specific PCR artifacts.

Another detection method commonly used with QMSP uses targeted fluorescent probes in the amplification. In contrast to the DNA-intercalating dye SYBR Green, these probes are sequence specific and are not affected by non-specific PCR products. There are a variety of probes that can be used for this purpose, such as molecular beacons, oligonucleotide probes or Scorpions probes (140). Scorpions probes are a composed of a stem-loop tail that brings a fluorophore and quencher in close proximity together with a PCR primer (131). During the PCR cycle, the primer is extended at the 3' end and incorporates the Scorpion probe into the target DNA product. When annealed, the recognition sequence in the Scorpion stem loop hybridizes to the complementary sequence within the same strand of the target PCR product. By breaking the stem loop the fluorophore and quencher are separated resulting in the fluorescence emission (**Figure 1.10)** (139). This approach was attractive with our clinical samples, as the unimolecular structure decreases the background fluorescence and the mechanism of action increases the specificity with limited amounts of clinical samples.

### 3.2.1 Generation of standards for QMSP assay

To quantify the promoter methylation of the genes from biopsy samples, we first needed to generate genomic standards to determine the absolute number of methylated copies of the promoter region of each gene (PRG). In this section we cloned the bisulfite converted promoter regions into a plasmid with a known molecular weight to use as a standard.

### 3.2.2 Bisulfite conversion

Genomic DNA from a malignant PCa cell line (LNCaP) was used as a template for TOPO cloning of bisulfite converted PRGs. While we used a commercial bisulfite solution for the conversion reactions we optimized both the temperature conditions and the template amount. We found that altering the temperature did not impact bisulfite conversion but unexpectedly the amount of the template strongly affected the yield of the reaction. Several different amounts of gDNA were used in the conversion reaction based on the manufacturers protocols (0.5pg - 2µg). From this, 500ng total genomic DNA was selected as the yield after the conversion did not improve with further amounts. The resulting bisulfite converted LNCaP gDNA was used for the generation of all QMSP genomic standards.

### 3.2.3 TOPO cloning

The promoter regions of ACTB, APC, GSTP1 and RARB2 were PCR amplified from bisulfite converted LNCaP gDNA. The specific sites were selected based off previous publications. Our APC, GSTP1 and RARB2 primers are specific for methylated DNA while the ACTB region did not contain any CpG and therefore will not be affected by bisulfite conversion. Primer sequences are given in **Table 2.2**. The PCR reactions from converted gDNA were optimized in terms of total volume and the annealing temperatures **(Figure 3.2, Figure 3.3).** The final amplified and purified products of each gene can be seen in **Figure 3.4.** Following gel purification, the PCR products were cloned into TOPO pCR4 vector by TOPO cloning (141). This vector was selected due to its relatively small size and ease of cloning. The resulting cloned plasmids were validated by diagnostic restriction endonuclease digestion and Sanger sequencing.

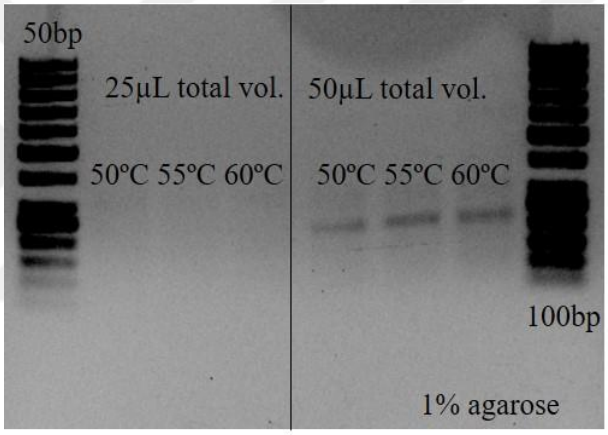


**Figure 3.2 Volume and temperature gradient for ACTB PCR.** *25µL of DreamTaq Green PCR MM (2X) was used with 10µM of final concentration of primers and 1ng of bisulfite converted LNCaP genomic DNA. Three temperatures with 5ºC increments were used to set gradient PCRs. While total reaction mixture of 25µL didn't result in any PCR products, the same concentration of primers and template in 50µL reaction resulted in single band amplifications.*

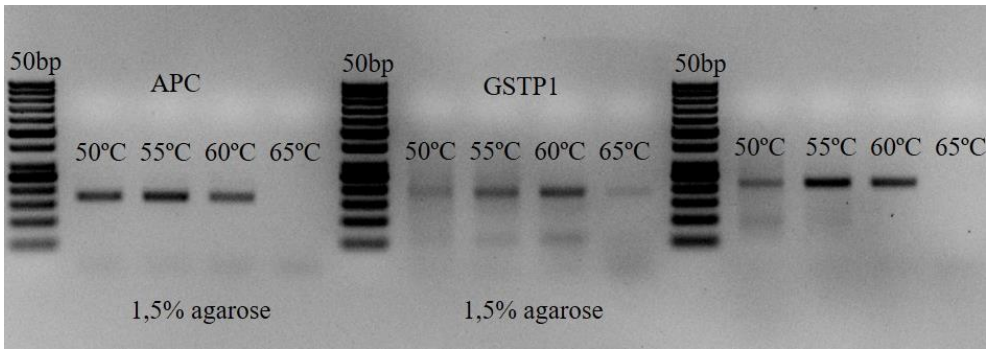


**Figure 3.3 Gradient PCRs for APC, GSTP1 and RARB2.** *Several temperatures were tested with 50µL reactions for APC, GSTP1 and RARB2 PCR.*

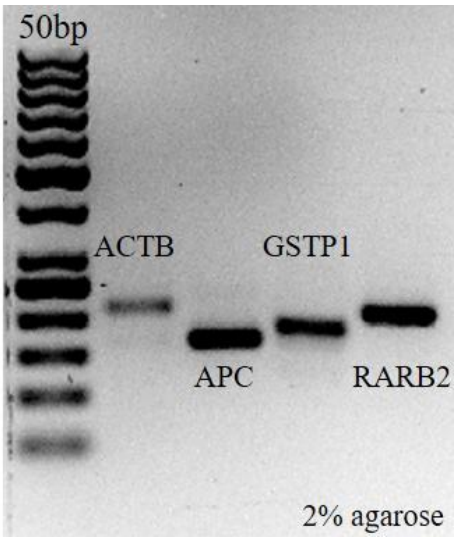


**Figure 3.4 Final PCR amplified products for all four genes.**

### 3.2.4 Standard curves

Using the cloned PRG plasmids we then generated QMSP standard curves. In this, the number of copies of an insert in a plasmid was calculated from the DNA amount using a fixed weight of 650 Daltons per base pair with the following formula:

$$\text{Number of copies} = \frac{\text{amount} * 6.022\text{x}10\text{\^{}}23}{\text{length} * 1\text{x}10\text{\^{}}9 * 650}$$

After calculating the plasmid copy number, we then serially diluted plasmids to generate a standard curve to correlate the insert copy numbers and the cycle thresholds (Ct) from QMSP. Using ACTB, the methylation independent genomic region, as an internal reference the absolute amount of gDNA from a biopsy sample can be quantified by these standard curves. The QMSP signal for the PRG will be normalized by the gDNA amounts calculated by ACTB to reduce false positives and negatives caused by varying yields of genetic material from individual clinical samples. The copy number calculation we obtained for ACTB were used to calculate the amount of sample in that particular reaction. This internal control enabled us to compare the normalized methylated copies of PRGs between different clinical samples.

#### 3.2.4.1 Optimizing the reaction mixture

Before optimizing our QMSP methodology with clinical samples we first needed to validate that our primer-probe pairs were binding to the designated region and could efficiently amplify the cloned insert. To simplify this initial optimization, we first used the forward primer without a Scorpion probes stem-loop or fluorophore. Instead the PCR

products were detected with SYBR Green **(Figure 3.5-Figure 3.8).** The initial qPCRs demonstrated that the primer pairs to be used in QMSP reactions were able to amplify all of our cloned genes. Furthermore, the plasmid standard curves demonstrated a good fit with an $R^2$>0.98. Therefore, we decided to proceed with incorporate our Scorpion probes and optimize the QMSP methodology.

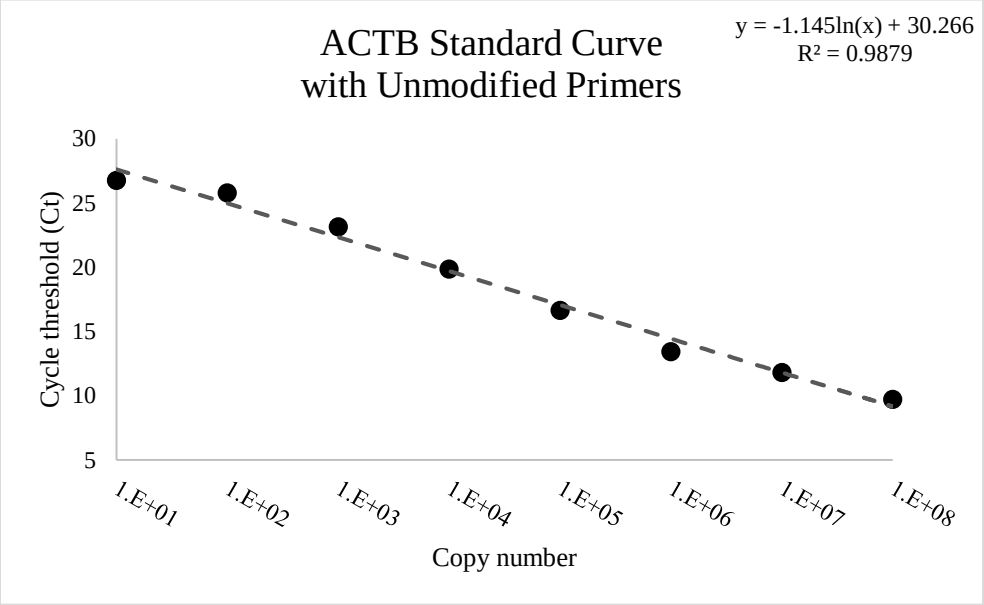


**Figure 3.5 ACTB standard curve with QPCR.** *Forward primer of ACTB Scorpion with reverse primer is used for the reaction. Curve generated with 3 technical replicas for each copy number dilution.*

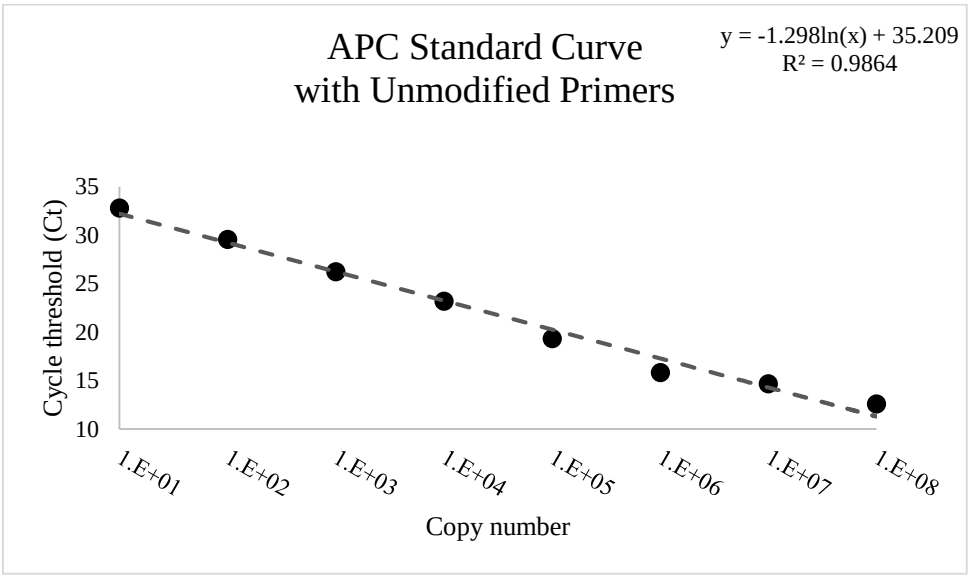


**Figure 3.6 APC standard curve with QPCR.** *Forward primer of APC Scorpion with reverse primer is used for the reaction. Curve generated with 3 technical replicas for each copy number dilution.*

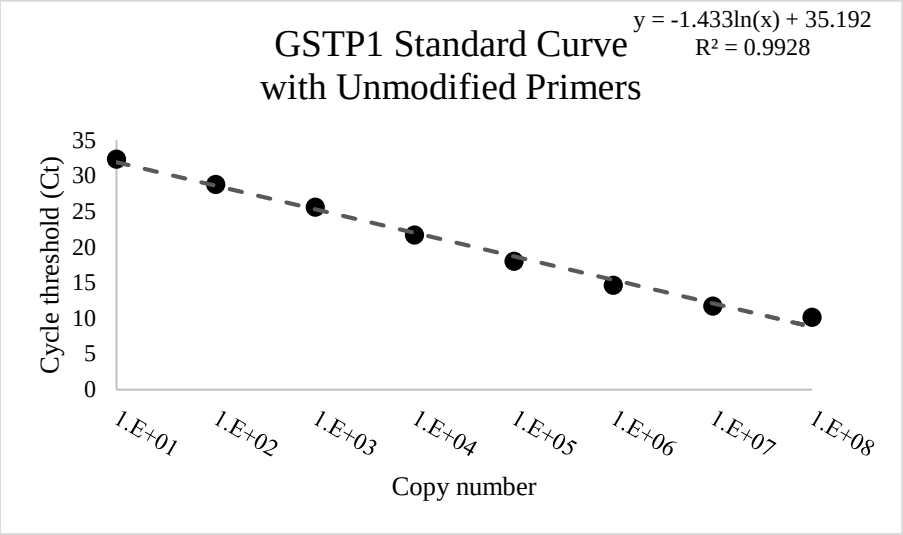


**Figure 3.7 GSTP1 standard curve with QPCR.** *Forward primer of GSTP1 Scorpion with reverse primer is used for the reaction. Curve generated with 3 technical replicas for each copy number dilution.*

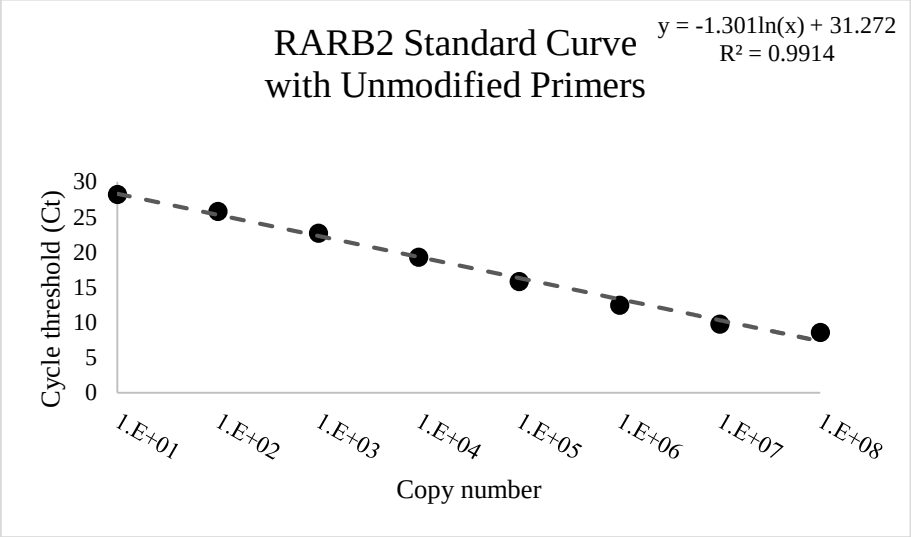


**Figure 3.8 RARB2 standard curve with QPCR**. *Forward primer of RARB2 Scorpion with reverse primer is used for the reaction. Curve generated with 3 technical replicas for each copy number dilution.*

Initial QMSP reactions were performed for ACTB and APC, using equal amounts of Scorpion probes, primers and Taq polymerase. The ACTB standard curve **(Figure 3.9)** indicated a good fit. However for APC, the linear correlation was not consistent across log-fold dilutions of the plasmid suggesting the assay could not quantify $<10^4$ copies **(Figure 3.10).** To understand if excess probe, primer and polymerase concentration is the reason hampering the amplification by improper binding, the final concentration of each of these parameters were lowered. The results for GSTP1 **(Figure 3.11)** and RARB2

**(Figure 3.12)** showed even more scattered signal then the initial reactions. At dilution points ranging from 10^2 to 10^6 copies, Ct values fluctuated within a range of approximately five cycles, which is narrower than expected. Although the differences in these curves could be attributed to different primer pairs, further optimizations were needed to achieve a sufficient wide range of sensitivity needed for clinical biopsies where DNA amounts are limited.

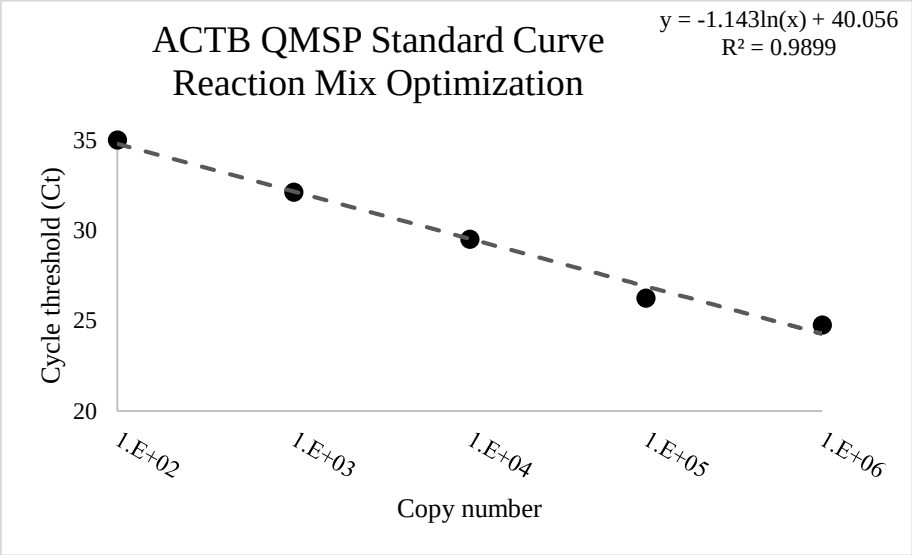


**Figure 3.9 ACTB standard curve with QMSP.** *Reaction mixture contained 3µM final concentration of Scorpions, primers and fast start Taq DNA polymerase. Same cycling conditions for initial QPCRs applied. Curve generated with 3 technical replicas for each copy number dilution.*

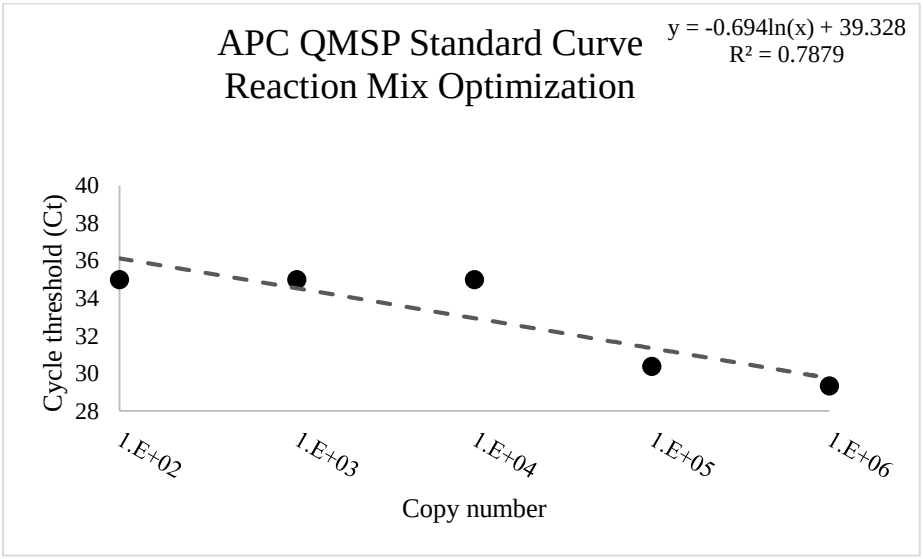


**Figure 3.10 APC standard curve with QMSP.** *Reaction mixture contained 3µM final concentration of Scorpions, primers and fast start Taq DNA polymerase. Same cycling conditions for initial QPCRs applied. Curve generated with 3 technical replicas for each copy number dilution.*

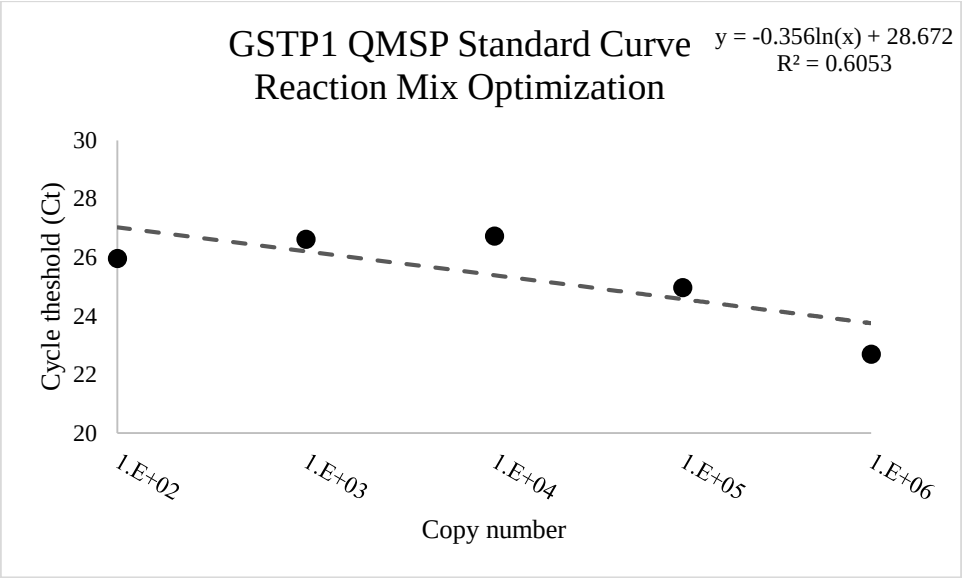


**Figure 3.11 GSTP1 standard curve with QMSP.** *Reaction mixture contained 1µM final concentration of Scorpions, primers and fast start Taq DNA polymerase. Same cycling conditions for initial QPCRs applied. Curve generated with 3 technical replicas for each copy number dilution.*

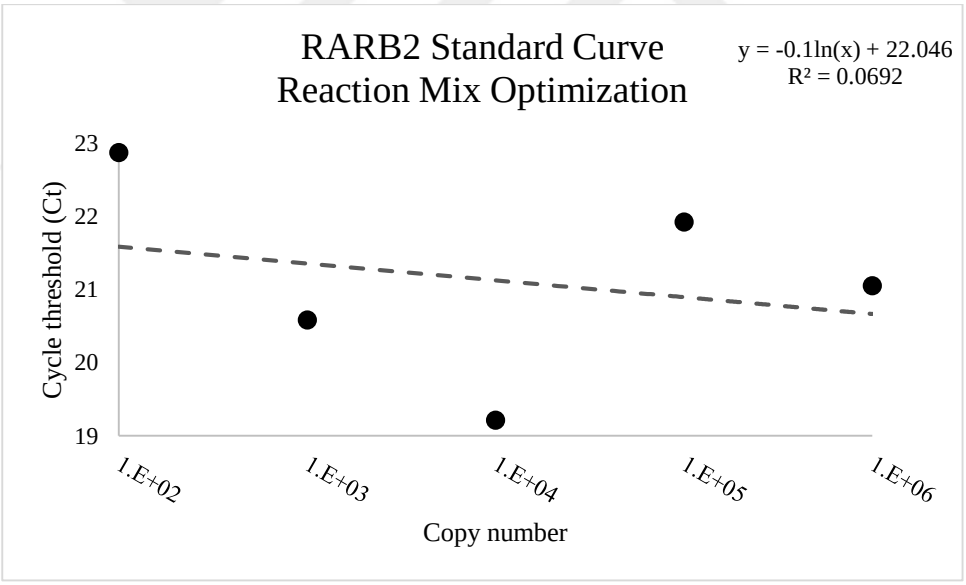


**Figure 3.12 RARB2 standard curve with QMSP.** *Reaction mixture contained 1µM final concentration of Scorpions, primers and fast start Taq DNA polymerase. Same cycling conditions for initial QPCRs applied. Curve generated with 3 technical replicas for each copy number dilution.*

### 3.2.4.2 Optimizing the cycling conditions

To improve the limit of detection of our initial assay we broadly optimized numerous features of the QMSP reaction including the volume of the reaction, final concentrations of the primers, probes used, polymerase and the qPCR instrument itself. Within this optimization matrix we used the initial QPCR conditions as a starting point for QMSP

optimization (**Figure 3.11, Figure 3.12**). All data points that had a Ct value >40 were considered to be non-detectable. Detection of DNA methylation from needle biopsy samples require a method that is accurate with limited genomic DNA. Hence, generating standard curves with as low limit of detection as possible was the main goal of our optimization. Based on published yields of genomic DNA from needle biopsy sections we calculated we would need a limit of detection greater than 10^2 copies of the specific genomic region.

*Reaction volume*

Due to the lower operating volumes, we chose to use a PikoReal light cycler for subsequent optimization. The reduction in total reaction volume to 10µL significantly reduces reagent costs while increasing the concentration of sample gDNA. However, no data points could be observed after dilution point 10^6 copies for ACTB (**Figure 3.13).** A similar result was obtained for RARB2 **(Figure 3.16)**. However, APC **(Figure 3.14)** and GSTP1 **(Figure 3.15)** had much better amplification and reached a plateau around 10^3 copies. All samples showed high Ct values even with the highest plasmid copies.

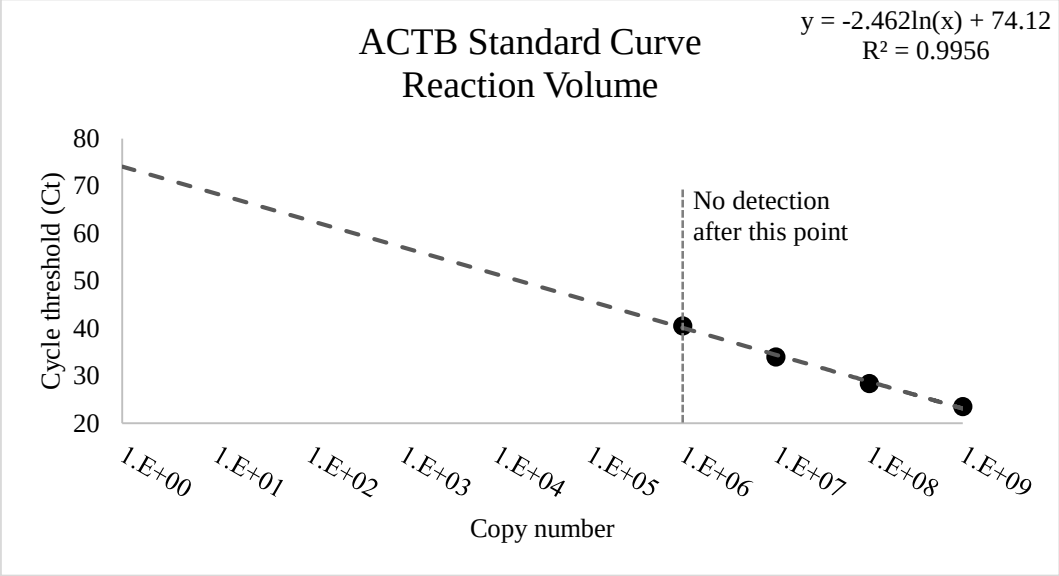


**Figure 3.13 ACTB standard curve in 10uL with PCR MM, run in PikoReal™**. *Cycling conditions used for initial set of QPCRs were applied. Curve generated with 2 technical replicas for each copy number dilution.*

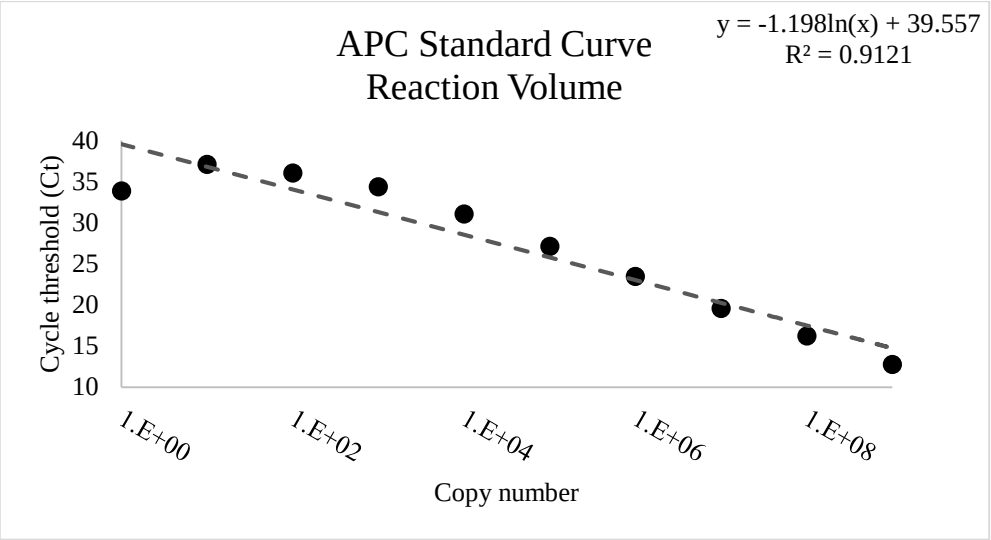


**Figure 3.14 APC standard curve in 10uL with PCR MM, run in PikoReal™.** *Cycling conditions used for initial set of QPCRs were applied. Curve generated with 2 technical replicas for each copy number dilution.*

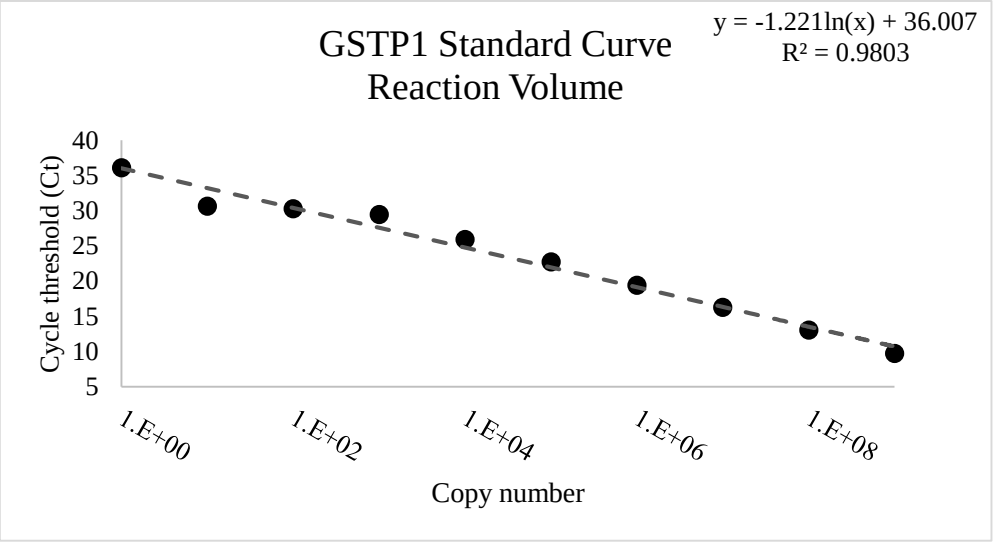


**Figure 3.15 GSTP1 standard curve in 10uL with PCR MM, run in PikoReal™**. *Cycling conditions used for initial set of QPCRs were applied. Curve generated with 2 technical replicas for each copy number dilution.*

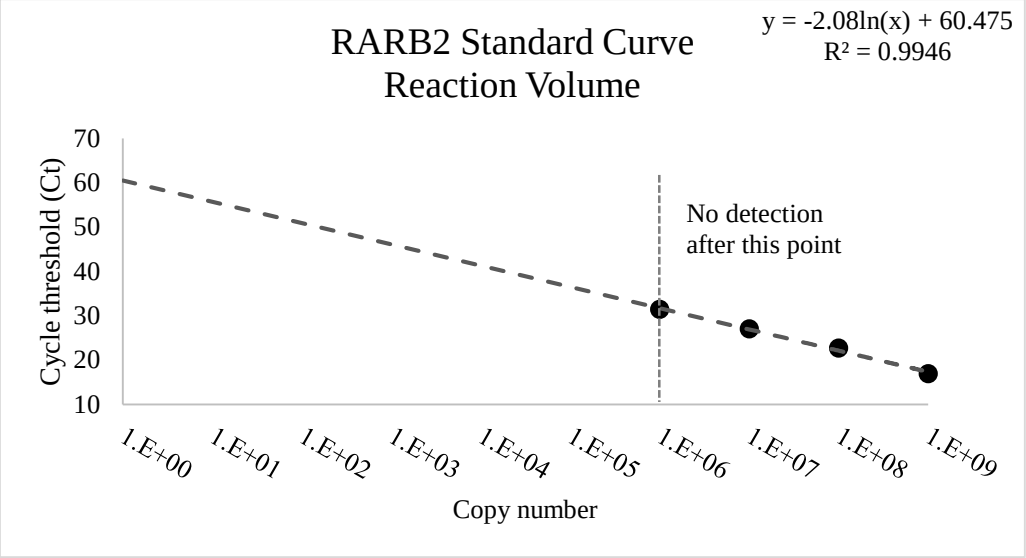


**Figure 3.16 RARB2 standard curve in 10uL with PCR MM, run in PikoReal™.** *Cycling conditions used for initial set of QPCRs were applied. Curve generated with 2 technical replicas for each copy number dilution.*

*Initial denaturation time*

Next we optimized the denaturation time of the QMSP. The goal was to understand if the denaturation time used was suitable with longer Scorpion probes for strand denaturation and could support primer – probe binding following amplification. An initial denaturation time of 10 or 15 min was used but no amplification was observed for 15 min in any runs. **Figure 3.17- Figure 3.20** show the amplifications with 10 minutes of initial denaturation. For ACTB, we detected amplification for the dilution points up to 10^4 (**Figure 3.17)**. Similarly, the dilution points up to 10^2 copies could be detected for RARB2 **(Figure 3.20)**. On the other hand, changing the initial denaturation time did not affect the GSTP1 curve **(Figure 3.19)**. Although APC showed a better fit **(Figure 3.18)** the limit of detection was reached earlier, at 10^5 copies.

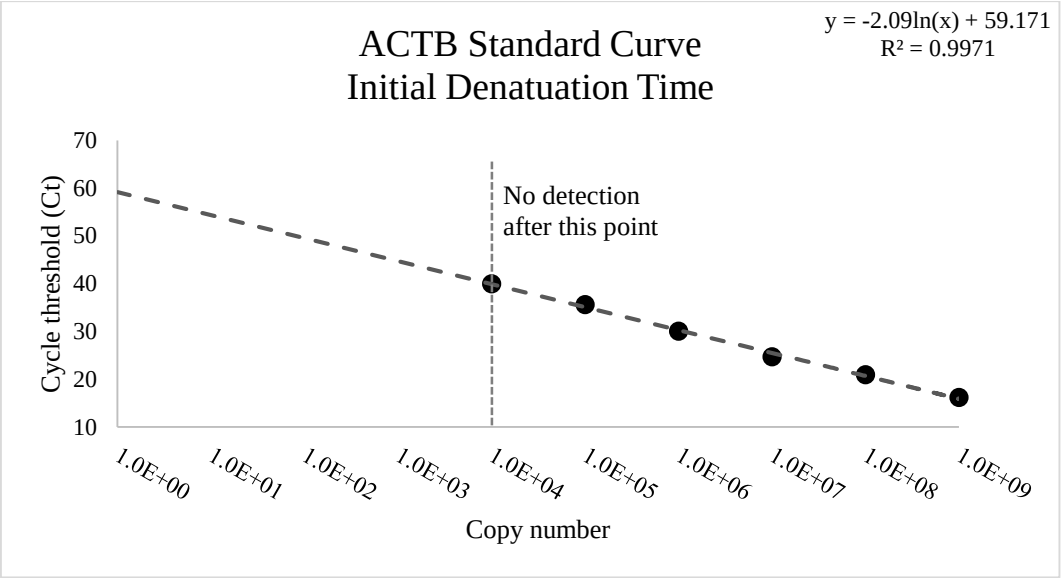


**Figure 3.17 ACTB QMSP standard curve with l0 mins initial denaturation.** *Curve generated with 2 technical replicas for each copy number dilution.*

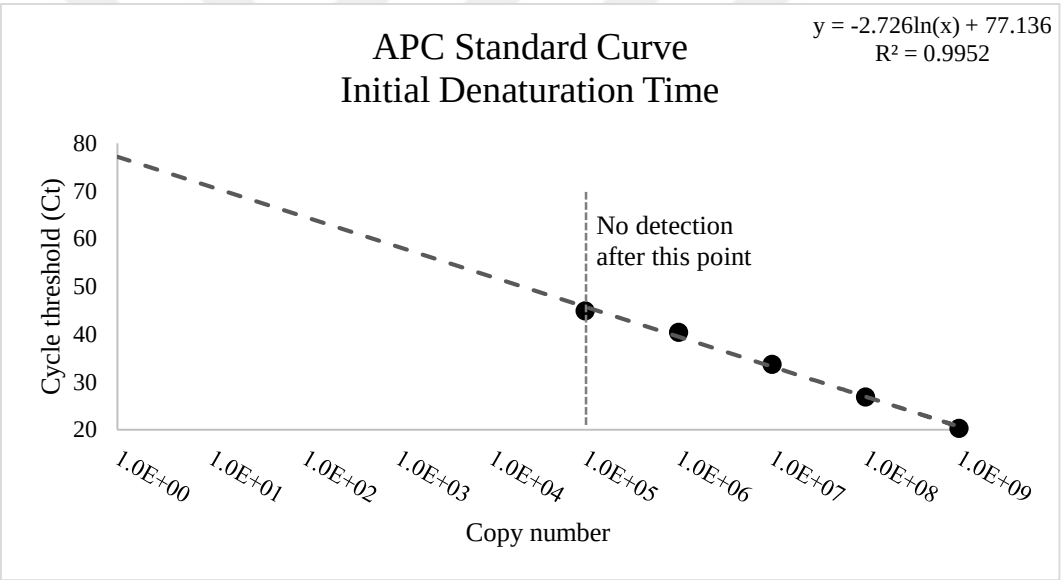


**Figure 3.18 APC QMSP standard curve with l0 mins initial denaturation.** *Curve generated with 2 technical replicas for each copy number dilution.*

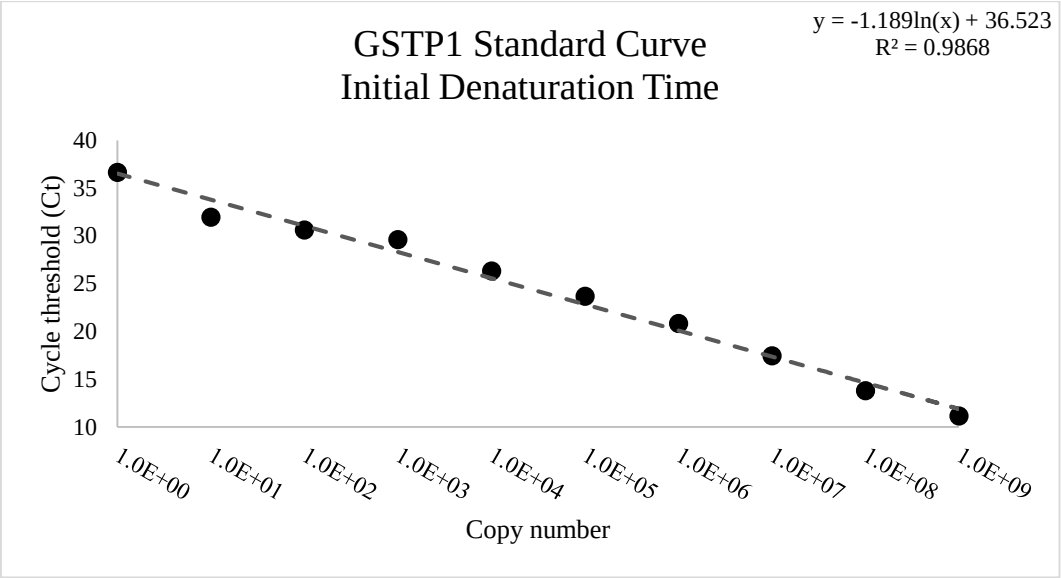


**Figure 3.19 GSTP1 QMSP standard curve with l0 mins initial denaturation.** *Curve generated with 2 technical replicas for each copy number dilution.*

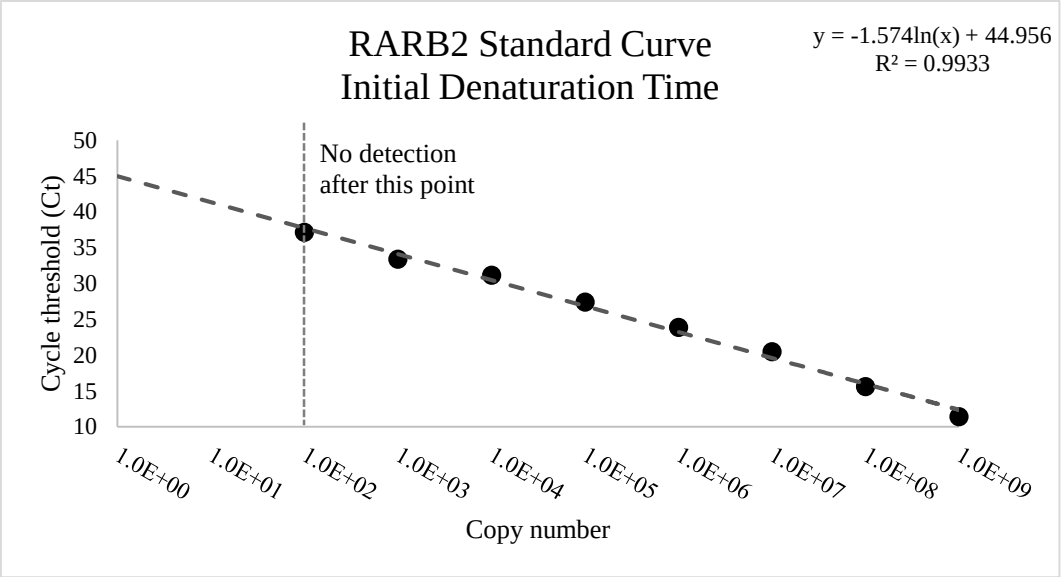


**Figure 3.20 ACTB QMSP standard curve with l0 mins initial denaturation.** *Curve generated with 2 technical replicas for each copy number dilution.*

*Duration of denaturation step*

Next we wanted to see the effect of changing denaturation step in the PCR. Given that ACTB is used as an internal normalization control and critical for a successful assay, we focused on optimizing this genomic region as the limit of detection was significantly worse than other promoters. Therefore, we tested the effect of 10 or 30 seconds denaturation. Although the prolonged time for initial denaturation changed the shape of the curves, we did not see a prominent change for varying the denaturation step **(Figure 3.21).** As there was no difference we chose 10 seconds for denaturation time.

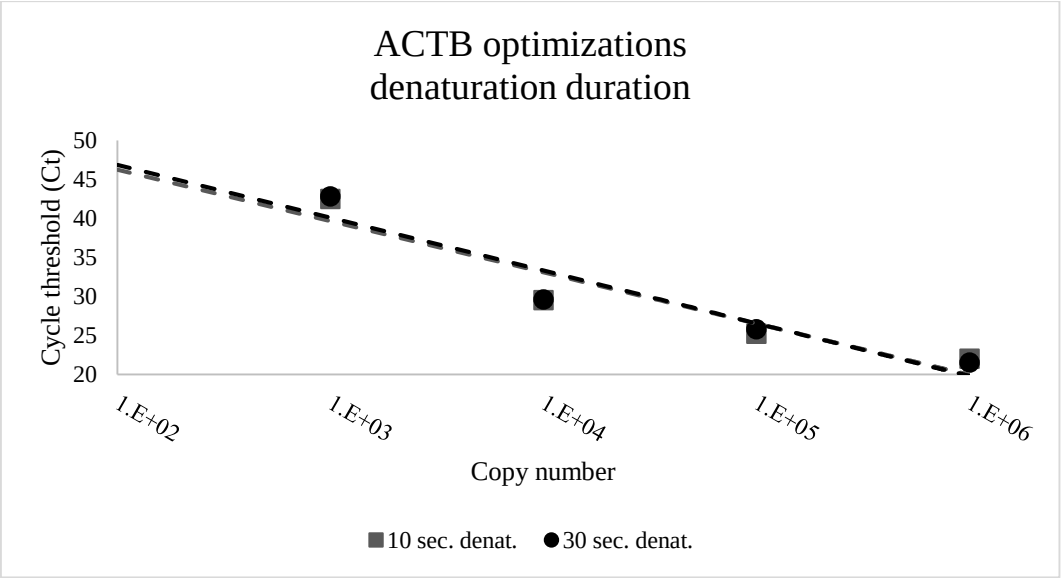


**Figure 3.21 ACTB optimizations for duration of denaturation step.** *No significant change was observed in the shape of the curve and the signal intensity depending on the duration of denaturation. Curves generated with 2 technical replicas for each copy number dilution.*

*Ramp rate of cycling steps*

Scorpion probe binding and extension is a complex process that may require fine adjustments to ensure successful detection of amplification. Therefore, we next tested the ramp rate of 1ºC/s, 2ºC/s or a mix of ramp rates to understand if the speed of temperature change would affect the amplification efficiency. With more concentrated DNA amounts the amplification was very similar with different ramp rates. However, a slight separation between the signals could be observed with lower concentrations **(Figure 3.22).** Given the technical variability at lower concentrations this is likely not significant suggesting that ramp rate does not influence QMSP assay sensitivity.

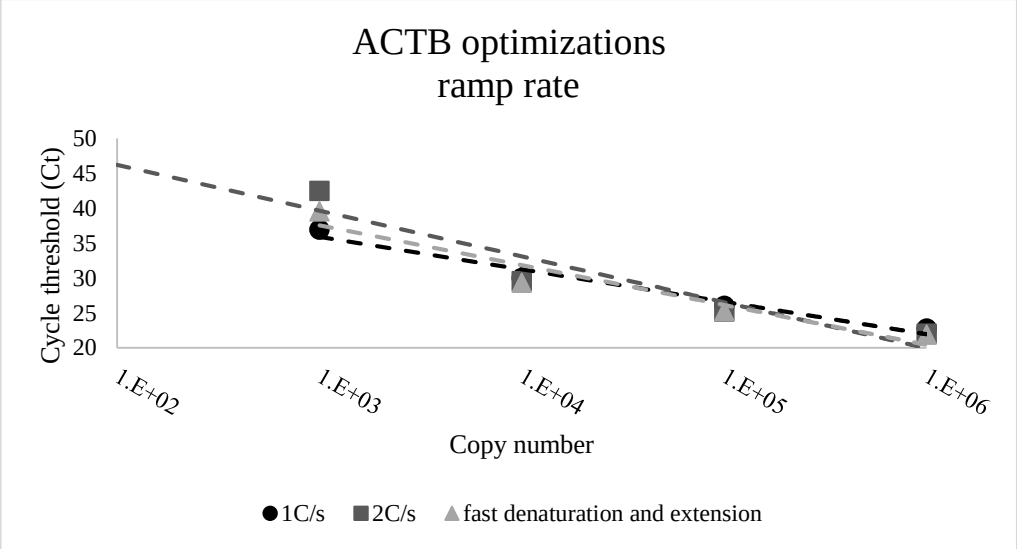


**Figure 3.22 ACTB optimizations for ramp rates of cycling steps.** *Three different curves displayed for steps with equal ramp rates during cycling (1ºC/s and 2ºC/s) and varying, faster temperature changes (4.4ºC/s, 2.2ºC/s, 4.4ºC/s for denaturation, annealing and extension, respectively). Ct values for all curves mostly overlap with more concentrated points, however, a slight separation could be observed for lower concentration points. Curves generated with 2 technical replicas for each copy number dilution.*

*Annealing and extension time*

Next, the annealing and extension time were optimized. We tested both 30 (shorter duration) or 60 second (longer duration) annealing steps. For ACTB we observed a significantly improved sensitivity with longer annealing and extension time compared to a shorter one.

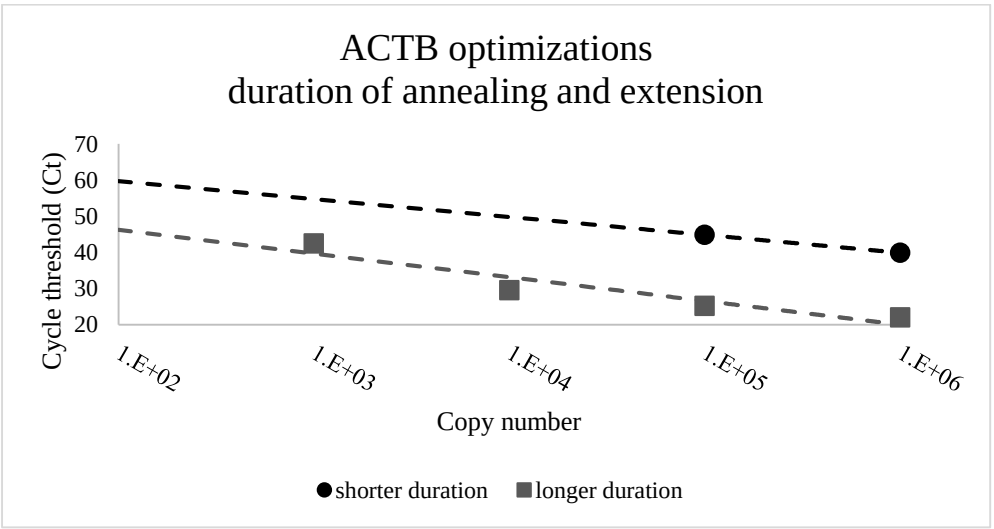


**Figure 3.23 ACTB optimizations for duration of annealing and extension steps.** *Longer annealing and extension time (over a minute) generated more signal points for the curve compared to the shorter times (less than 30 secs). Curves generated with 2 technical replicas for each copy number dilution.*

Given the improved sensitivity we then further increased the duration of the annealing to both 1.5 and 2 minutes and found that this improved the ACTB limit of detection **(**Error! Reference source not found.**).** We did not observe significant difference between 1.5 and 2 minutes and therefore chose to use the lower 1.5 minutes annealing time.

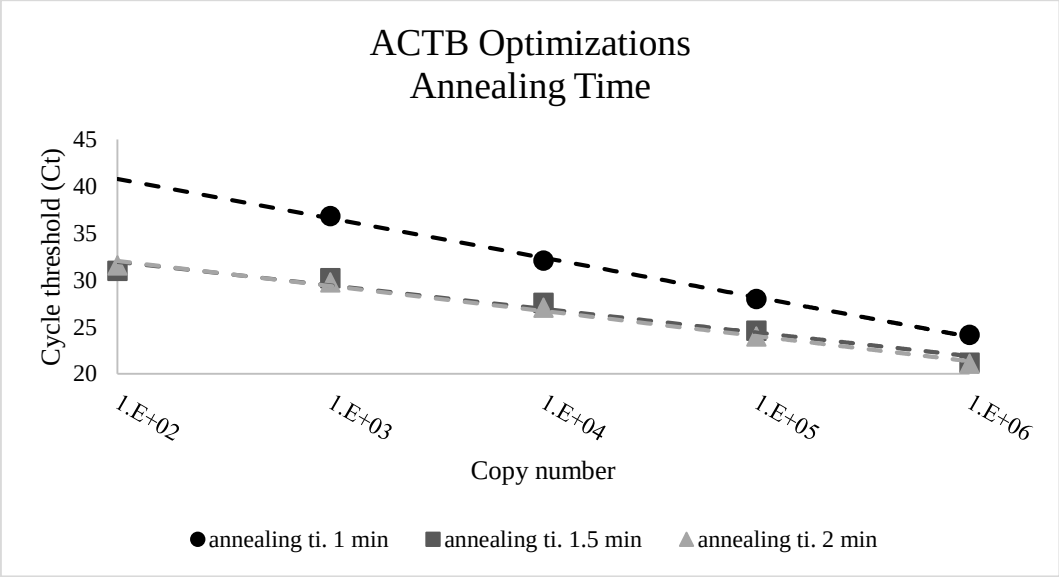


**Figure 3.24 ACTB optimizations for annealing time for fixed duration and ramp rates for the rest of the cycling steps.** *Longer annealing time with a low ramp rate generated a better standard curve for ACTB. Curves generated with 2 technical replicas for each copy number dilution.*

Having optimized and improved the QMSP conditions for ACTB we then wanted to test how these would worked with APC, GSTP1 and RARB2 **(Figure 3.25-Figure 3.27)**.

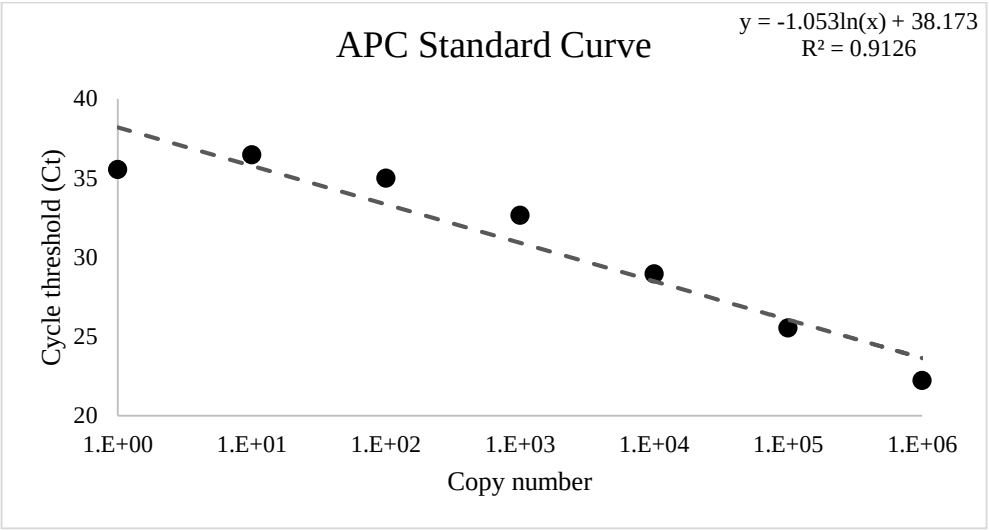


**Figure 3.25 APC standard curve with the conditions optimized with ACTB.** *Curve generated with 2 technical replicas for each copy number dilution.*

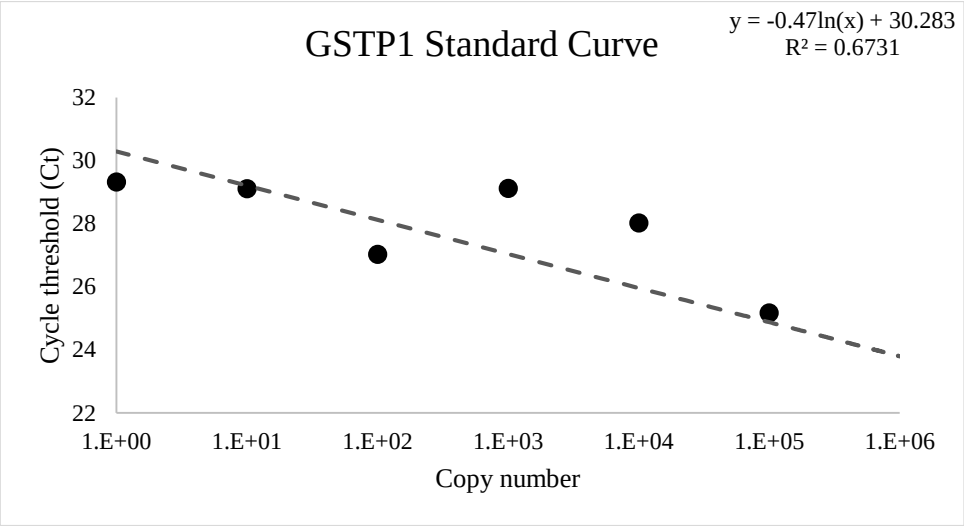


**Figure 3.26 GSTP1 standard curve with the conditions optimized with ACTB.** *Curve generated with 2 technical replicas for each copy number dilution.*

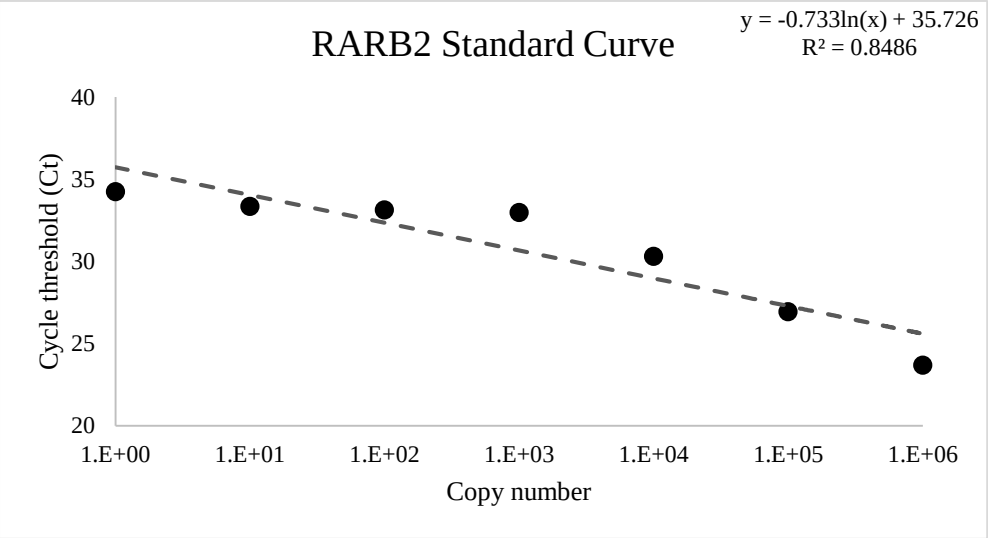


**Figure 3.27 RARB2 standard curve with the conditions optimized with ACTB.** *Curve generated with 2 technical replicas for each copy number dilution.*

The results for these optimized Scorpion probes were mixed. For APC, the limit of detection was 10^2 copies with Ct values similar to ACTB standard curve **(Figure 3.25).** For RARB2, the detection limit stayed at 10^3 copies **(Figure 3.27).** However, for GSTP1 our observed data points provided a poor fit suggesting that this condition did not work for these primer pairs **(Figure 3.26).**

*Second set of primer-probe pairs for ACTB, GSTP1 and RARB2*

To determine if another probe-primer pair would provide a better amplification we chose to design a new Scorpion primer with Serial Cloner targeting ACTB, GSTP1 and RARB2. No new pair was tried for APC as our the initial probe and primer generated a reproducible standard curve with a good fit and wide dynamic range **(Figure 3.28).**

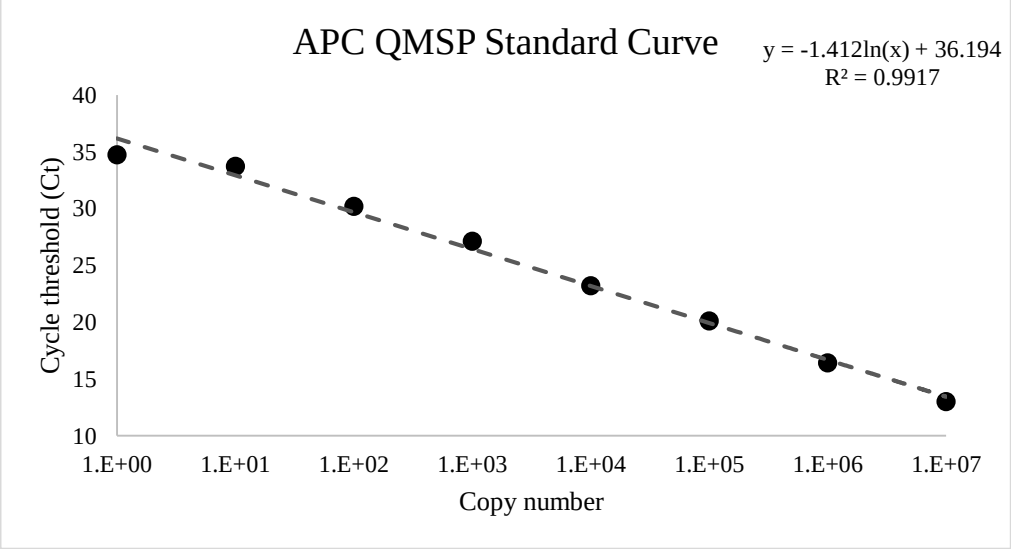


**Figure 3.28 APC standard curve after the final cycling condition optimizations.** *Freshly prepared plasmid standards and new dilutions of primer – probe pair for APC QMSP reactions showed a good fitting, reproducible curve with good separation between dilution points. Curve generated with 2 technical replicas for each copy number dilution.*

With the second set of primer pairs we first performed qPCRs using unmodified oligonucleotides and SYBR-Green **(Figure 3.29-Figure 3.31)**. Similar to the first set of primers, these could efficiently amplify the targets. We did not detect a significant improvement in the standard curve fit or the range compared to the first set. However, as the previous primer pair showed there can be marked differences in the sensitivity of QPCR and QMSP reactions, we also tested the QMSP reaction of the new primer pair with Scorpions probes. **(Figure 3.32-Figure 3.34).**

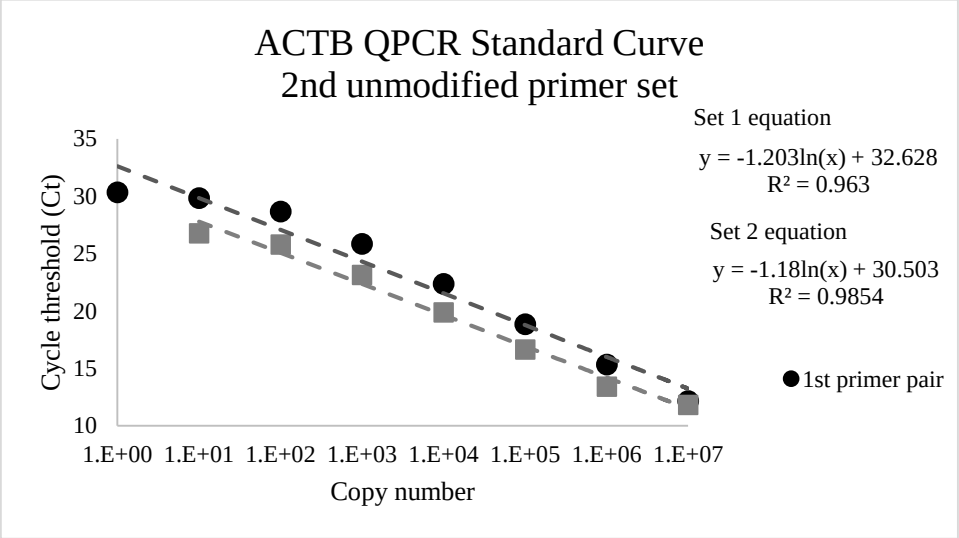


**Figure 3.29 ACTB QPCR St. Curve, 2nd primer set.** *Curves generated with 2 technical replicas for each copy number dilution.*

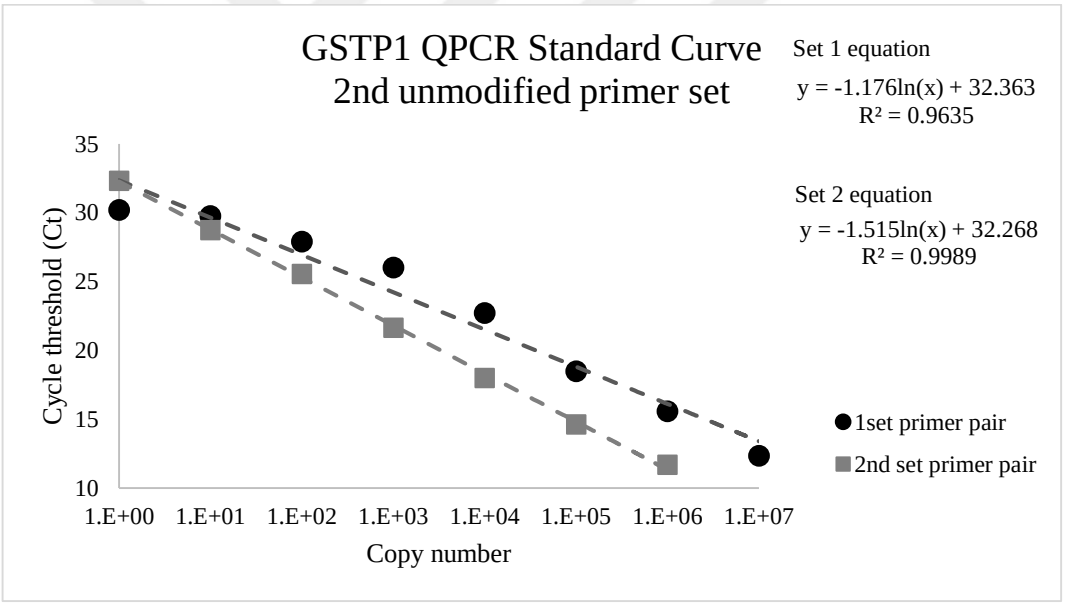


**Figure 3.30 GSTP1 QPCR St. Curve, 2nd primer set.** *Curves generated with 2 technical replicas for each copy number dilution.*

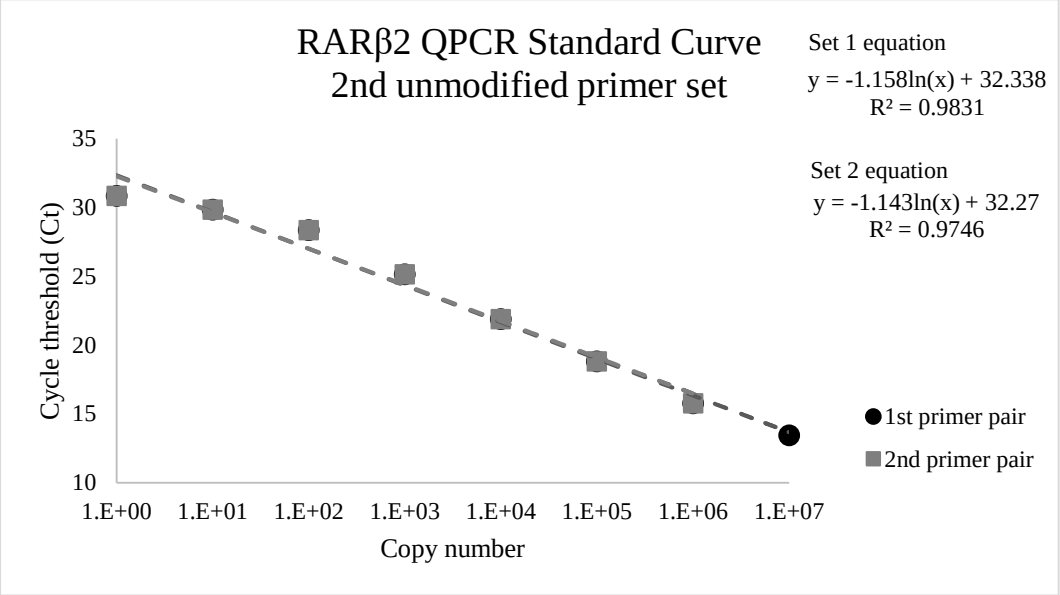


**Figure 3.31 RARβ2 QPCR St. Curve, 2nd primer set**. *Curves generated with 2 technical replicas for each copy number dilution.*

The second set of primers produced slightly better curve for ACTB than the first one. While the second pair had a better fit for GSTP1, it did not improve RARB2 curve.

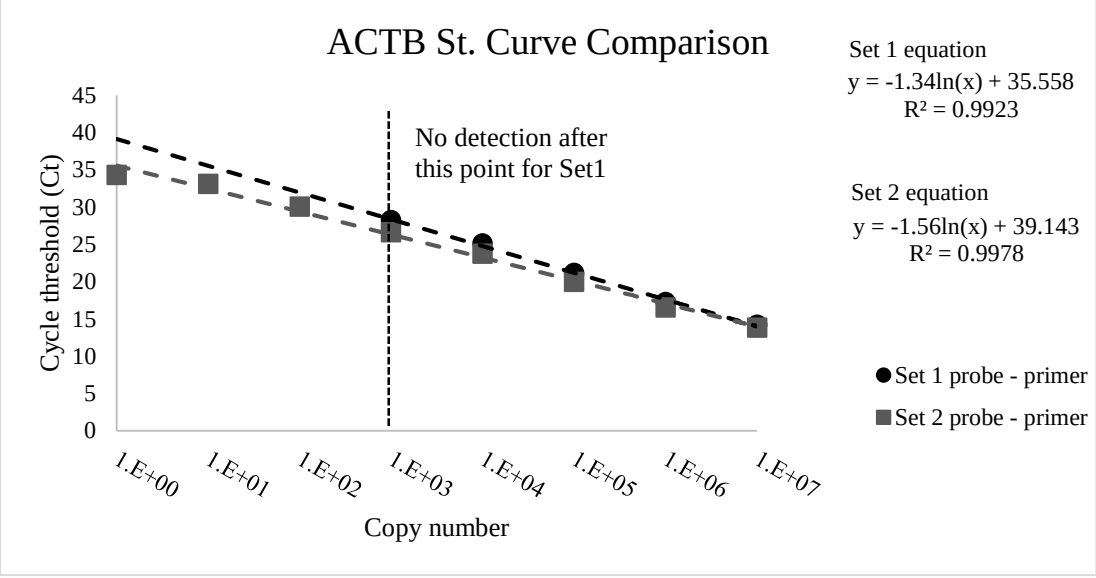


**Figure 3.32 Comparison of two different primer – probe pairs for ACTB amplification.** *Curves generated with 2 technical replicas for each copy number dilution.*

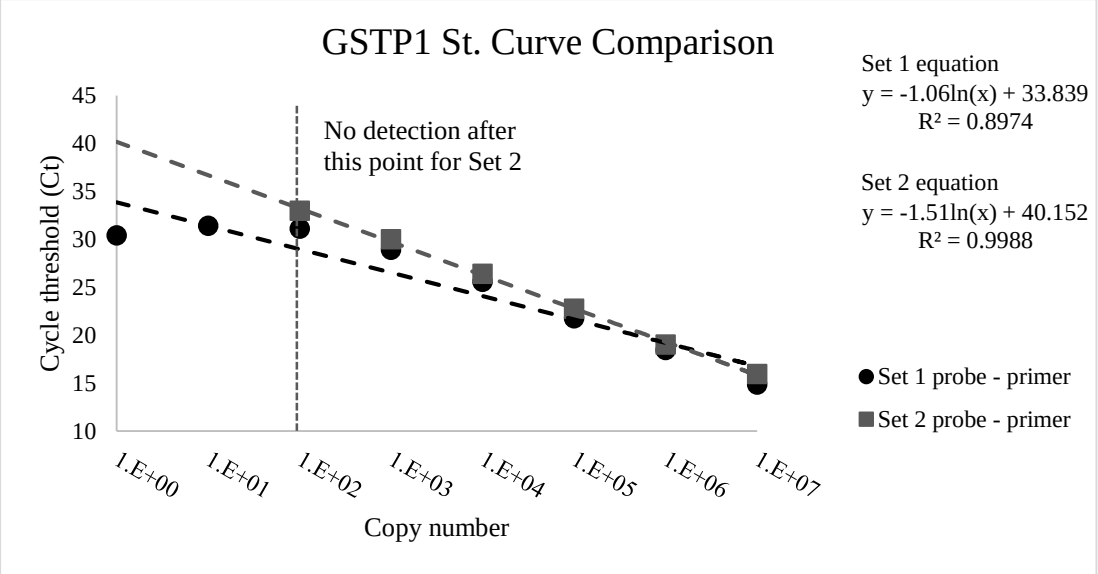


**Figure 3.33 Comparison of two different primer – probe pairs for GSTP1 amplification.**
*Curves generated with 2 technical replicas for each copy number dilution.*

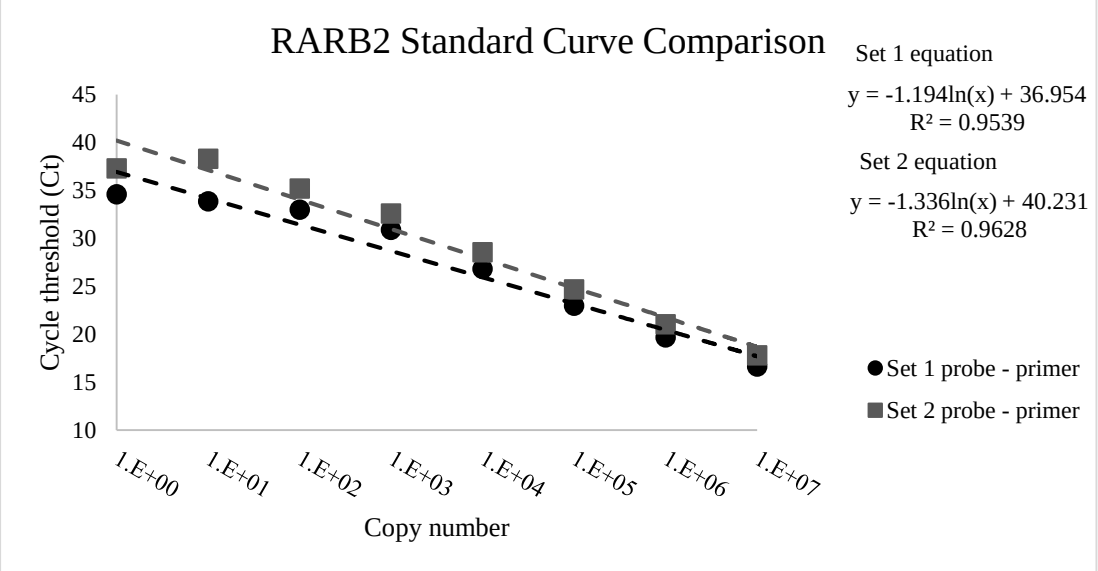


**Figure 3.34 Comparison of two different primer – probe pairs for RARB2 amplification.**
*Curves generated with 2 technical replicas for each copy number dilution.*

*Assay controls*

Having initially optimized assay conditions with Scorpion Probes we then tested the signal strength of our QMSP assay with universal methylated and unmethylated gDNA. These two references can therefore both confirm the selectivity of a probe-primer pair to a single genomic region as well as the experimental limit of detection with gDNA.

Two different commercially available universal methylated and unmethylated gDNA controls were used in the QPCR and QMSP runs. One set required bisulfite reaction while the other was already bisulfite converted. This allowed us to selectively test both the bisulfite conversion assay and QMSP. Therefore, we initially tested the non-bisulfite converted controls to ensure that our commercially available conversion assay was functional before moving on to the pre-converted gDNA.

**Figure 3.35** shows the universal methylated and unmethylated gDNA controls for the first primer probe pairs with 0.5ng gDNA or ~145 genome copies. As expected we observed a similar signal with the methylated and unmethylated gDNA with our normalization control (ACTB) as this genomic region is not methylated. However, the Ct value was close to our limit of detection. For both APC and RARB2 we observed a clear separation between methylated and unmethylated gDNA demonstrating that the assay is working. In contrast with GSTP1 we didn't see any separation between the two controls. Next we tested the universally methylated or unmethylated gDNAs with the second set of primer – probe pairs **Figure 3.36.** Although ACTB showed no separation between the controls, the Ct values were once again quite close to the limit of detection of the standard curve. Further while RARB2 demonstrated improved separation between the controls compared to first primer pair **(Figure 3.35),** no signal was obtained for GSTP1 as the second Scorpion probe did not work.

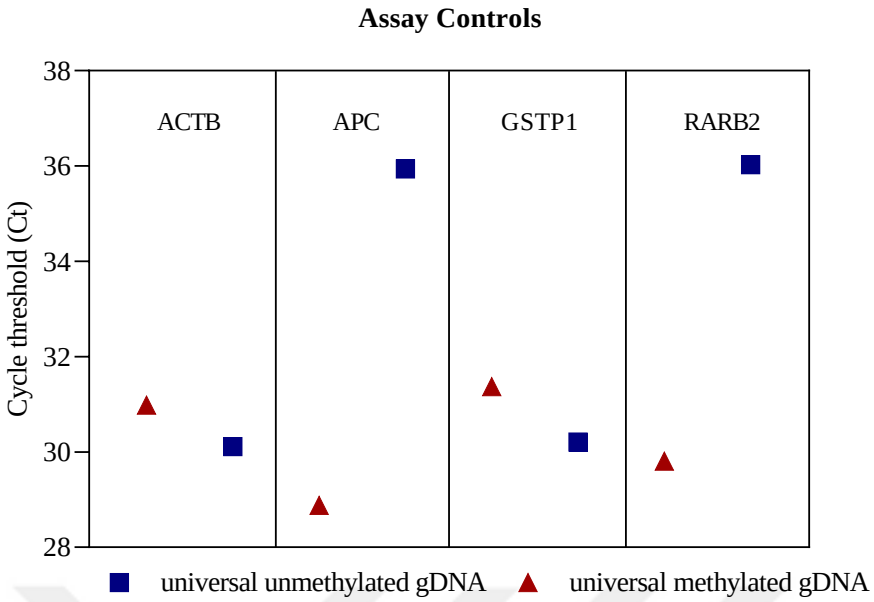


**Figure 3.35 QMSP Assay controls with universal methylated and unmethylated gDNA.** *All controls were run at the same conditions, volume and concentration. First set of primer – probe pairs were used.*

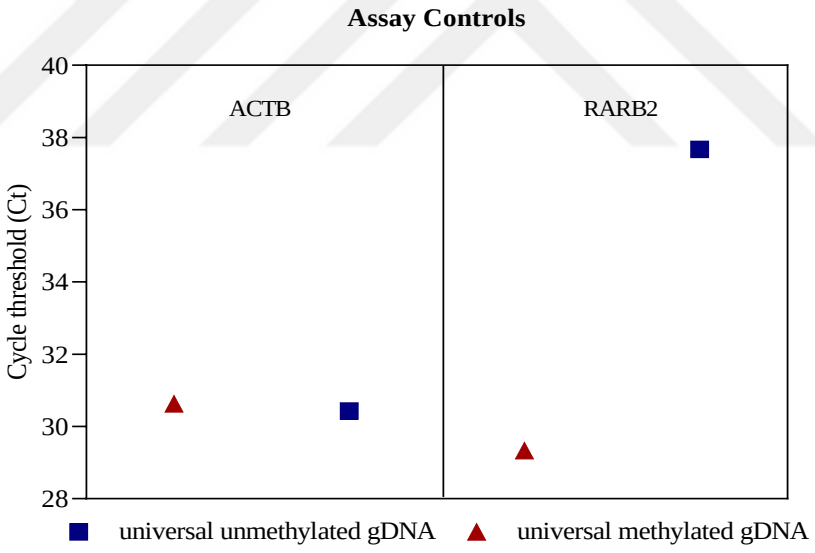


**Figure 3.36 QMSP Assay controls with universal methylated and unmethylated gDNA.** *All controls were run at the same conditions, volume and concentration. Second set of primer – probe pairs were used. No signals could be observed for GSTP1, and APC is not displayed since primer – probe couple was not changed for the region.*

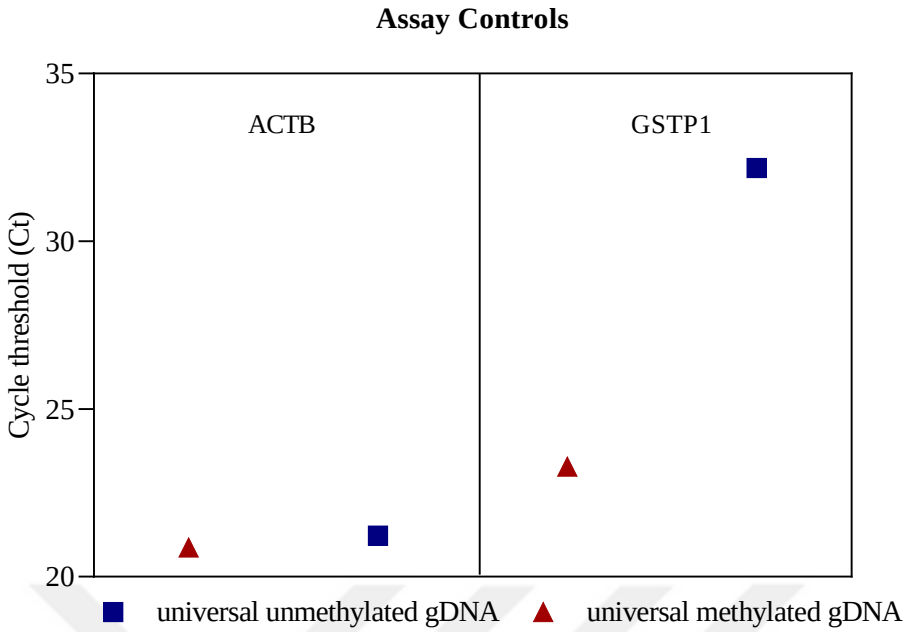


**Figure 3.37 QPCR assay controls with universal methylated and unmethylated gDNA.** All controls were run at the same conditions, volume and concentration. *Forward primer sequence of the second Scorpion probe used for ACTB. Forward primer sequence of the first Scorpion probe used for GSTP1.*

Given the poor limit of detection and amplification with our Scorpion probes for ACTB and GSTP1 we then attempted a QPCR assay with our control samples using with SYBR green as our detection method. With this we observed excellent amplification and separation between the universally methylated and unmethylated genomic DNA. Importantly, we only observed a single product in the melting curve analysis of these PCR products. From these results we chose to use a hybrid of methylation assays. Specifically, we would use our optimized QMSP assay for both APC and RARB2 while we would use a QPCR assay for ACTB and GSTP1. With this mixed approach we obtained excellent detection in both our universally methylated and unmethylated controls **(Figure 3.38)** and standard curves **(Figure 3.39-Figure 3.42)**. Overall, these reactions were very reproducible with a good fit and low limit of detection.

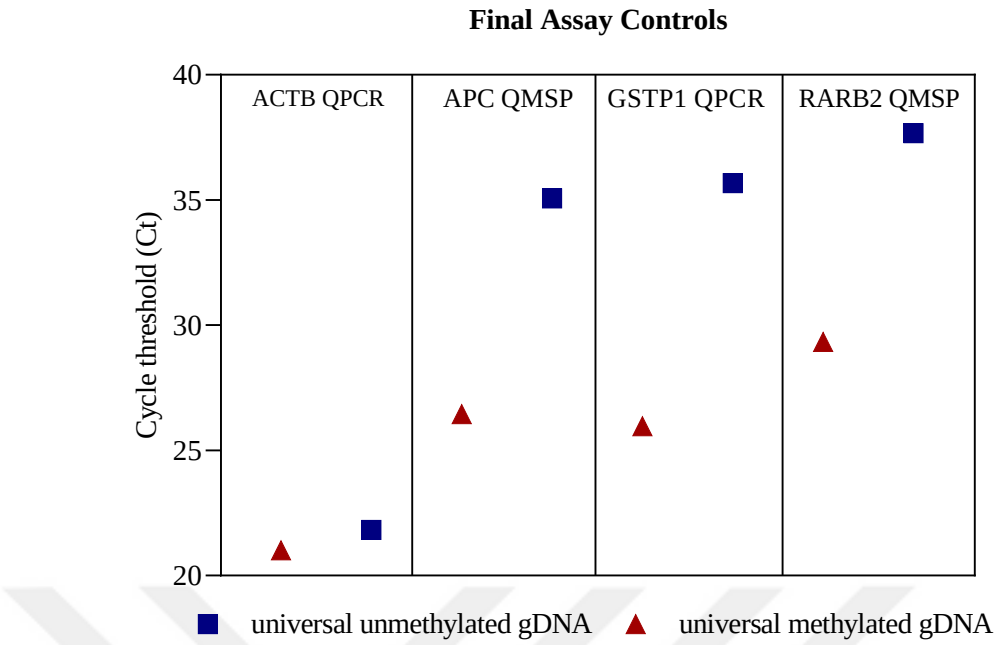


**Figure 3.38 Assay controls with universal methylated and unmethylated gDNA.** *ACTB and GSTP1 controls were run in QPCR; APC and RARB2 controls were run in QMSP reactions with the corresponding primers or probes.*

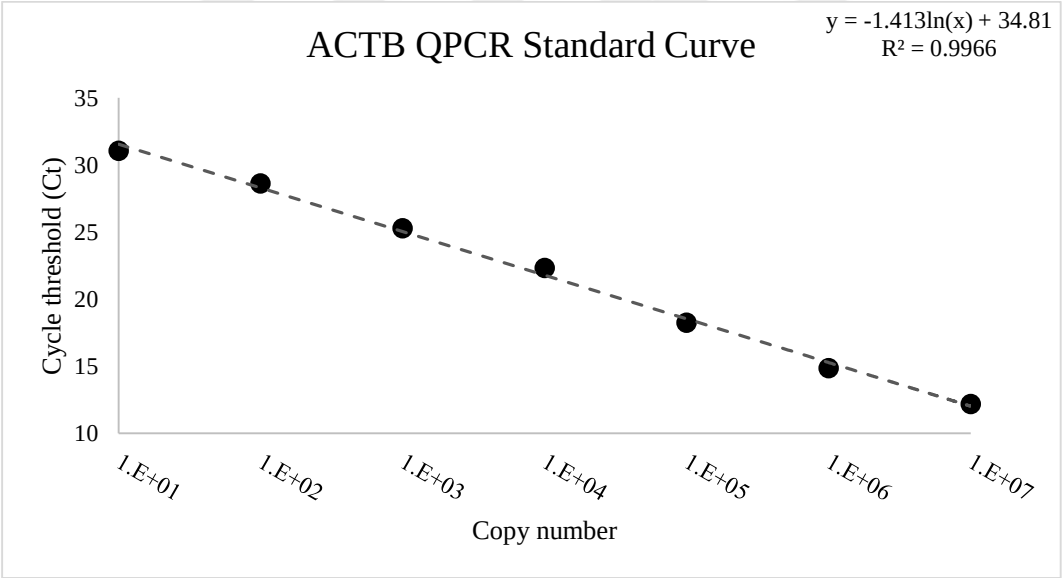


**Figure 3.39 ACTB QPCR standard curve.** *The curve is generated with respect to the final decision on primer couples and the optimized mixture and cycling conditions. Curve generated with 2 technical replicas for each copy number dilution.*

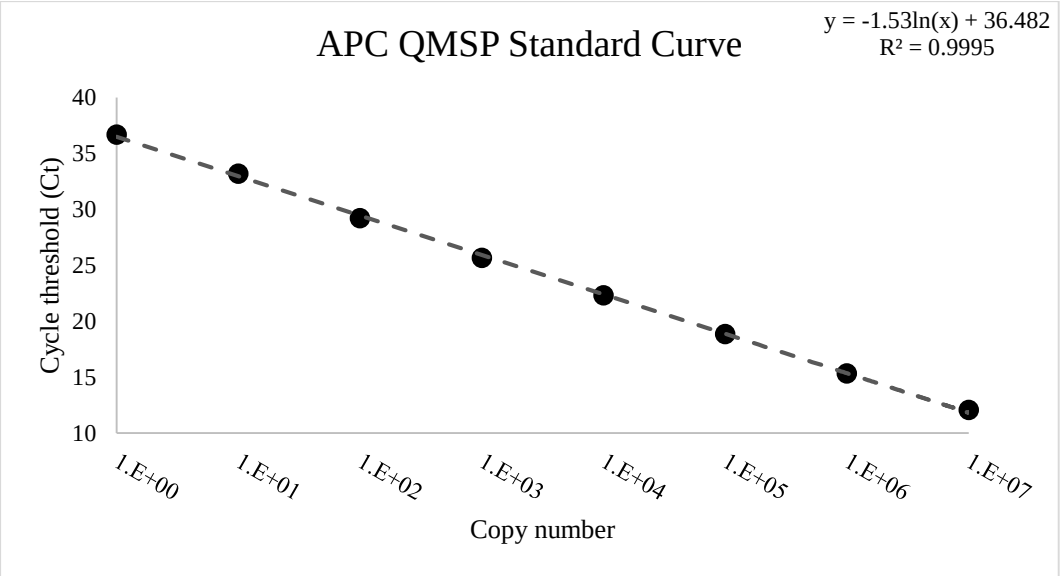


**Figure 3.40 APC QMSP standard curve.** *The curve is generated with respect to the final decision on primer – probe pairs and the optimized mixture and cycling conditions. Curve generated with 2 technical replicas for each copy number dilution.*

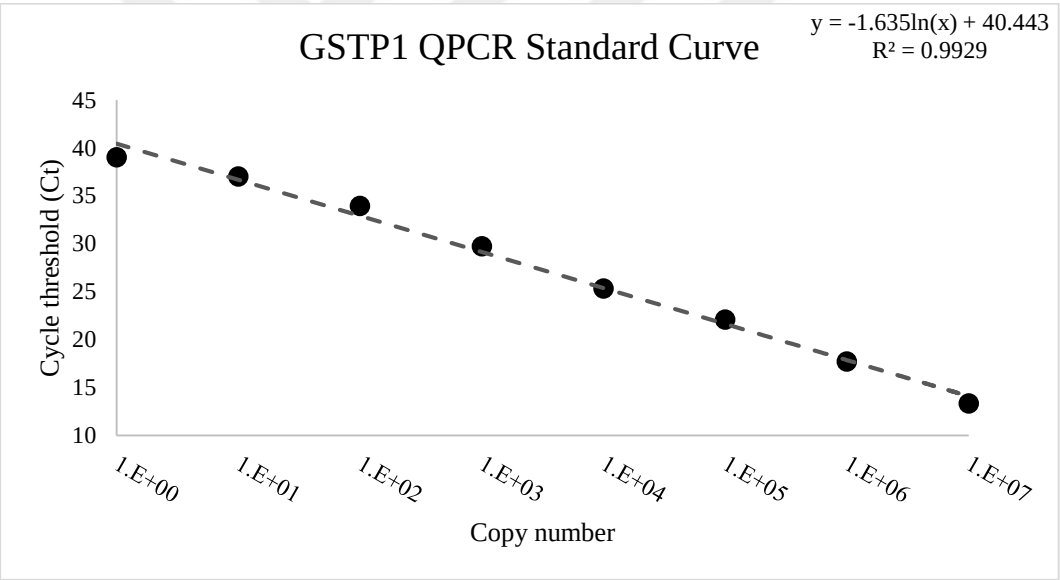


**Figure 3.41 GSTP1 QPCR standard curve.** *The curve is generated with respect to the final decision on primer – probe pairs and the optimized mixture and cycling conditions. Curve generated with 2 technical replicas for each copy number dilution.*

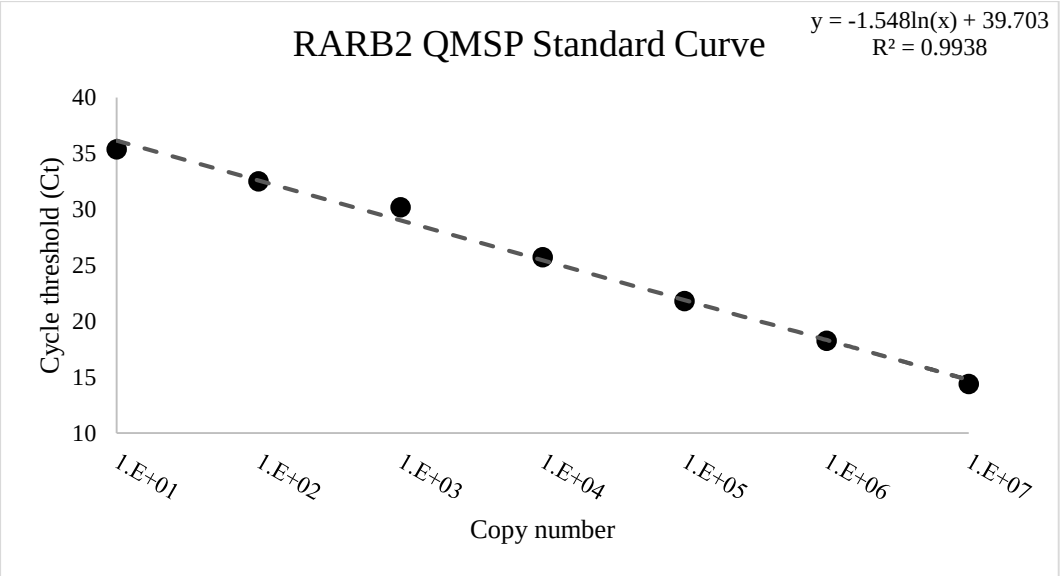


**Figure 3.42 RARB2 QMSP standard curve.** *The curve is generated with respect to the final decision on primer – probe pairs and the optimized mixture and cycling conditions. Curve generated with 2 technical replicas for each copy number dilution.*

### 3.2.4.3 Utility of the optimized QMSP and QPCR assays with clinical samples

Next we tested our optimized QMSP and QPCR assays with a small number of clinical prostate samples. We used FFPE tissues with confirmed benign or malignant histopathology and aimed to test the separation between the tissues of two distinct characteristics. We used a 10µM paraffin sections from needle biopsies of the malignant samples to match the proposed protocol in our mpMRI cohort. With these sections, tissues were deparaffinized and gDNA isolated. Then, bisulfite converted and used as templates in the assays. **Figure 3.43** shows the ACTB copies of benign and malignant group of tissues and **Figure 3.44** shows the ACTB normalized QPCR and QMSP results of the three epigenetic markers. Amplification was observed at different levels for different genes due to relative gDNA yields. High Ct values observed for some samples suggest that we will likely have samples beyond our detection limit. From this and the universally methylated controls we selected an ACTB threshold of 150 copies to ensure sufficient template for each sample analyzed.

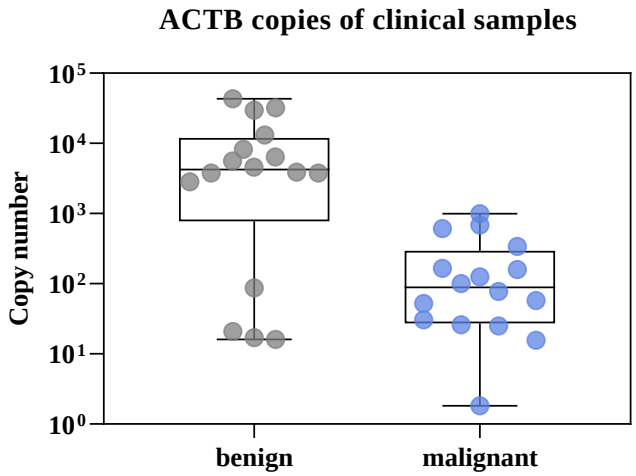


**Figure 3.43 ACTB copy number of the clinical samples run in ACTB QPCR assay.**

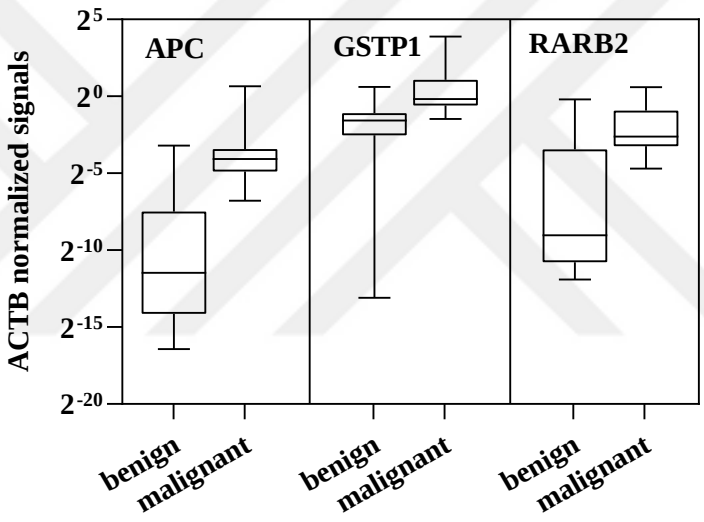


**Figure 3.44 ACTB normalized signals of epigenetic markers.**

## 3.3 Application of QMSP method

### 3.3.1 Patient data and samples

Radiographically suspicious but histopathologic benign prostate biopsies were collected with the help of Drs. Ömer Acar and Mert Kılıç from patients who were treated at the American Hospital (Istanbul, Turkey) from 2012-2020. Samples were collected mpMRI guided in-bore biopsy by a single radiologist with extensive experience thereby limiting potential variability or sampling errors. All radiologically suspicious biopsy lesions were classified in accordance with the Prostate Imaging – Reporting and Data System version 2 (PI-RADS) on a 1-5 scale. Lesions deemed to be radiographically suspicious were scored as either group 4 or 5, suggesting that these biopsies are likely or highly likely to

be clinically significant cancer. A representation of these radiographically suspicious regions are shown in **Figure 3.45** and **Figure 3.46.** Multiple biopsies were collected if possible from each patient to limit sample collection artifacts. Similar mpMRI guided in-bore biopsies (PIRAD 4 or 5) were also collected from patients who had histopathologic malignant lesions.

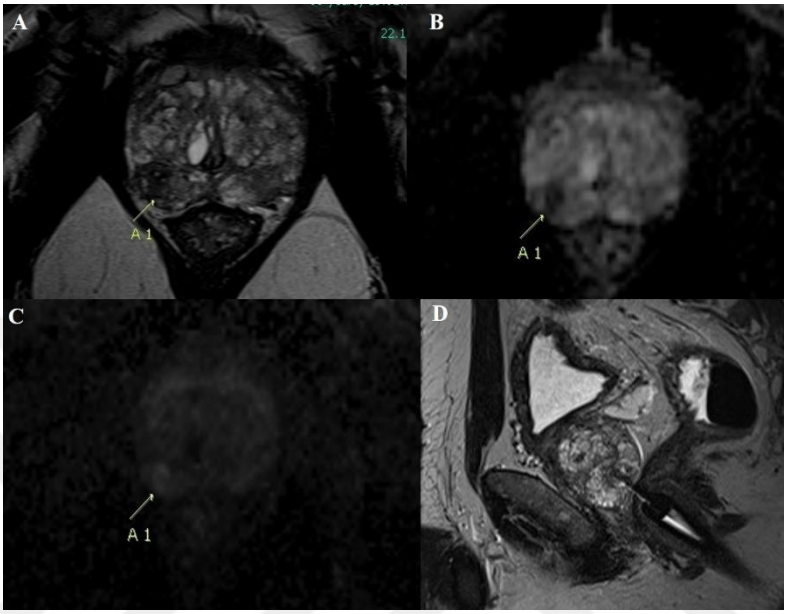


**Figure 3.45 A 60-year-old man with elevated PSA of 2.8 ng/mL.** *(A) Axial T2W image shows an area of decreased T2 signal intensity in the right peripheral zone at the level of apex (arrow). (B) Axial ADC map and (C) axial calculated high b-value DWI (b=1600 s/mm2) demonstrate corresponding marked restricted diffusion (arrow). The lesion is compatible with a PI-RADS category 5. (D) Image obtained with the needle guide in the appropriate position for biopsy shows insertion of an 18-gauge MR-compatible biopsy needle directed to the target lesion. Pathology result was benign.*

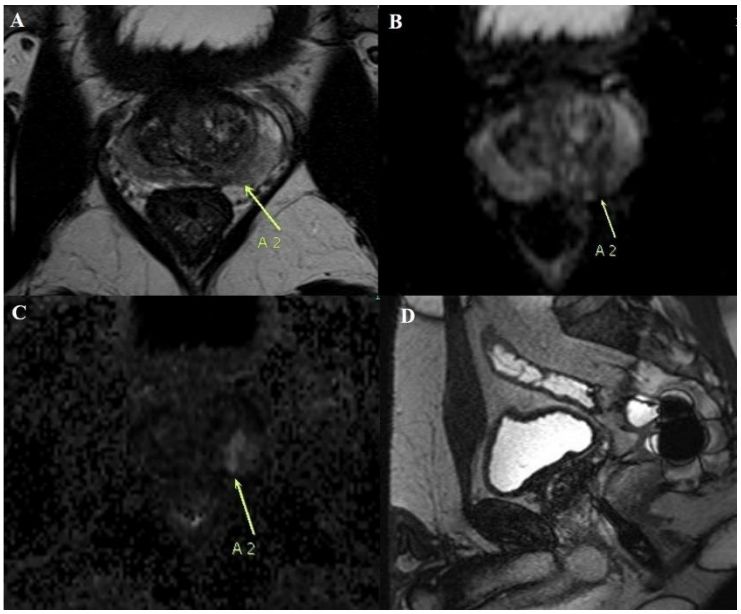


**Figure 3.46 A 58-year-old man presenting with elevated PSA (5.4 ng/mL).** *(A) Axial T2W image shows area of hypointensity in the left peripheral zone. The mass shows low signal intensity on ADC map (B) and high signal intensity on calculated high b-value (b=1600 s/mm2) DWI (C) (arrow). The PI-RADS assessment category is 4. (D) Note the biopsy needle directed to the target area. Target biopsy revealed prostatic adenocarcinoma, Gleason score 8(4+4) involving 48% of 5 cores.*

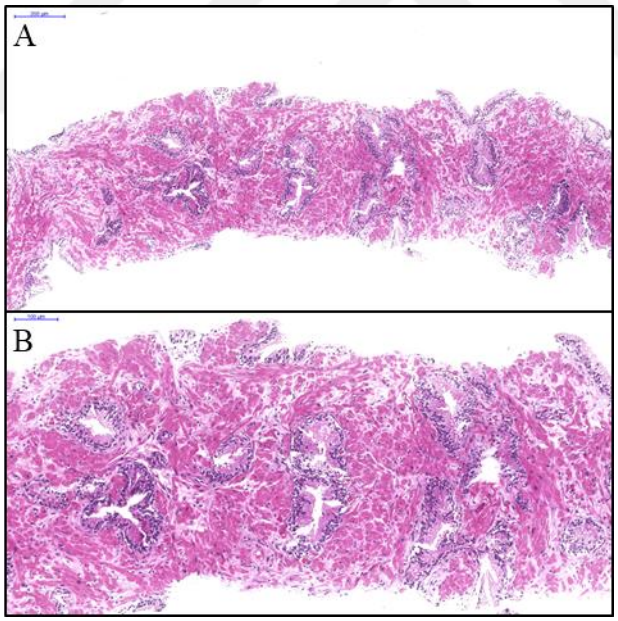


**Figure 3.47 Histopathology images of a patient in MRI group.** *(A) Benign prostatic glands in fibromuscular stroma (H&E, 8.3x). (B) Benign prostatic glands (H&E, 14.4x).*

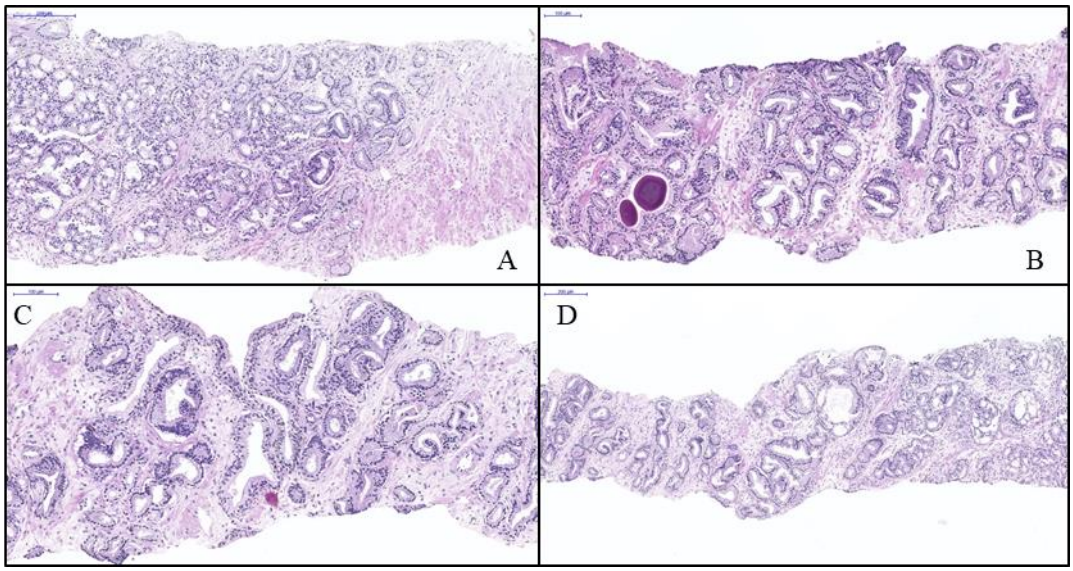


**Figure 3.48 Histopathology images of a patient in malignant group.** *(A) (Left) Large tumor nodules create cribriform pattern (Gleason pattern 4) and to the right well-formed glands (Gleason pattern 3). (Right) Benign prostate glands (H&E, 11.6x). (B) Gleason 3+3 carcinoma mixed with benign glands, one of them containing corpora amylacea within the lumina. (H&E, 13.7x). (C) Gleason pattern 3 adenocarcinoma mixed with benign glands (H&E, 16.7x). (D) Pattern 3 (left) and pattern 4 (right); Stromal reaction is generally not evident in prostate cancer (H&E, 8.1x).*

As mpMRI biopsies will only be collected in those patients who likely have PCa it was not possible to have a negative control group of benign prostate tissue collected with the same protocol. Therefore, we utilized a transurethral resection of prostate (TURP) from 12 patients admitted to American and Acibadem Hospital (Istanbul, Turkey) who were treated for BPH. Importantly, all benign TURP samples were confirmed by histopathology.

From these patients, a total of 150 biopsy cores consisting of 138 in-bore biopsies and 12 TURP sections ("benign") were retrospectively collected. Within the in-bore biopsies, 82 paraffin sections from 28 patients were found to be both radiologically and histopathologically malignant ("malignant"). The remaining 56 paraffin sections from 18 patients were radiologically suspicious but histopathological benign ("MRI"). Representative histopathology for MRI and malignant group of patients were shown in **Figure 3.47** and **Figure 3.48** respectively. The clinical information for the MRI and malignant patients is shown in **Table 3.1**. As described, all patients in this study were either PIRADS 4 or 5 **(Figure 3.53).** We did not observe any significant difference in patient clinical parameters including age (unpaired t-test with Welch's correction, $p$=0.32, 95%CI), or PSA levels (p= 0.14, 95%CI) **(Figure 3.49, Figure 3.50).** The majority of patients in the malignant group identified as ISUP 2 **(Figure 3.52),** formerly described as

Gleason 3+4 or Grade Group II. Multiple cores were collected from each patient during mpMRI guided biopsies to reduce potential sample artefacts. On average, 3.0±1.2 cores were collected from each patient in the malignant group and 3.0±1.3 cores for the ones in the MRI group. The distribution of the total number of cores per patient in each patient pool are shown in **Figure 3.53.**

**Table 3.1 Clinical data for the patients used in this study.**

| | Malignant | MRI |
|---|---|---|
| Number of patients [N] | 28 | 18 |
| Number of cores | 82 | 56 |
| Age | | |
| Mean [years] | 65.5 | 62.7 |
| Median [years] | 66.5 | 64.5 |
| Range [years] | 55-78 | 45-70 |
| Preoperative PSA [ng/mL] | | |
| Mean | 6.9 | 7.7 |
| Median | 6.1 | 6.1 |
| Range | 2.9-17 | 2.5-30 |
| < 4 [n] | 8 | 3 |
| 4-10 [n] | 14 | 11 |
| > 10 [n] | 6 | 3 |
| unknown | 0 | 1 |
| ISUP Grading [n] | | |
| 1 | 4 | N/A |
| 2 | 14 | N/A |
| 3 | 5 | N/A |
| 4 | 3 | N/A |
| 5 | 1 | N/A |
| unknown | 1 | N/A |
| PI-RADS Group [n] | | |
| 4 | 19 | 13 |
| 5 | 9 | 5 |

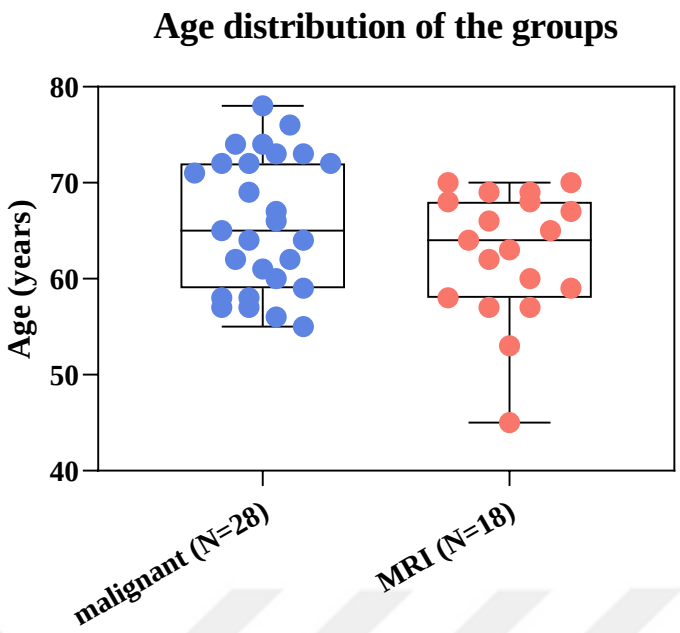


**Figure 3.49 Age distribution across the malignant and MRI group.**

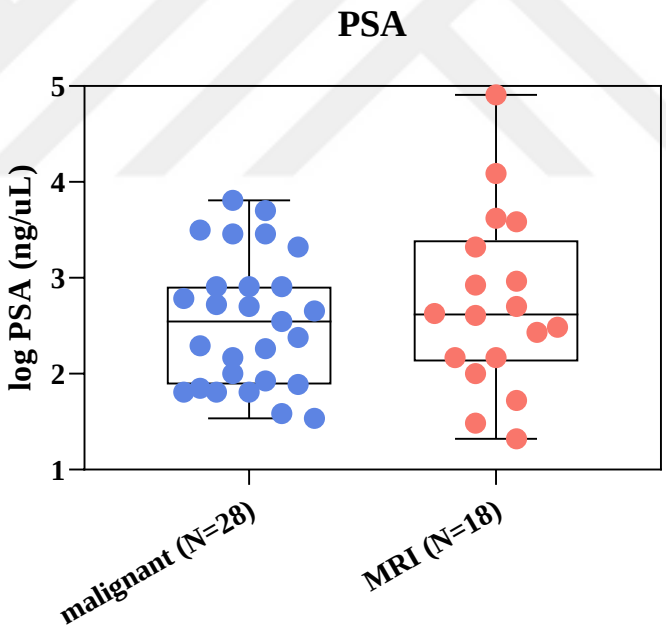


**Figure 3.50 Distribution of PSA level across malignant and MRI group.**

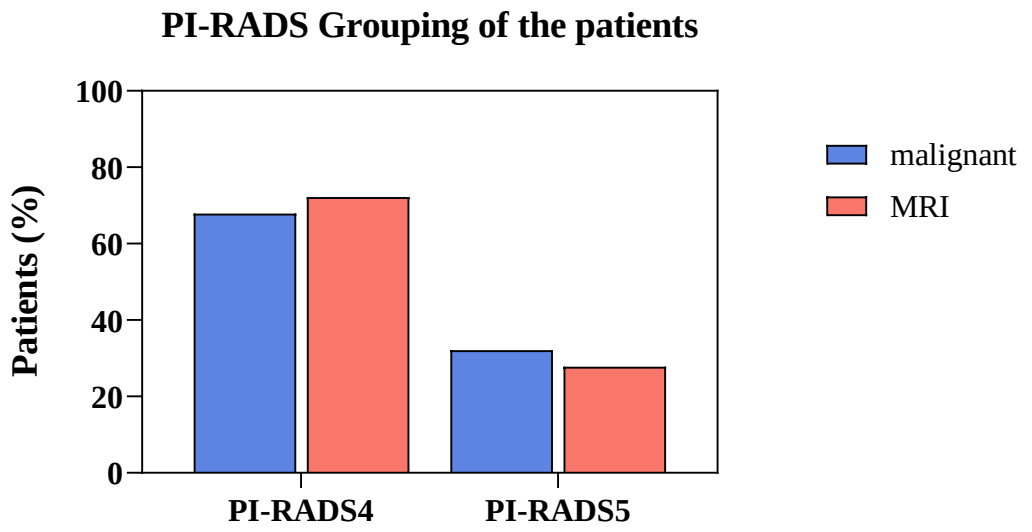


**Figure 3.51 Distribution of patients in PI-RADS groups.**

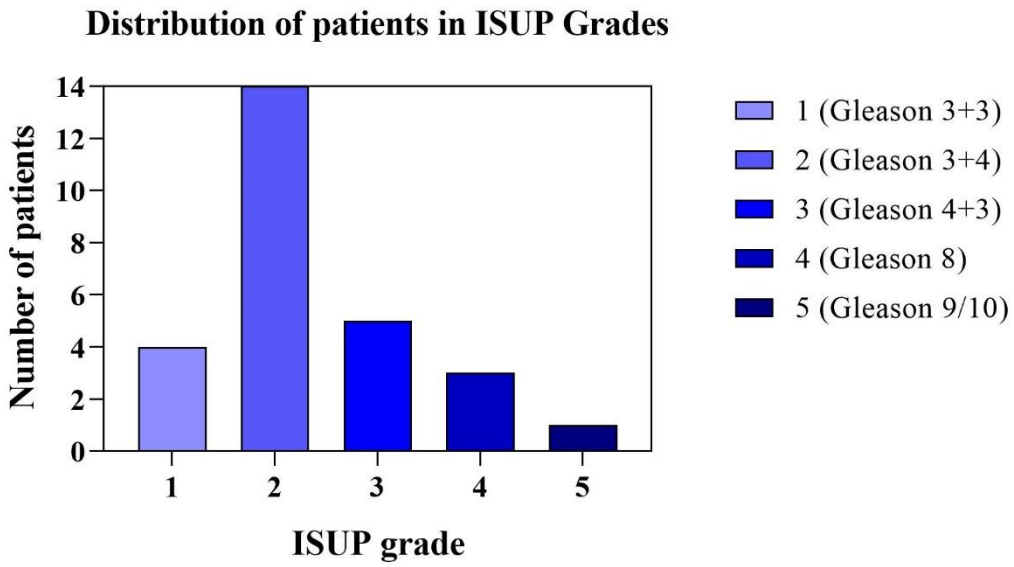


**Figure 3.52 Distribution of number of patients in ISUP groups.**

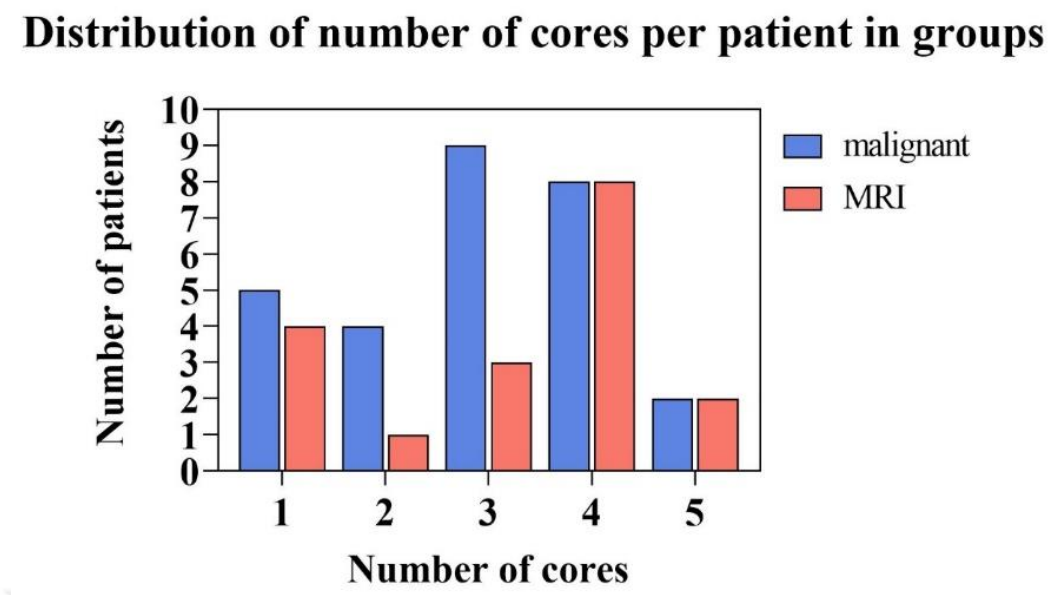


**Figure 3.53 Distribution of cores per patient in groups.**

### 3.3.2 Quantification of methylation in MRI cohort

The MRI cohort were composed of patients presenting radiographically suspicious lesions that were histopathologically benign. Their unconfirmed malignancy may potentially be due to epigenetic alterations that occur during PCa development. To quantify these alterations in these biopsy samples we utilized our optimized DNA methylation assay.

The first step of the analysis was to isolate and convert gDNA from each clinical sample. With bisulfite converted gDNA we then quantified the PRG methylation using our optimized assay. First we generated a standard curve of the cloned plasmids to calculate the copy numbers of each sample. This was performed with each PCR plate to reduce variability and error. Next, the ACTB copy numbers were calculated to determine the amount of gDNA in each sample. This value was used to normalize the copy numbers obtained for APC, GSTP1 and RARβ2. We set a minimum threshold of 150 genome copies calculated by ACTB to ensure a sufficient amount of template.

The ACTB normalized samples in **Figure 3.54** shows that the distribution of signals differ dramatically for APC, GSTP1 and RARβ2 in our clinical cohorts. As expected **(Figure 3.54),** benign patient group samples showed the weakest signals within each PRG, while malignant group had the strongest. Excluding APC, the MRI group samples had methylation levels that were lower than malignant group but higher than benign group.

For APC, the malignant group showed the strongest normalized readouts with a mean and standard deviation of 2.97±5.86. However, compared to malignant group, the benign and MRI group of samples were quite low with 0.11±0.21 and 0.01±5.86 respectively. For GSTP1, the malignant group again had the strongest normalized readouts with a mean of 726.8±698.5 while for the MRI group also had markedly elevated DNA methylation with a mean normalized readouts of 691.1±929.0. In contrast the benign group only had normalized readouts of 37.4±24.5. Finally, RARβ2 had a similar trend as GSTP1, with malignant samples having the highest mean of readouts obtained (12.96±19.75). While reduced, the MRI group also had an increased average readout (0.90±1.54) compared to the benign group (0.17±0.11). To better characterize each sample in the corresponding groups, the cores were scored in a binary fashion as either methylated (positive) or non-methylated (negative). The methylation cut-off ratio for each region were chosen heuristically from both the benign and malignant groups and the universally methylated and unmethylated controls **(Figure 3.54)**.

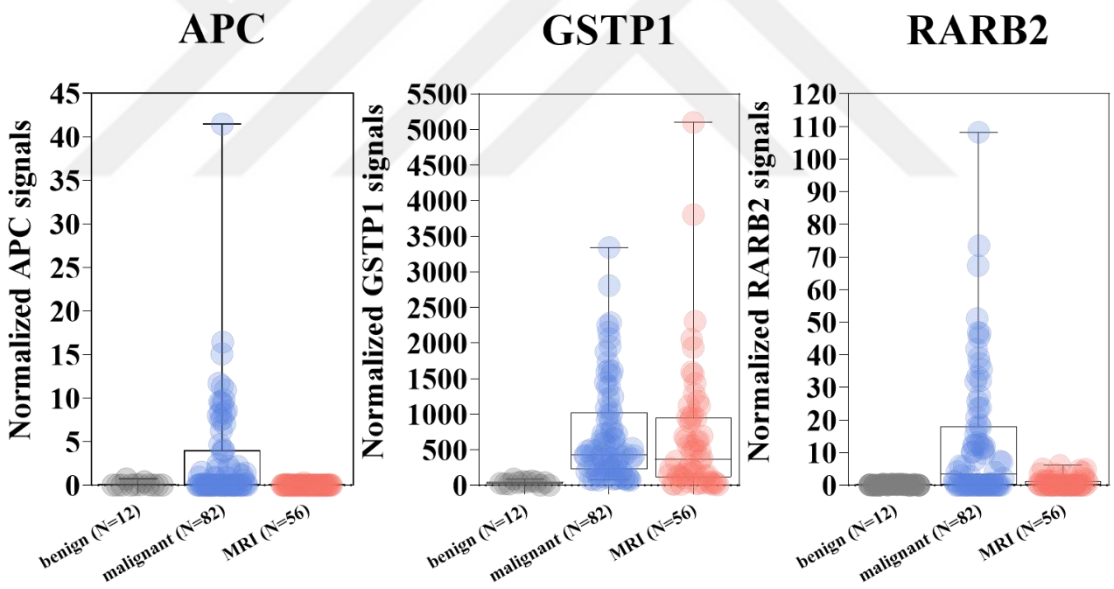


**Figure 3.54 ACTB normalized signals for the epigenetic markers.**

### 3.3.3 Percent methylation in patient groups

Consistent with previous reports (97,111,113,142), the malignant patient biopsies were frequently methylation positive in these genetic regions while all biopsies in the benign group were methylation negative. This obvious difference between the two groups clearly demonstrates that our methodology can distinguish between these sample populations. Interestingly, the proportion of methylation positive samples in MRI group was also

increased compared to the benign group for all regions except for APC. In the malignant group, APC was methylated in 37.8% samples (31/82 cores) while no cores in the MRI or benign group were methylated. However the proportion of methylated APC biopsies within the malignant group, was similar to previously publications that typically ranged from 27% to 90% (111–113). GSTP1 showed the clearest difference between the groups with, 92.7% (76/82 cores) of malignant samples, 0% (0/12 cores) of benign and 76.8% (43/56 cores) of MRI samples being methylated. Finally, RARβ2 was methylated in 57.3% (47/82 cores) of malignant samples, 0% (0/12) of benign samples and 33.9% of MRI samples (19/56 cores). The percentage of cores with methylated gene promoters across the patient groups is shown in **Figure 3.55**. The three gene promoters had different efficiencies at distinguishing malignant and benign samples. With GSTP1 and RARβ2, both the number of positive cores and the difference between malignant and benign group is very prominent. In contrast APC methylation was only observed in a portion of the malignant samples. Overall, these results demonstrate that there is a difference in the epigenetic profile of radiographic suspicious malignant and benign prostate tissue.

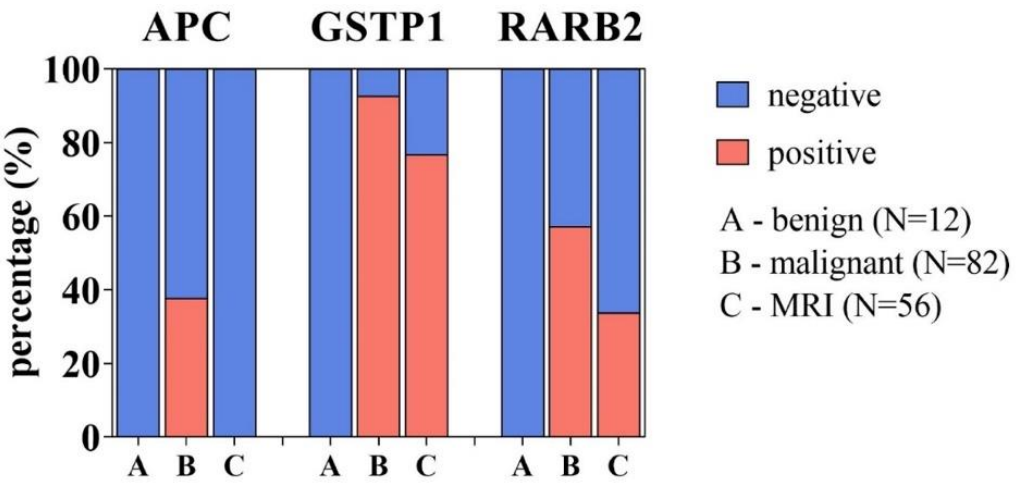


**Figure 3.55 Percent of cores showing signals in each patient group for all three markers.**

There was heterogeneity observed in the proportion of methylation positive PRG from a single biopsy. For the malignant group, there was a 0 cores (0%) with no methylation positive promoters, 35 cores (42.68%) with a single promoter, 19 cores (23.17%) with two promoters and 28 cores (34.15%) with all three promoters. In MRI group, 9 cores (16.07%) didn't show any methylation positive promoters, 32 cores (57.14%) had a single positive promoter, 15 cores (26.79%) with two positive markers promoters **(Figure 3.56).**

No core was positive in the MRI group for all three genes due to the lack of APC methylation observed in this cohort **(Figure 3.56).**

The total number of biopsies from a single patient that were methylated was quite variable due to the differing number of cores collected per patient **(Figure 3.53)**. For each patient in the cohort, all needle biopsy cores that were obtained at the time of the mpMRI was included to the analysis. However, not all collected cores provided sufficient genomic DNA and therefore were excluded from the analysis (**Figure 3.57**). This elimination meant some patients were also excluded from the study, creating a difference in the number of biopsy cores or patients included. The number of positive signals for each marker per individual patient is shown in **Figure 3.58.** Demonstrating the tumor heterogeneity, cores biopsied from the same patient were not always positive for the same markers. As expected, more biopsy cores analyzed from a single patient increased the chances of a variety in the marker positivity. This might be thought as a bias in the overall marker positivity, however, PCa is a multifocal and heterogeneous disease. Moreover, samples in mpMRI are generally collected from different lesions. Therefore, every different needle could be considered as a different sample even if it was taken from the same patient. This is also supported by the differences of positivity in the cores of the same patient. Namely, as shown in figure **Figure 3.58** and **Figure 3.62** each core from a single patient had different number of positive signals and also from different markers.

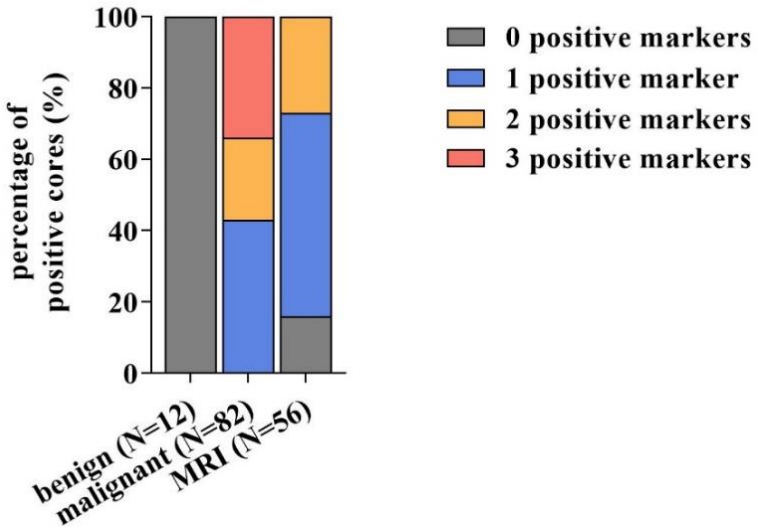


**Figure 3.56 Share of cores showing no signal, signals in one, two, or all three markers simultaneously across groups.**

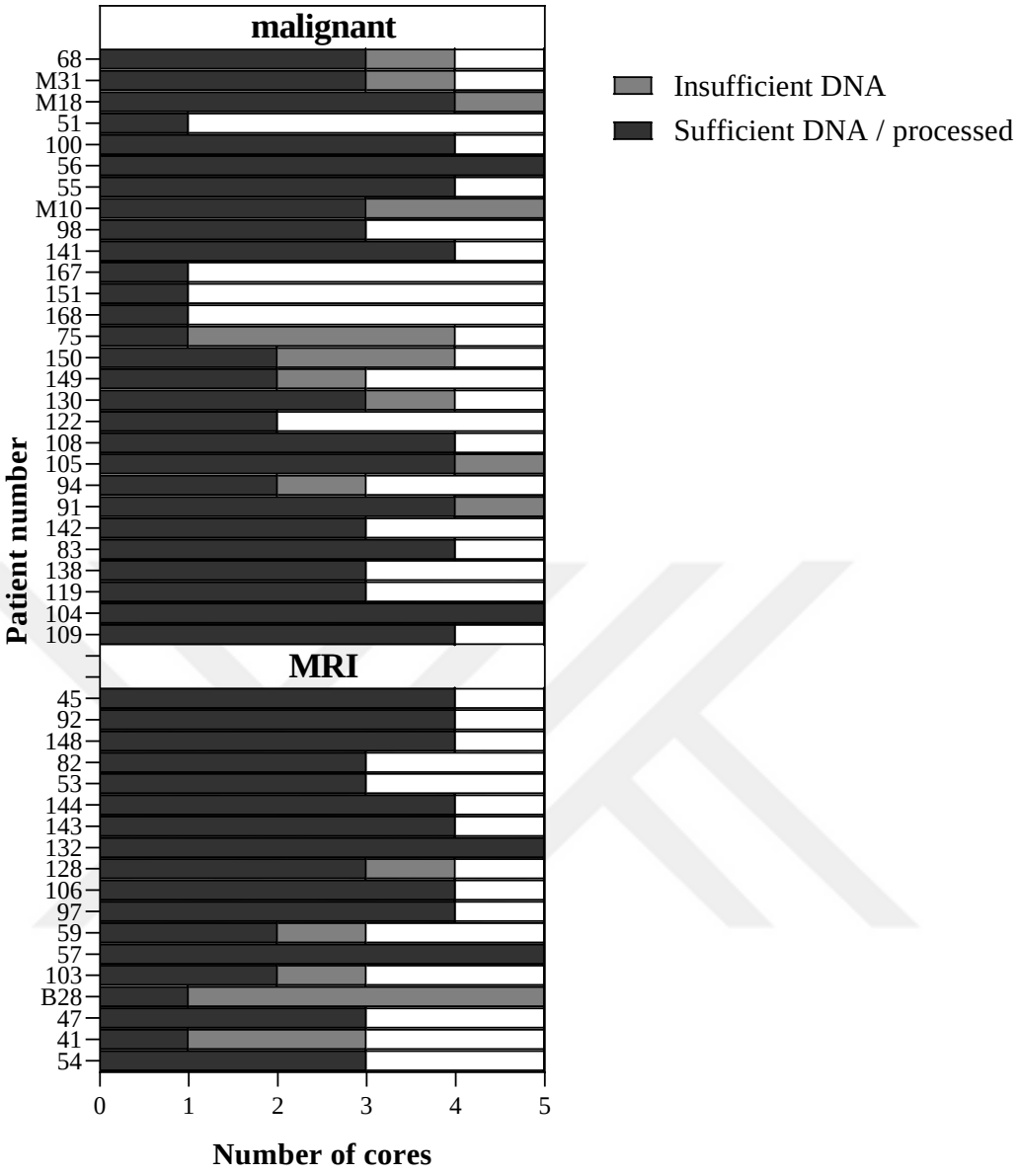


**Figure 3.57 Total number of cores analyzed per patient.**

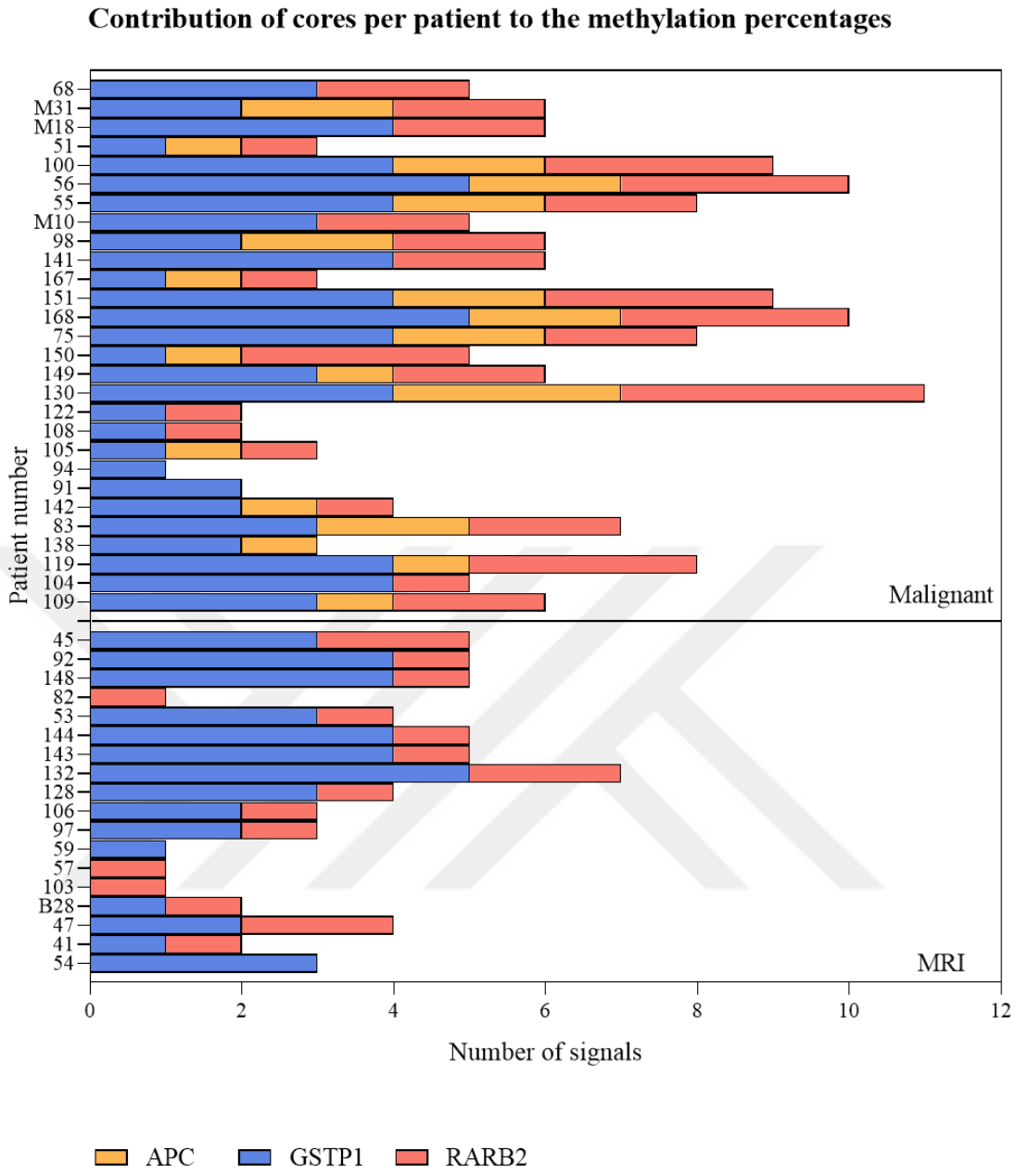


**Figure 3.58 Number of positive signals per patient across groups with respect to individual markers.**

Looking at the heterogeneity in methylation across all biopsies collected from a single patient, we observed marked variability between individual genes. The frequency of APC positivity from those biopsies collected from a single patient were different than the positivity pattern of GSTP1 and RARβ2 which could be a result of those samples with no signal (**Figure 3.59)**. For GSTP1, all but three cores in the malignant group were positive (**Figure 3.60)**. Similarly, most of the cores in MRI group were also positive and there was only one patient (Patient #57) in MRI group that did not show any positivity in any of the five analyzed biopsies. While GSTP1 methylation in MRI group was observed more than

half of the cores (76%) this was still a lower percentage than the malignant group (93%). This suggests, together with the strong radiological indication, the biopsy cores in our MRI group of patients could indeed be premalignant lesions. For RARβ2, the heterogeneity of positive samples were more than that of APC but less than GSTP1 (**Figure 3.61)**. Similar to GSTP1 methylation, the MRI group patient cores had lower overall methylation level than malignant group. More than half of the of malignant samples (57.3%) were methylation positive while 33.9% of the MRI patient cores were positive for RARB2. Most of the MRI group of patients only had a single cores positive for RARB2 while most of patients in malignant group had several positive cores.

At the patient level, there was no pattern observed for individual core positivity **(Figure 3.62).** However, in malignant group overlapping APC and RARB2 positivity was observed in half of the patients. When comparing these results to clinical parameters or outcome we could not find any obvious correlation due to the relatively small number patients in this study. Overall our results suggest that radiographically suspicious but histopathologic benign samples undergo epigenetic alternations similar to premalignant lesions.

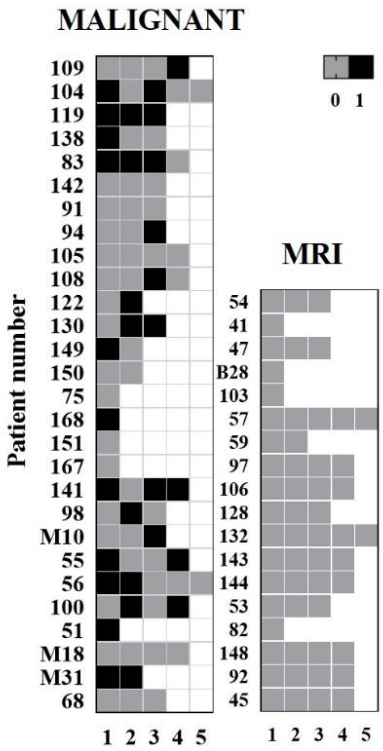


**Figure 3.59 APC positivity of each marker per patient in malignant and MRI groups.** *Grey cells indicate negativity and black ones positivity for APC. White cells indicate that there is no core available for the given patient. The bottom axis denotes the number of the core for each patient across the groups listed by its code along the vertical axis.*

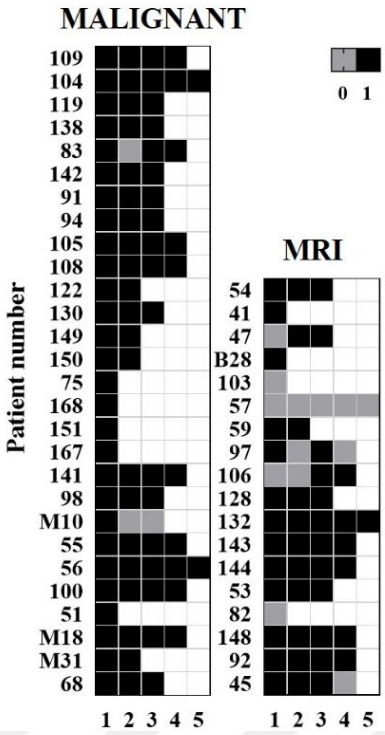


**Figure 3.60 GSTP1 positivity of each marker per patient in malignant and MRI groups.** *Grey cells indicate negativity and black ones the positivity for GSTP1. White cells indicate that there is no core available for the given patient. The bottom axis denotes the number of the core for each patient across the groups listed by its code along the vertical axis.*

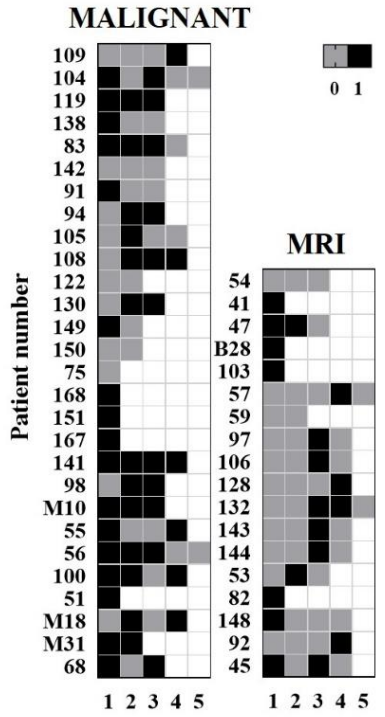


**Figure 3.61. RARβ2 positivity of each marker per patient in malignant and MRI groups.** *Grey cells indicate negativity and black cells denote the positivity for RARβ2. White cells indicate that there is no core available for the given patient. The bottom axis denotes the number of the core for each patient across the groups listed by its code along the vertical axis.*

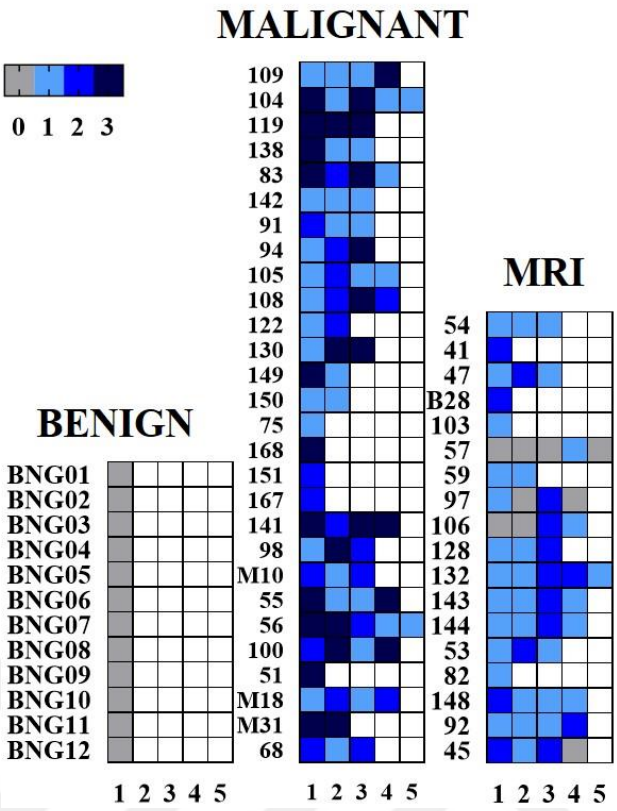


**Figure 3.62. Distribution of marker positivity per core per patient across groups.** *The color gradient cells show the level of positivity (0-3) for any of the three markers. White cells indicate that there is no core available for the given patient. The bottom axis denotes the number of the core for each patient listed by its code along the vertical axis.*

**Table 3.2 Clinical follow-up of patients in malignant group.**

| | Malignant group of patients (n=28) | |
|---|---|---|
| Treatment offered | # of patients | (%) |
| No follow up | 5 | 17.9 |
| Active surveliance | 2 | 7.1 |
| Radical prostatectomy | 13 | 46.4 |
| Radiotherapy | 7 | 25.0 |
| Hormonotherapy followed by radiotherapy | 1 | 3.6 |

**Table 3.3 Clinical follow-up of patients in MRI group.**

| | MRI group of patients (n=18) | |
|---|---|---|
| | # of patients | (%) |
| No new mpMRI | 11 | 61.8 |
| Regression in previous lesions | 6 | 33.3 |
| No change in previous lesions | 1 | 5.6 |

To determine if these epigenetically altered lesions in the MRI group progressed to malignant tumors we collected retrospective clinical information for all patients **(Table 3.3, Table 3.2).** As expected all patients in the malignant group were treated for PCa with most of them receiving a radical prostatectomy (46%) or radiotherapy (21%). For the available patient in the MRI group more than half of the patients (61%) did not have any further MRIs, biopsies or treatment due to either no change or slight increase in their PSA levels. Interestingly, of those these patients that further MRIs (n=6) only one had a stable lesion while the tumor actually regressed in the remaining six patients. To note, the MRI group of patients included in the study were admitted to American Hospital between 2014-2018 **(Figure 3.63)**. This suggests that the longest duration after the diagnosis of any patient can at most be 6 years. Since PCa is a slow progressing disease, this interval might not be long enough for us to confirm our suspicion of malignancy for these patients. While further follow up is needed our preliminary analysis suggests that the non-malignant lesions in the MRI group do not progress to a neoplastic tumor.

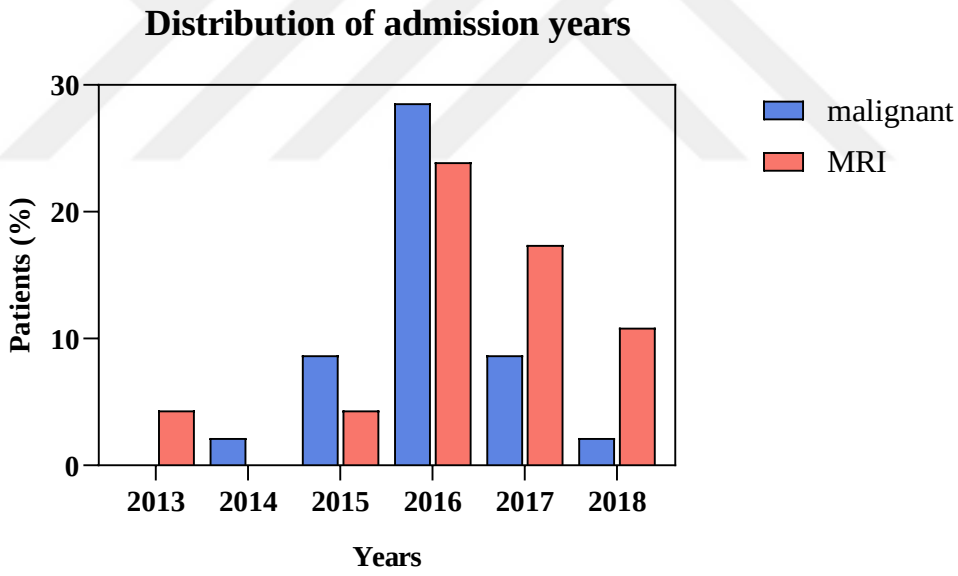


**Figure 3.63. Admission years of the patients in groups.**

# 4. DISCUSSION

In this thesis work, we characterized the DNA methylation of radiographically suspicious but histopathologically benign mpMRI in-bore prostate biopsies. The introduction of mpMRI has significantly improved PCa detection. However, it still is affected by a ~10% rate of false positives. Given the robust nature of MRI it is unclear if these false positive contain premalignant alterations or are simply a technical artifact.

To characterize the epigenetic alterations in these highly suspicious mpMRI-guided biopsies, we focused on three well characterized gene promoters, APC, GSTP1 and RARB2, which are commonly inactivated by hypermethylation early in PCa development (143–145). To analyze with these clinical samples, we first optimized a methylation assay that was compatible with challenging FFPE needle biopsies. Following extensive work, we developed a QMSP methodology with both Scorpion probes or SYBR green to quantify the methylation at these genomic regions. As expected we found that the overall methylation of these three markers was the highest in the malignant group and all the cores analyzed were positive for at least one of the three markers. In contrast, there was almost no methylation in any benign samples. This is similar to previous publications reporting a very low frequency or no methylation in these genomic regions (82,96,111–113,146). Overall, this demonstrated that our optimized methylation assay could be used with FFPE needle biopsy samples and could robustly differentiate malignant and benign samples.

Having demonstrated the feasibility of this method, we then analyzed the promoter methylation of radiographically suspicious but histopathologically benign samples. In these, the percent methylation observed for each marker was lower than the malignant tumors, but significantly higher than the benign group. This was in line with our hypothesis that these lesions carry premalignant characteristics but had not completely progressed into a malignant state. Considering the high promoter methylation observed in the MRI group compared to benign samples, our results suggest that it is unlikely that mpMRI false positive biopsies are sampling errors but likely represent premalignant lesions.

We observed differing sensitivity and detection with each gene promoter. Among the three markers we analyzed, APC, could robustly separate histopathologic positive and negative biopsies. However, the detection with APC was very poor and only 37%

malignant samples were methylated. Although similar to some of the previously published studies (111–113,147), the percentage of methylation was lower in malignant group compared to GSTP1 and RARB2. Although APC is a well-defined tumor suppressor, there is discrepancy among the published data in both its prognostic and diagnostic potential and the relative methylation levels (111,113). It has been shown in several studies to be a sensitive marker for cancer development (135), that is detected early in carcinogenesis (98,113). However, there is conflicting evidence. Fiano *et al* reported no association of APC with PCa detection (148). Considering the variety of results published, it was hard to evaluate our results with the MRI group. However, APC is proposed to have over 90% negative predictive value (149) thereby offering a potential for preventing unnecessary biopsies and overtreatment. Furthermore, while APC is one of the DNA methylation markers suggested marking a premalignant state of the prostate tissue, the time of its exact occurrence throughout the PCa development pathway is not known. The fact that APC methylation was heterogeneous in the malignant population suggests that this is not required for neoplastic transformation. Moreover, while we strongly suspect a premalignant characteristic in our MRI group, lack of APC methylation can also be a result of different degrees of methylation for different markers.

GSTP1 promoter hypermethylation is the most extensively studied epigenetic biomarker for PCa (150). Over 90% of PCa tissues in published work showed hypermethylation for of this gene promoter(82). Some studies suggest that up to 70% of PIN display this hypermethylation, making it one of the strongest markers of a premalignant lesion (81,82). It is rarely observed in normal prostate or other tissue types (112,151) and has been proposed as a PCa biomarker for tissues and body fluids (152). In our cohort, both MRI and malignant group of patients showed high levels of GSTP1 positivity with a greater number of positive cores compared to APC and RARB2. Only 3 cores (3.6%) were not positive for GSTP1 in malignant group and all the patients had at least one core positive. For the MRI group, only 3 patients did not have any GSTP1 positive cores. It is believed that GSTP1 methylation is stable over time starting from the early point of multistep progression of PC and thus correlates with cancer development (148).

RARB2 promoter methylation in both malignant and MRI groups were consistent with previous publications (111,146). High levels of RARB2 methylation was previously observed in both PCa tissues, HGPIN and to a significantly lesser extent, in BPH (153). RARβ2 promoter methylation is also suggested to occur early in PCa etiology and is

associated with cancer initiation. (96–98). There are studies (97) reported that RARB2 methylation levels are significantly different between PCa, BPH and PIN. Methylation levels observed in MRI and malignant group of patients indicated a similar tendency. Predominantly, a single positive core observed for each patient in MRI group, while it was more frequent in malignant group of patients potentially due to the significantly higher level of methylation observed in the MRI and malignant cohorts.

We then investigated the clinical outcome for our MRI cohort by collecting follow up data including PSA, additional mpMRI imaging and treatment if applicable. In the malignant group of patients (n=23), only two were under active surveillance while the remaining 21 patients received either radical prostatectomy, radiotherapy or hormonotherapy. In contrast, the follow up of MRI group of patients were unexpected. More than half of the patients (11/18) did not have any further MRIs due to either no change or slight increase in their PSA levels. One patient in this group, had a TURP and was later diagnosed with ISUP 1 (GS 3+3) adenocarcinoma. Interestingly, in 7/18 of the patients that had further MRIs, only one of them was stable while the other reported lesions actually regressed which correlated with a decrease in PSA levels. Overall, this suggests that although these radiographically suspicious lesions had strong premalignant characteristics, they do not transition to a malignant tumor and show even further stability or regression. Therefore, although the samples were obtained with the guidance of a highly specific mpMRI methodology, histopathology should still remain the gold-standard for diagnosing patients. Potentially, this regression might be due to an immune response. Aberrant promoter methylation was established to be occurring in normal aging prostate tissues (154,155). During that time, prostate cells continuously get exposed to damaging agents, however, they can still activate self-repair until the number of the alterations accumulate to drive the cells through transformation (156).

Separate from this work there are numerous studies trying to correlate the clinical outcome of PCa with DNA promoter hypermethylation as a diagnostic or prognostic biomarker to aid diagnosis. However, these studies have a different end-point results than our work and they commonly include risk stratification and clinical outcome in form of BCR, relapse and PCa caused death. However, as PCa is a very slow growing disease the full assessment of the potential of the DNA markers require long term follow up (>15 years) (157). Due to these challenges, there is no consensus in the reported ability of these DNA methylation markers of predicting the disease progression and outcome (158). In

our cohort, the biomarker positivity could not be correlated with GS or PI-RAD grade due to the small patient numbers in each group. Moreover, the recent admission time of the patients and short-term follow up information limited our time dependent observations.

In conclusion, our study showed radiographically suspicious but histologically benign tissues have aberrant DNA methylation that inactivates common tumor suppressors. However, while these patients demonstrate similar radiographic and epigenetic features as histopathologic malignant samples, they largely did not progress as neoplastic tumors. Overall this work demonstrates that radiographically suspicious lesions do indeed have epigenetic alterations but this is not sufficient to drive transformation. This work demonstrates while mpMRI can robustly identify potential lesions, histopathology is essential to successfully diagnose PCa. However, given the sensitivity of specific markers, particularly APC, a DNA methylation assays combined with highly specific mpMRI visualization can potentially improve diagnosis and prognosis.

# 5. FUTURE STUDIES

In this thesis work, one of the bottlenecks was the limited number of patients. The reliable correlation of the clinical outcome and DNA methylation profile could definitely be achieved by analysis of data from larger cohorts. Also, both radiographic and treatment follow-up history up to 15 years would give us a clear path of accumulation of DNA methylation events.

Furthermore, the inclusion of different prostate tissue types to cohort would help us better identify the premalignant characteristics. While the options are limited for benign group, the suspicious group could further be divided in the PIA, PIN or HGPIN groups to be able to correlate and understand how frequent the tissues in these group proceed to malignancy and how their methylation profile differ from each other. Adding more promoter regions to this analysis would also enable us to mark the stepwise PCa development with varying methylation levels. Furthermore, addition of other clinical samples from the patients such as urine, would provide an additional possible validation step of premalignant characteristic.

Finally, analyzing the methylation levels with more than one assay would be a validation for both primer-probe pairs and the methylation levels.

# 6. BIBLIOGRAPHY


1. Lee CH, Akin-Olugbade O, Kirschenbaum A. Overview of Prostate Anatomy, Histology, and Pathology. Endocrinol Metab Clin North Am. 2011 Sep;40(3):565–75.

2. Aaron L, Franco OE, Hayward SW. Review of Prostate Anatomy and Embryology and the Etiology of Benign Prostatic Hyperplasia. Urol Clin North Am. 2016 Aug;43(3):279–88.

3. Lee JJ, Thomas I-C, Nolley R, Ferrari M, Brooks JD, Leppert JT. Biologic differences between peripheral and transition zone prostate cancer. Prostate. 2015 Feb;75(2):183–90.

4. Prostate Cancer [Internet]. Available from: https://www.cdc.gov/cancer/prostate/basic_info/what-is-prostate-cancer.htm#:~:text=The prostate is a part,empties urine from the bladder). Accessed on:18/08/2020

5. Liu AY, True LD. Characterization of Prostate Cell Types by CD Cell Surface Molecules. Am J Pathol. 2002 Jan;160(1):37–43.

6. Kavoussi L, Partin A, Novick AC, Peters CC, editors. CAMPBELL-WALSH UROLOGY. 10th ed. Philadelphia: Elsevier; 2011. 3831 p.

7. Huang Y-H, Zhang Y, Huang J. Neuroendocrine cells of prostate cancer: biologic functions and molecular mechanisms. Asian J Androl. 2019;21(3):291–5.

8. Sathianathen NJ, Konety BR, Crook J, Saad F, Lawrentschuk N. Landmarks in prostate cancer. Nat Rev Urol. 2018 Oct 31;15(10):627–42.

9. Pernar CH, Ebot EM, Wilson KM, Mucci LA. The Epidemiology of Prostate Cancer. Cold Spring Harb Perspect Med. 2018 Dec;8(12):a030361.

10. Gann PH. Risk factors for prostate cancer. Rev Urol. 2002 Feb;4 Suppl 5(2):S3–10.

11. James N. Primer on Prostate Cancer. Tarporley: Springer Healthcare Ltd.; 2014.

12. Stenman U-H, Leinonen J, Zhang W-M, Finne P. Prostate-specific antigen. Semin Cancer Biol. 1999 Apr 1;9(2):83–93.

13. Bax C, Taverna G, Eusebio L, Sironi S, Grizzi F, Guazzoni G, et al. Innovative Diagnostic Methods for Early Prostate Cancer Detection through Urine Analysis: A Review. Cancers (Basel). 2018 Apr 18;10(4):123.

14. Schrecengost R, Knudsen KE. Molecular Pathogenesis and Progression of Prostate Cancer. Semin Oncol. 2013 Jun;40(3):244–58.

15. Bostwick DG, Liu L, Brawer MK, Qian J. High-grade prostatic intraepithelial neoplasia. Rev Urol. 2004;6(4):171–9.

16. Ayala AG, Ro JY. Prostatic intraepithelial neoplasia: recent advances. Arch Pathol Lab Med. 2007 Aug;131(8):1257–66.

17. Leite KRM, Camara-Lopes LH, Cury J, Dall'Oglio MF, Sañudo A, Srougi M. Prostate cancer detection at rebiopsy after an initial benign diagnosis: results using sextant extended prostate biopsy. Clinics. 2008;63(3):339–42.

18. Tolkach Y, Kristiansen G. Is high-grade prostatic intraepithelial neoplasia (HGPIN) a reliable precursor for prostate carcinoma? Implications for clonal evolution and early detection strategies. J Pathol. 2018 Apr;244(4):389–93.

19. Moreira DM, de O Freitas DM, Nickel JC, Andriole GL, Castro-Santamaria R, Freedland SJ. The combination of histological prostate atrophy and inflammation is associated with lower risk of prostate cancer in biopsy specimens. Prostate Cancer Prostatic Dis. 2017 Dec 6;20(4):413–7.

20. Celma A, Servián P, Planas J, Placer J, Quilez MT, Arbós MA, et al. Clinical significance of proliferative inflammatory atrophy in prostate biopsy. Actas Urológicas Españolas (English Ed. 2014 Mar;38(2):122–6.

21. Bostwick DG, Brawer MK. Prostatic Intra-Epithelial Neoplasia and Early Invasion in Prostate Cancer. Cancer. 1987 Feb 15;59(4):788–94.

22. Yegnasubramanian S, Lin X, Haffner MC, DeMarzo AM, Nelson WG. Combination of methylated-DNA precipitation and methylation-sensitive restriction enzymes (COMPARE-MS) for the rapid, sensitive and quantitative detection of DNA methylation. Nucleic Acids Res. 2006;34(3):1–14.

23. Hernandez J, Thompson IM. Diagnosis and treatment of prostate cancer. Med Clin North Am. 2004 Mar;88(2):267–79.

24. Chen N, Zhou Q. The evolving Gleason grading system. Chin J Cancer Res. 2016 Feb;28(1):58–64.

25. Moch H, Cubilla AL, Humphrey PA, Reuter VE, Ulbright TM. The 2016 WHO Classification of Tumours of the Urinary System and Male Genital Organs—Part A: Renal, Penile, and Testicular Tumours. Eur Urol. 2016 Jul;70(1):93–105.

26. Velonas V, Woo H, Remedios C, Assinder S. Current Status of Biomarkers for Prostate Cancer. Int J Mol Sci. 2013 May 24;14(6):11034–60.

27. Porten SP, Whitson JM, Cowan JE, Cooperberg MR, Shinohara K, Perez N, et al. Changes in Prostate Cancer Grade on Serial Biopsy in Men Undergoing Active Surveillance. J Clin Oncol. 2011 Jul 10;29(20):2795–800.

28. Lima AR, Bastos M de L, Carvalho M, Guedes de Pinho P. Biomarker Discovery in Human Prostate Cancer: an Update in Metabolomics Studies. Transl Oncol. 2016 Aug;9(4):357–70.

29. Lecornet E, Ahmed HU, Hu Y, Moore CM, Nevoux P, Barratt D, et al. The Accuracy of Different Biopsy Strategies for the Detection of Clinically Important Prostate Cancer: A Computer Simulation. J Urol. 2012 Sep;188(3):974–80.

30. Kvåle R, Møller B, Wahlqvist R, Fosså SD, Berner A, Busch C, et al. Concordance between Gleason scores of needle biopsies and radical prostatectomy specimens: a population-based study. BJU Int. 2009 Jun;103(12):1647–54.

31. Jones JS. Saturation biopsy for detecting and characterizing prostate cancer. BJU Int. 2007 Jun;99(6):1340–4.

32. Lane BR, Zippe CD, Abouassaly R, Schoenfield L, Magi-Galluzzi C, Jones JS. Saturation Technique Does Not Decrease Cancer Detection During Followup After Initial Prostate Biopsy. J Urol. 2008 May;179(5):1746–50.

33. Eichler K, Hempel S, Wilby J, Myers L, Bachmann LM, Kleijnen J. Diagnostic Value of Systematic Biopsy Methods in the Investigation of Prostate Cancer: A Systematic Review. J Urol. 2006 May;175(5):1605–12.

34. Salami SS, Ben-Levi E, Yaskiv O, Ryniker L, Turkbey B, Kavoussi LR, et al. In patients with a previous negative prostate biopsy and a suspicious lesion on magnetic resonance imaging, is a 12-core biopsy still necessary in addition to a

targeted biopsy? BJU Int. 2015 Apr;115(4):562–70.

35. Woodrum D, Gorny K, Greenwood B, Mynderse L. MRI-Guided Prostate Biopsy of Native and Recurrent Prostate Cancer. Semin Intervent Radiol. 2016 Aug 30;33(03):196–205.

36. Turkbey B, Albert PS, Kurdziel K, Choyke PL. Imaging Localized Prostate Cancer: Current Approaches and New Developments. Am J Roentgenol. 2009 Jun;192(6):1471–80.

37. Murphey A, Gaillard F. MRI Sequences (Overview) [Internet]. Available from: https://radiopaedia.org/articles/mri-sequences-overview. Accessed on:18/08/2020

38. Lovegrove CE, Matanhelia M, Randeva J, Eldred-Evans D, Tam H, Miah S, et al. Prostate imaging features that indicate benign or malignant pathology on biopsy. Transl Androl Urol. 2018 Sep;7(S4):S420–35.

39. Barrett T. What is Multiparametric-MRI of the Prostate and Why Do We Need It ? J Imaging Interv Radiol. 2015;1:13–7.

40. Ludwig DR, Fraum TJ, Fowler KJ, Ippolito JE. Imaging in Prostate Cancer: Magnetic Resonance Imaging and Beyond. Mo Med. 2018;115(2):135–41.

41. Mussi TC, Martins T, Dantas GC, Garcia RG, Filippi RZ, Lemos GC, et al. Comparison between multiparametric MRI with and without post - contrast sequences for clinically significant prostate cancer detection. Int braz j urol. 2018 Dec;44(6):1129–38.

42. Turkbey B, Mani H, Shah V, Rastinehad AR, Bernardo M, Pohida T, et al. Multiparametric 3T Prostate Magnetic Resonance Imaging to Detect Cancer: Histopathological Correlation Using Prostatectomy Specimens Processed in Customized Magnetic Resonance Imaging Based Molds. J Urol. 2011 Nov 22;186(5):1818–24.

43. Ahmed HU, Kirkham A, Arya M, Illing R, Freeman A, Allen C, et al. Is it time to consider a role for MRI before prostate biopsy? Nat Rev Clin Oncol. 2009 Apr;6(4):197–206.

44. Bjurlin MA, Mendhiratta N, Wysock JS, Taneja SS. Multiparametric MRI and targeted prostate biopsy: Improvements in cancer detection, localization, and risk

assessment. Cent Eur J Urol. 2016;69(1):9–18.

45. Moore CM, Kasivisvanathan V, Eggener S, Emberton M, Fütterer JJ, Gill IS, et al. Standards of Reporting for MRI-targeted Biopsy Studies (START) of the Prostate: Recommendations from an International Working Group. Eur Urol. 2013 Oct;64(4):544–52.

46. Moore CM, Robertson NL, Arsanious N, Middleton T, Villers A, Klotz L, et al. Image-Guided Prostate Biopsy Using Magnetic Resonance Imaging–Derived Targets: A Systematic Review. Eur Urol. 2013 Jan;63(1):125–40.

47. Barentsz JO, Weinreb JC, Verma S, Thoeny HC, Tempany CM, Shtern F, et al. Synopsis of the PI-RADS v2 Guidelines for Multiparametric Prostate Magnetic Resonance Imaging and Recommendations for Use. Eur Urol. 2016 Jan;69(1):41–9.

48. Zhou Y, Zhou Z, Li Q, Xu Y, Sun H, Xiao Y, et al. Diagnostic accuracy of magnetic resonance-guided prostate biopsy and template-guided transperineal saturation biopsy. Medicine (Baltimore). 2018 Sep;97(38):e12495.

49. Barentsz JO, Richenberg J, Clements R, Choyke P, Verma S, Villeirs G, et al. ESUR prostate MR guidelines 2012. Eur Radiol. 2012 Apr 10;22(4):746–57.

50. Haffner J, Lemaitre L, Puech P, Haber G-P, Leroy X, Jones JS, et al. Role of magnetic resonance imaging before initial biopsy: comparison of magnetic resonance imaging-targeted and systematic biopsy for significant prostate cancer detection. BJU Int. 2011 Oct;108(8b):E171–8.

51. Park BK, Park JW, Park SY, Kim CK, Lee HM, Jeon SS, et al. Prospective Evaluation of 3-T MRI Performed Before Initial Transrectal Ultrasound–Guided Prostate Biopsy in Patients With High Prostate-Specific Antigen and No Previous Biopsy. Am J Roentgenol. 2011 Nov;197(5):W876–81.

52. Pinto PA, Chung PH, Rastinehad AR, Baccala AA, Kruecker J, Benjamin CJ, et al. Magnetic Resonance Imaging/Ultrasound Fusion Guided Prostate Biopsy Improves Cancer Detection Following Transrectal Ultrasound Biopsy and Correlates With Multiparametric Magnetic Resonance Imaging. J Urol. 2011 Oct;186(4):1281–5.

53. Sonn GA, Natarajan S, Margolis DJA, MacAiran M, Lieu P, Huang J, et al. Targeted Biopsy in the Detection of Prostate Cancer Using an Office Based Magnetic Resonance Ultrasound Fusion Device. J Urol. 2013 Jan;189(1):86–92.

54. Rais-Bahrami S, Siddiqui MM, Turkbey B, Stamatakis L, Logan J, Hoang AN, et al. Utility of Multiparametric Magnetic Resonance Imaging Suspicion Levels for Detecting Prostate Cancer. J Urol. 2013 Nov;190(5):1721–7.

55. Fütterer JJ, Barentsz JO. MRI-guided and robotic-assisted prostate biopsy. Curr Opin Urol. 2012 Jul;22(4):316–9.

56. Puech P, Ouzzane A, Gaillard V, Betrouni N, Renard B, Villers A, et al. Multiparametric MRI-Targeted TRUS Prostate Biopsies Using Visual Registration. Biomed Res Int. 2014;2014:1–11.

57. Overduin CG, Fütterer JJ, Barentsz JO. MRI-Guided Biopsy for Prostate Cancer Detection: A Systematic Review of Current Clinical Results. Curr Urol Rep. 2013 Jun 9;14(3):209–13.

58. Kilic M, Vural M, Coskun B, Acar Ö, Saglican Y, Akpek S, et al. Accuracy of Sampling PI-RADS 4–5 Index Lesions Alone by MRI-guided In-bore Biopsy in Biopsy–naive Patients Undergoing Radical Prostatectomy. Eur Urol Focus. 2020 Mar;6(2):249–54.

59. Bjurlin MA, Meng X, Le Nobin J, Wysock JS, Lepor H, Rosenkrantz AB, et al. Optimization of Prostate Biopsy: the Role of Magnetic Resonance Imaging Targeted Biopsy in Detection, Localization and Risk Assessment. J Urol. 2014 Sep;192(3):648–58.

60. Bjurlin MA, Taneja SS. Standards for prostate biopsy. Curr Opin Urol. 2014 Mar;24(2):155–61.

61. Bird A. CpG-rich islands and the function of DNA methylation. Nature. 1986;321:209–13.

62. Gardiner-Garden M, Froomer M. CpG Islands in Vertebrate Genomes. J Mol Biol. 1987;261–82.

63. Takai D, Jones PA. Comprehensive analysis of CpG islands in human chromosomes 21 and 22. Proc Natl Acad Sci. 2002;99(6):3740–5.

64. Cooper DN, Krawczak M. Cytosine methylation and the fate of CpG dinucleotides in vertebrate genomes. Hum Genet. 1989;83(2):181–8.

65. Yoder JA, Walsh CP, Bestor TH. Cytosine methylation and the ecology of intragenomic parasites. Trends Genet. 1997;13(8):335–40.

66. Wang Y, Leung FCC. An evaluation of new criteria for CpG islands in the human genome as gene markers. Bioinformatics. 2004;20(7):1170–7.

67. Perry AS, Watson RWG, Lawler M, Hollywood D. The epigenome as a therapeutic target in prostate cancer. Nat Rev Urol. 2010;7(12):668–80.

68. Johnson CA, Laherty CD, Ng H-H, Eisenman RN, Turner BM, Nan X, et al. Transcriptional repression by the methyl-CpG-binding protein MeCP2 involves a histone deacetylase complex. Nature. 1998;393:386–9.

69. Landsberger N, Strouboulis J, Wolffe AP, Vermaak D, Jones PL, Kass SU, et al. Methylated DNA and MeCP2 recruit histone deacetylase to repress transcription. Nat Genet. 1998;19(2):187–91.

70. Bestor TH. Methylation meets acetylation. Nature. 1998;393(6683):311–2.

71. Chodavarapu RK, Feng S, Bernatavichute Y V., Chen P-Y, Stroud H, Yu Y, et al. Relationship between nucleosome positioning and DNA methylation. Nature. 2010 Jul 30;466(7304):388–92.

72. Pakneshan P, Hongmei Xing R, Rabbani SA. Methylation status of uPA promoter as a molecular mechanism regulating prostate cancer invasion and growth in vitro and in vivo. FASEB. 2003;17:1081–8.

73. Li LC, Zhao H, Shiina H, Kane CJ, Dahiya R. PGDB: A curated and integrated database of genes related to the prostate. Nucleic Acids Res. 2003;31(1):291–3.

74. Schulz WA, Hatina J. Epigenetics of prostate cancer: Beyond DNA methylation. J Cell Mol Med. 2006;10(1):100–25.

75. Majumdar S, Buckles E, Estrada J, Koochekpour S. Aberrant DNA Methylation and Prostate Cancer. Curr Genomics. 2012 Nov 1;12(7):486–505.

76. Graça I, Pereira-Silva E, Henrique R, Packham G, Crabb SJ, Jerónimo C. Epigenetic modulators as therapeutic targets in prostate cancer. Clin Epigenetics.

2016 Dec 15;8(1):98.

77. Lee WH, Morton RA, Epstein JI, Brooks JD, Campbell PA, Bova GS, et al. Cytidine methylation of regulatory sequences near the pi-class glutathione S-transferase gene accompanies human prostatic carcinogenesis. Proc Natl Acad Sci U S A. 1994;91(24):11733–7.

78. Joseph DB, Strand DW, Vezina CM. DNA methylation in development and disease: an overview for prostate researchers. Am J Clin Exp Urol. 2018;6(6):197–218.

79. Berhane K, Widersten M, Engstrom A, Kozarich JW, Mannervik B. Detoxication of base propenals and other alpha, beta-unsaturated aldehyde products of radical reactions and lipid peroxidation by human glutathione transferases. Proc Natl Acad Sci. 1994;91(4):1480–4.

80. Glutathione SP, Nelson CP, Kidd LCR, Sauvageot J, Isaacs WB, Marzo AM De, et al. Protection against 2-Hydroxyamino-1-methyl-6-phenylimidazo [ 4 , 5- b ] pyridine Cytotoxicity and DNA Adduct Formation in Human Prostate by. 2001;103–9.

81. Brooks JD, Weinstein M, Lin X, Sun Y, Pin SS, Bova GS, et al. CG island methylation changes near the GSTP1 gene in prostatic intraepithelial neoplasia. Cancer Epidemiol Biomarkers Prev. 1998;7(6):531–6.

82. Nakayama M, Bennett CJ, Hicks JL, Epstein JI, Platz EA, Nelson WG, et al. Hypermethylation of the human glutathione S-transferase-π gene (GSTP1) CpG island is present in a subset of proliferative inflammatory atrophy lesions but not in normal or hyperplastic epithelium of the prostate: A detailed study using laser-capture micro. Am J Pathol. 2003;163(3):923–33.

83. Hoque MO, Topaloglu O, Begum S, Henrique R, Rosenbaum E, Van Criekinge W, et al. Quantitative Methylation-Specific Polymerase Chain Reaction Gene Patterns in Urine Sediment Distinguish Prostate Cancer Patients From Control Subjects. J Clin Oncol. 2005 Sep 20;23(27):6569–75.

84. Goessl C, Müller M, Heicappell R, Krause H, Miller K. DNA-based detection of prostate cancer in blood, urine, and ejaculates. Ann N Y Acad Sci. 2001 Sep;945:51–8.

85. Suh C., Shanafelt T, May D., Shroyer K., Bobak J., Crawford E., et al. Comparison of telomerase activity and GSTP1 promoter methylation in ejaculate as potential screening tests for prostate cancer. Mol Cell Probes. 2000 Jun;14(4):211–7.

86. Park JY. Promoter Hypermethylation in Prostate Cancer. Cancer Control. 2010 Oct;17(4):245–55.

87. Allenby G, Bocquel MT, Saunders M, Kazmer S, Speck J, Rosenberger M, et al. Retinoic acid receptors and retinoid X receptors: Interactions with endogenous retinoic acids. Proc Natl Acad Sci U S A. 1993;90(1):30–4.

88. Gao T, He B, Pan Y, Li R, Xu Y, Chen L, et al. The Association of Retinoic Acid Receptor Beta2(RARβ2) Methylation Status and Prostate Cancer Risk: A Systematic Review and Meta-Analysis. Campbell M, editor. PLoS One. 2013 May 13;8(5):e62950.

89. Wang X -f. Epigenetic Modulation of Retinoic Acid Receptor 2 by the Histone Deacetylase Inhibitor MS-275 in Human Renal Cell Carcinoma. Clin Cancer Res. 2005 May 1;11(9):3535–42.

90. Sirchia SM, Ren M, Pili R, Sironi E, Somenzi G, Ghidoni R, et al. Endogenous reactivation of the RARbeta2 tumor suppressor gene epigenetically silenced in breast cancer. Cancer Res. 2002 May 1;62(9):2455–61.

91. Fang C, Jian Z-Y, Shen X-F, Wei X-M, Yu G-Z, Zeng X-T. Promoter Methylation of the Retinoic Acid Receptor Beta2 (RARβ2) Is Associated with Increased Risk of Breast Cancer: A PRISMA Compliant Meta-Analysis. PLoS One. 2015;10(10):e0140329.

92. Lotan Y, Xu XC, Shalev M, Lotan R, Williams R, Wheeler TM, et al. Differential Expression of Nuclear Retinoid Receptors in Normal and Malignant Prostates. J Clin Oncol. 2000 Jan 1;18(1):116–116.

93. De Luca LM. Retinoids and their receptors in differentiation, embryogenesis, and neoplasia. FASEB J. 1991 Nov;5(14):2924–33.

94. Yang Q, Mori I, Shan L, Nakamura M, Nakamura Y, Utsunomiya H, et al. Biallelic Inactivation of Retinoic Acid Receptor β2 Gene by Epigenetic Change in Breast Cancer. Am J Pathol. 2001 Jan;158(1):299–303.

95. Ivanova T, Petrenko A, Gritsko T, Vinokourova S, Eshilev E, Kobzeva V, et al. Methylation and silencing of the retinoic acid receptor-β2 gene in cervical cancer. BMC Cancer. 2002 Dec 21;2(1):4.

96. Nakayama T, Watanabe M, Yamanaka M, Hirokawa Y, Suzuki H, Ito H, et al. The Role of Epigenetic Modifications in Retinoic Acid Receptor β2 Gene Expression in Human Prostate Cancers. Lab Investig. 2001 Jul 1;81(7):1049–57.

97. Yamanaka M, Watanabe M, Yamada Y, Takagi A, Murata T, Takahashi H, et al. Altered methylation of multiple genes in carcinogenesis of the prostate. Int J Cancer. 2003;106(3):382–7.

98. Li LC, Okino ST, Dahiya R. DNA methylation in prostate cancer. Biochim Biophys Acta - Rev Cancer. 2004;1704(2):87–102.

99. Takeichi M. Cadherin cell adhesion receptors as a morphogenetic regulator. Science (80- ). 1991 Mar 22;251(5000):1451–5.

100. Fearnhead NS. The ABC of APC. Hum Mol Genet. 2001 Apr 1;10(7):721–33.

101. Nathke IS. The adenomatous polyposis coli protein. Mol Pathol. 1999 Aug 1;52(4):169–73.

102. Noordermeer J, Klingensmith J, Perrimon N, Nusse R. dishevelled and armadillo act in the Wingless signalling pathway in Drosophila. Nature. 1994 Jan;367(6458):80–3.

103. Willert K, Shibamoto S, Nusse R. Wnt-induced dephosphorylation of Axin releases beta -catenin from the Axin complex. Genes Dev. 1999 Jul 15;13(14):1768–73.

104. Hankey W, Frankel WL, Groden J. Functions of the APC tumor suppressor protein dependent and independent of canonical WNT signaling: implications for therapeutic targeting. Cancer Metastasis Rev. 2018 Mar 9;37(1):159–72.

105. He T. Identification of c-MYC as a Target of the APC Pathway. Science (80- ). 1998 Sep 4;281(5382):1509–12.

106. Shtutman M, Zhurinsky J, Simcha I, Albanese C, D'Amico M, Pestell R, et al. The cyclin D1 gene is a target of the -catenin/LEF-1 pathway. Proc Natl Acad Sci. 1999

May 11;96(10):5522–7.

107. Tetsu O, McCormick F. β-catenin regulates expression of cyclin D1 in colon carcinoma cells. Nature. 1999;398(6726):422–6.

108. Heinen CD, Goss KH, Cornelius JR, Babcock GF, Knudsen ES, Kowalik T, et al. The APC tumor suppressor controls entry into S-phase through its ability to regulate the cyclin D/RB pathway. Gastroenterology. 2002 Sep;123(3):751–63.

109. Esteller M, Corn PG, Baylin SB, Herman JG. A gene hypermethylation profile of human cancer. Cancer Res. 2001 Apr 15;61(8):3225–9.

110. Yang M, Park JY. DNA Methylation in Promoter Region as Biomarkers in Prostate Cancer. In: Dumitrescu RG, Verma M, editors. Cancer. Totowa, NJ: Humana Press; 2012. p. 67–109. (Methods in Molecular Biology; vol. 863).

111. Maruyama R, Toyooka S, Toyooka KO, Virmani AK, Zöchbaurer-Müller S, A.J. F, et al. Aberrant Promoter Methylation Profile of Prostate Cancers and Its Relationship to Clinicopathological Features. Clin Cancer Res. 2002;8:514–9.

112. Yegnasubramanian S, Kowalski J, Gonzalgo ML, Zahurak M, Piantadosi S, Walsh PC, et al. Hypermethylation of CpG Islands in Primary and Metastatic Human Prostate Cancer. Cancer Res. 2004 Mar 15;64(6):1975–86.

113. Kang GH, Lee S, Lee HJ, Hwang KS. Aberrant CpG island hypermethylation of multiple genes in prostate cancer and prostatic intraepithelial neoplasia. J Pathol. 2004 Feb;202(2):233–40.

114. Perry AS, Foley R, Woodson K, Lawler M. The emerging roles of DNA methylation in the clinical management of prostate cancer. Endocr Relat Cancer. 2006;357–77.

115. Hoque MO. DNA methylation changes in prostate cancer: Current developments and future clinical implementation. Expert Rev Mol Diagn. 2009 Apr 9;9(3):243–57.

116. Laird PW. Principles and challenges of genome-wide DNA methylation analysis. Nat Rev Genet. 2010 Mar 2;11(3):191–203.

117. Beck S, Rakyan VK. The methylome: approaches for global DNA methylation

profiling. Trends Genet. 2008 May;24(5):231–7.

118. Pharo HD. Quantitative methylation-specific PCR - optimization and application. 2014;

119. Saluz H, Jost J-P. Major techniques to study DNA methylation. In: DNA Methylation. Basel: Birkhäuser Basel; 1993. p. 11–26.

120. Grigg G, Clark S. Sequencing 5-methylcytosine Residues in Genomic DNA. BioEssays. 1994;16(6):431–6.

121. Rein T, DePamphilis ML, Zorbas H. Identifying 5-methylcytosine and related modifications in DNA genomes. Nucleic Acids Res. 1998 May 1;26(10):2255–64.

122. Sepulveda AR, Jones D, Ogino S, Samowitz W, Gulley ML, Edwards R, et al. CpG Methylation Analysis—Current Status of Clinical Assays and Potential Applications in Molecular Diagnostics. J Mol Diagnostics. 2009 Jul;11(4):266–78.

123. Fraga MF, Esteller M. Review DNA Methylation : A Profile of Methods. Biotechniques. 2002;33(3).

124. Harrison A, Parle-McDermott A. DNA Methylation: A Timeline of Methods and Applications. Front Genet. 2011;2(OCT):1–13.

125. Cedar H, Solage A, Glaser G, Razin A. Direct detection of methylated cytosine in DNA by use of the restriction enzyme MspI. Nucleic Acids Res. 1979;6(6):2125–32.

126. Frommer M, McDonald LE, Millar DS, Collis CM, Watt F, Grigg GW, et al. A genomic sequencing protocol that yields a positive display of 5-methylcytosine residues in individual DNA strands. Proc Natl Acad Sci. 1992 Mar 1;89(5):1827–31.

127. DNA Methylation [Internet]. Available from: https://www.diagenode.com/en/applications/dna-bisulfite-conversion. Accessed on:18/08/2020

128. Pharo Dietrichson H. Quantitative methylation-specific PCR - optimization and application. University of Oslo; 2014.

129. Eads CA. MethyLight: a high-throughput assay to measure DNA methylation.

Nucleic Acids Res. 2000;28(8):32e – 0.

130. Cairns P. Gene methylation and early detection of genitourinary cancer: the road ahead. Nat Rev Cancer. 2007 Jul;7(7):531–43.

131. Thelwell N. Mode of action and application of Scorpion primers to mutation detection. Nucleic Acids Res. 2000 Oct 1;28(19):3752–61.

132. © 2020 Merck KGaA, Darmstadt G and/or its affiliates. Quantitative PCR and Digital PCR Detection Methods [Internet]. Available from: https://www.sigmaaldrich.com/technical-documents/articles/biology/quantitative-pcr-and-digital-pcr-detection-methods.html Accessed on: 18/09/2020.

133. Kornberg Z, Cooperberg MR, Spratt DE, Feng FY. Genomic biomarkers in prostate cancer. Transl Androl Urol. 2018 Jun;7(3):459–71.

134. Stewart GD, Van Neste L, Delvenne P, Delrée P, Delga A, McNeill SA, et al. Clinical Utility of an Epigenetic Assay to Detect Occult Prostate Cancer in Histopathologically Negative Biopsies: Results of the MATLOC Study. J Urol. 2013 Mar;189(3):1110–6.

135. Partin AW, Van Neste L, Klein EA, Marks LS, Gee JR, Troyer DA, et al. Clinical Validation of an Epigenetic Assay to Predict Negative Histopathological Results in Repeat Prostate Biopsies. J Urol. 2014 Oct;192(4):1081–7.

136. Van Neste L, Partin AW, Stewart GD, Epstein JI, Harrison DJ, Van Criekinge W. Risk score predicts high-grade prostate cancer in DNA-methylation positive, histopathologically negative biopsies. Prostate. 2016 Sep 28;76(12):1078–87.

137. Chai H, Brown RE. Field effect in cancer-an update. Ann Clin Lab Sci. 2009;39(4):331–7.

138. Shuman S. DNA strand transfer reactions catalyzed by vaccinia topoisomerase I. J Biol Chem. 1992 Apr 25;267(12):8620–7.

139. Van Der Velden VHJ, Hochhaus A, Cazzaniga G, Szczepanski T, Gabert J, van Dongen JJM. Detection of minimal residual disease in hematologic malignancies by real-time quantitative PCR: principles, approaches, and laboratory aspects. Leukemia. 2003 Jun 23;17(6):1013–34.

140. Tyagi S, Kramer FR. Molecular Beacons: Probes that Fluoresce upon Hybridization. Nat Biotechnol. 1996 Mar;14(3):303–8.

141. Thermo Fisher Scientific Inc. TOPO ® TA Cloning ® Kit for Sequencing. Carlsbad; 2014.

142. Jerónimo C, Henrique R, Hoque MO, Mambo E, Ribeiro FR, Varzim G, et al. A quantitative promoter methylation profile of prostate cancer. Clin Cancer Res. 2004;10(24):8472–8.

143. Wolffe AP, Matzke MA. Epigenetics: Regulation Through Repression. Science (80- ). 1999 Oct 15;286(5439):481–6.

144. Jones PA. Functions of DNA methylation: Islands, start sites, gene bodies and beyond. Nat Rev Genet. 2012;13(7):484–92.

145. Baylin SB. Aberrant patterns of DNA methylation, chromatin formation and gene expression in cancer. Hum Mol Genet. 2001 Apr 1;10(7):687–92.

146. Yamanaka M, Watanabe M, Yamada Y, Takagi A, Murata T, Takahashi H, et al. Altered methylation of multiple genes in carcinogenesis of the prostate. Int J Cancer. 2003 Sep 1;106(3):382–7.

147. Perry AS, Foley R, Woodson K, Lawler M. The emerging roles of DNA methylation in the clinical management of prostate cancer. Endocr Relat Cancer. 2006 Jun;91(2):357–77.

148. Fiano V, Zugna D, Grasso C, Trevisan M, Delsedime L, Molinaro L, et al. DNA methylation in repeat negative prostate biopsies as a marker of missed prostate cancer. Clin Epigenetics. 2019;11(1):1–10.

149. Trock BJ, Brotzman MJ, Mangold LA, Bigley JW, Epstein JI, McLeod D, et al. Evaluation of GSTP1 and APC methylation as indicators for repeat biopsy in a high-risk cohort of men with negative initial prostate biopsies. BJU Int. 2012;110(1):56–62.

150. Van Neste L, Herman JG, Otto G, Bigley JW, Epstein JI, Van Criekinge W. The Epigenetic promise for prostate cancer diagnosis. Prostate. 2012;72(11):1248–61.

151. Nakayama M, Gonzalgo ML, Yegnasubramanian S, Lin X, De Marzo AM, Nelson

WG. GSTP1 CpG island hypermethylation as a molecular biomarker for prostate cancer. J Cell Biochem. 2004 Feb 15;91(3):540–52.

152. Strand S, Orntoft T, Sorensen K. Prognostic DNA Methylation Markers for Prostate Cancer. Int J Mol Sci. 2014 Sep 18;15(9):16544–76.

153. Jerónimo C, Henrique R, Hoque MO, Ribeiro FR, Oliveira J, Fonseca D, et al. Quantitative RARβ2 hypermethylation: A promising prostate cancer marker. Clin Cancer Res. 2004;10(12 I):4010–4.

154. Jung M, Pfeifer GP. Aging and DNA methylation. BMC Biol. 2015 Dec 31;13(1):7.

155. Richardson B. Impact of aging on DNA methylation. Ageing Res Rev. 2003 Jul;2(3):245–61.

156. Otsetov A, Wanders A, Buckland R, Bergh AB. Epigenetics in the Development of Prostate Cancer Precursors. J Urol Ren Dis. 2017;2017(05):1–4.

157. Albertsen PC. 20-Year Outcomes Following Conservative Management of Clinically Localized Prostate Cancer. JAMA. 2005 May 4;293(17):2095.

158. Lam D, Clark S, Stirzaker C, Pidsley R. Advances in Prognostic Methylation Biomarkers for Prostate Cancer. Cancers (Basel). 2020 Oct 15;12(10):2993.